ITS UCDAVIS
INSTITUTE OF TRANSPORTATION STUDIES

Research Report – UCD-ITS-RR-11-19

Accelerated Traffic Load Testing of Expansion Joints for the Self-Anchored Suspension Section of the New San Francisco-Oakland Bay Bridge East Span

December 2011

David Jones
Rongzong Wu

Institute of Transportation Studies ◦ University of California, Davis
One Shields Avenue ◦ Davis, California 95616
PHONE (530) 752-6548 ◦ FAX (530) 752-6572
www.its.ucdavis.edu

December 2011
Research Report: UCPRC-RR-2011-06

Accelerated Traffic Load Testing of Expansion Joints for the Self-Anchored Suspension Section of the New San Francisco–Oakland Bay Bridge East Span

Authors:
D. Jones and R. Wu

Partnered Pavement Research Center (PPRC) Contract Strategic Plan Element 3.16:
Bay Bridge Expansion Joint Testing Study

PREPARED FOR:

California Department of Transportation
Division of Research and Innovation
Office of Roadway Research

PREPARED BY:

University of California
Pavement Research Center
UC Davis, UC Berkeley

DOCUMENT RETRIEVAL PAGE			**Research Report: UCPRC-RR-2011-06**
Title: Accelerated Traffic Load Testing of Expansion Joints for the Self-anchored Suspension Section of the New San Francisco–Oakland Bay Bridge East Span			
Authors: David Jones and Rongzong Wu			
Prepared for: Caltrans	**FHWA No:** CA122255A	**Work submitted:** 03-19-2012	**Date** December 2011
Strategic Plan Element No: 3.16	**Status:** Stage 6 Final		**Version No.:** 1

Abstract:

A relatively unique opportunity was recently identified for accelerated traffic load testing of a new bridge expansion joint design. This study was part of the construction of the new East Span of the San Francisco–Oakland Bay Bridge and assessed whether these new Caltrans seismic expansion joints (which were designed to function in harmony with the bridge decks in the event of a high-magnitude earthquake) linking the Self-anchored Span with the Transition and Skyway spans would withstand truck traffic loading. A test structure incorporating one of the full-scale joints was constructed close to the actual bridge and tested with the California Department of Transportation / University of California Pavement Research Center Heavy Vehicle Simulator in a series of phases.

A total of 1.36 million load repetitions, equating to about 46 million equivalent standard axle loads, were applied in seven phases during the three-month test. On completion of this testing, no structural damage was recorded by any of the Linear Variable Differential Transducers or strain gauges installed on the steel plates, steel frames, bolts, or washers. There was also no visible damage on any of these components. Excessive overloading with a 150 kN half-axle load in the last phase of the test caused some damage to the Trelleborg unit of the joint. This included abrasion, tearing, shoving and permanent deformation of the rubber inserts, and deformation and shearing of one of the steel supports directly under the wheel load. Based on the results of this limited testing, it was concluded that the Caltrans seismic expansion joint would perform adequately under typical Bay Bridge traffic. The distress observed to the Trelleborg unit under the high loads in the last phase of testing is unlikely to occur under normal traffic. However, the Trelleborg unit was found to be the weakest point of the expansion joint, as expected. On the actual bridge structure, these units will require periodic maintenance and replacement in line with manufacturer's specifications.

The findings from this study indicate that the Caltrans seismic expansion joint tested would be appropriate for typical Bay Bridge traffic.

No seismic or structural testing was undertaken on the seismic expansion joint as part of this study and no recommendations toward its seismic or structural performance are made. Ride quality, skid resistance, and tire noise studies were carried out by Caltrans in a separate study and are reported on in separate Caltrans reports.

Keywords:
San Francisco–Oakland Bay Bridge, Expansion Joint, Accelerated Traffic Load Test, Heavy Vehicle Simulator

Proposals for implementation:
Caltrans seismic expansion joint as tested is expected to withstand normal traffic loading

Related documents:
None

Signatures:

D. Jones **1st Author**	J. Harvey **Technical Review**	D. Spinner **Editor**	J. Harvey **Principal Investigator**	T.J. Holland **Caltrans Contract Manager**

DISCLAIMER

The contents of this report reflect the views of the authors who are responsible for the facts and accuracy of the data presented herein. The contents do not necessarily reflect the official views or policies of the State of California or the Federal Highway Administration. This report does not constitute a standard, specification, or regulation.

In this study, a new Caltrans seismic expansion joint was assessed for performance under accelerated truck traffic loading only. No seismic or structural testing was undertaken on the seismic expansion joint as part of this study and no recommendations toward its seismic or structural performance are made. Ride quality, skid resistance, and tire noise studies were carried out by Caltrans in a separate study and are reported on in separate Caltrans reports.

PROJECT OBJECTIVES

The objective of this study on accelerated traffic load testing of a Caltrans seismic expansion joint for the self-anchored suspension section of the new San Francisco–Oakland Bay Bridge East Span Bay Bridge was to provide a rapid indication of whether the expansion joint would perform adequately under typical Bay Bridge vehicle loading. This was achieved through the following tasks:

1. Identify any fatal flaws in the design related to vehicle trafficking;
2. Determine how the expansion joint will fail under vehicle trafficking.

No seismic or structural testing was undertaken on the seismic expansion joint as part of this study and no recommendations toward its seismic or structural performance are made. Ride quality, skid resistance, and tire noise studies were carried out by Caltrans in a separate study and are reported on in separate Caltrans reports.

ACKNOWLEDGEMENTS

The University of California Pavement Research Center acknowledges the following individuals and organizations who contributed to the project:

- Dr. Joe Holland, Caltrans Division of Research and Innovation
- Mr. Jason Wilcox, Mr. Mike Whiteside, and Mr. Ric Maggenti, Caltrans Toll Bridge Program
- Mr. Hardik Patel and Mr. Charles Redfield, T.Y. Lin International Group
- The UCPRC Heavy Vehicle Simulator Crew under the leadership of Mr. Peter Millar

EXECUTIVE SUMMARY

A relatively unique opportunity was recently identified for accelerated traffic load testing of a new bridge expansion joint design not previously used in California. This study was part of the construction of the new East Span of the San Francisco–Oakland Bay Bridge and assessed whether the new expansion joints (which were designed to function in harmony with the bridge decks in the event of a high-magnitude earthquake) planned for linking the Self-anchored Span with the Transition and Skyway spans would withstand truck traffic loading. A test structure incorporating one of the full-scale joints was constructed close to the actual bridge and tested with the California Department of Transportation / University of California Pavement Research Center Heavy Vehicle Simulator in a series of phases.

A total of 1.36 million load repetitions, equating to about 46 million equivalent standard axle loads on a highway pavement, were applied in seven phases during the three-month test. On completion of this testing, no structural damage was recorded by any of the Linear Variable Differential Transducers (LVDTs) or strain gauges installed on the steel plates, steel frames, bolts, and washers. There was also no visible damage on any of these components. Excessive overloading with a 150 kN half-axle load (approximately four times the standard axle load) on an aircraft tire in the last phase of the test caused some damage to the Trelleborg unit in the joint. The damage included abrasion, tearing, shoving and permanent deformation of the rubber inserts, and deformation and shearing of one of the steel supports directly under the wheel load.

Although no vehicle suspension dynamics (i.e., vehicle bounce) or speed effects were considered, based on the results of this limited testing, it was concluded that the Caltrans seismic expansion joint would perform adequately under typical Bay Bridge traffic. The distresses observed on the Trelleborg unit under high loads in the last phase of testing are unlikely to occur under normal traffic. However, the Trelleborg unit was found to be the weakest point of the expansion joint, as expected. On the actual bridge structure, these units should be checked periodically to confirm the findings of this study, and to assess any effects of higher speeds and vehicle dynamics that were not identified. The joints will require periodic maintenance and replacement in line with manufacturer's specifications.

The findings from this study indicate that the Caltrans seismic expansion joint tested would be appropriate for typical Bay Bridge traffic.

No seismic or structural testing was undertaken and no recommendations toward the expansion joint's seismic or structural performance are made. Ride quality, skid resistance, and tire noise studies were carried out by Caltrans in a separate study and are reported on in separate Caltrans reports.

TABLE OF CONTENTS

LIST OF TABLES

LIST OF FIGURES

CONVERSION FACTORS

SI* (MODERN METRIC) CONVERSION FACTORS				
Symbol	**Convert From**	**Convert To**	**Symbol**	**Conversion**
LENGTH				
mm	millimeters	inches	in	mm x 0.039
m	meters	feet	ft	m x 3.28
km	kilometers	mile	mile	km x 1.609
AREA				
mm^2	square millimeters	square inches	in^2	mm^2 x 0.0016
m^2	square meters	square feet	ft^2	m^2 x 10.764
VOLUME				
m^3	cubic meters	cubic feet	ft^3	m^3 x 35.314
kg/m^3	kilograms/cubic meter	pounds/cubic feet	lb/ft^3	kg/m^3 x 0.062
L	liters	gallons	gal	L x 0.264
L/m^2	liters/square meter	gallons/square yard	gal/yd^2	L/m^2 x 0.221
MASS				
kg	kilograms	pounds	lb	kg x 2.202
TEMPERATURE (exact degrees)				
C	Celsius	Fahrenheit	F	°C x 1.8 + 32
FORCE and PRESSURE or STRESS				
N	newtons	poundforce	lbf	N x 0.225
kPa	kilopascals	poundforce/square inch	lbf/in^2	kPa x 0.145

*SI is the symbol for the International System of Units. Appropriate rounding should be made to comply with Section 4 of ASTM E380. (Revised March 2003)

1. INTRODUCTION

1.1 Background

The 13.5 km (8.4 mi.) San Francisco–Oakland Bay Bridge connects the city of San Francisco with the East Bay cities of Oakland, Emeryville and Berkeley and is the start point of the Interstate 80 (I-80) corridor. Based on data collected at the toll plaza, the bridge carries approximately 270,000 vehicles per day (compared to the 100,000 carried by the Golden Gate Bridge), of which about three percent is truck traffic. It currently consists of two separate bridges linked by a short tunnel on Yerba Buena Island. The existing East Span, a steel box girder design constructed in 1936, was damaged by the 7.1-magnitude Loma Prieta earthquake in 1989, during which a section of the top span, carrying the five westbound lanes, collapsed onto the lower eastbound lanes. Although repairs were made and the bridge reopened approximately one month after the earthquake, a complete seismic retrofit of the East Span to withstand future similar or more severe earthquakes was not considered viable and construction of a new bridge was approved. The West Span, which consists of two suspension bridge spans connected at a center anchorage, was easier to retrofit to accommodate higher magnitude earthquakes. Retrofit work on this part of the bridge was completed in 2004 and retrofit work on the West Approach was completed in 2009.

The new East Span consists of four separate parts (Figure 1.1):

- The Oakland Touchdown, linking the new bridge to the existing I-80 infrastructure.
- The Skyway, two side-by-side 1.9 km (1.2 mi.) long concrete spans (completed in 2008).
- The Self-anchored Suspension Span (SAS), two side-by-side 470 m (1,540 ft.) long spans supported by a single tower, which is still under construction. It will be the longest bridge of its kind in the world. The span's single 160 m (525 ft.) tall tower will match the height of the West Span's towers. Its placement closer to the west end of the structure creates a distinctive asymmetrical design, with the single 1.6 km (1.0 mi.) long main cable presenting a sharper angle on the west side and a more sloping appearance on the east.
- The Yerba Buena Island Transition Structure (YBITS), still under construction, will connect the Self-anchored Suspension Span to Yerba Buena Island (YBI), and will transition the new East Span's side-by-side road decks to the upper and lower decks of the Yerba Buena Island tunnel and West Span.

The three radically different structures also required a new expansion joint design to link the three main parts (Skyway, Self-anchored Suspension Span, and Yerba Buena Island Transition Structure) while integrating with the seismic functioning of the entire bridge system. This new expansion joint was subsequently designed by the California Department of Transportation (Caltrans) and T.Y. Lin International Group and incorporates a Trelleborg Transflex 2400 expansion joint, a steel connector plate,

and fastening systems. The main focus of the design was to ensure that the joint acted in harmony with the three structures during seismic activity. A secondary focus was the requirement that each lane incorporate separate joints, in order to facilitate maintenance without major disruption to traffic. During review of the joint design, questions were raised with regard to how the joints would perform under traffic loading, given the focus on their seismic and maintenance requirements. An accelerated loading test, using the California Department of Transportation / University of California Pavement Research Center Heavy Vehicle Simulator (HVS) was therefore undertaken to provide a quick indication of how the joint would perform under truck traffic.

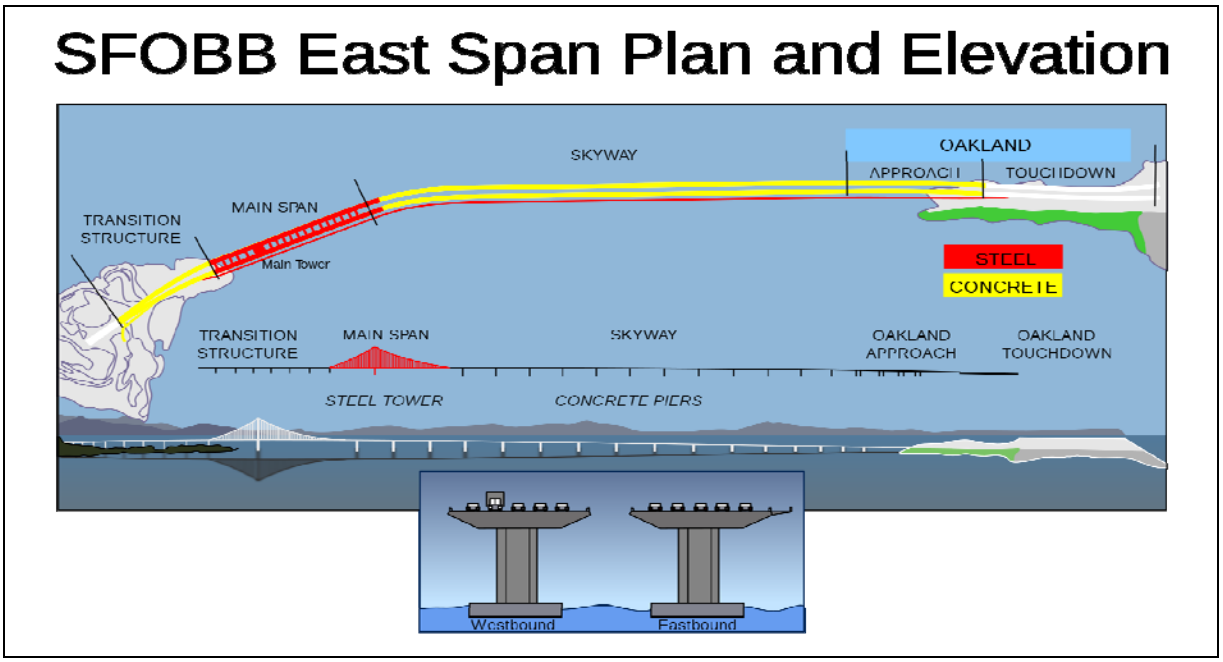

Figure 1.1: Schematic of the new East Span of the San Francisco–Oakland Bay Bridge.

(http://en.wikipedia.org/wiki/File:SFOBBEastSpan.svg)

1.2 Project Objectives

The research presented in this report is part of Partnered Pavement Research Center Strategic Plan Element 3.16 (PPRC SPE 3.16), titled "Bay Bridge Expansion Joint Testing Study," undertaken for the California Department of Transportation (Caltrans) by the University of California Pavement Research Center (UCPRC). The objective of this project was to provide a rapid indication of whether the expansion joint would perform adequately under typical Bay Bridge vehicle loading. This was achieved through the following tasks:

- Identify any fatal flaws in the seismic expansion joint design related to vehicle trafficking
- Determine how the seismic expansion joint will fail under vehicle trafficking

No seismic or structural testing was undertaken on the seismic expansion joint as part of this study, and no recommendations toward its seismic or structural performance are made. Ride quality, skid resistance, and tire noise studies were carried out by Caltrans in a separate study and are reported on in separate Caltrans reports.

1.3 Literature Review

A review of the literature found no published reference to any similar studies where equipment used for accelerated pavement testing was used to test bridge expansion joints.

1.4 Structure and Content of this Report

This report presents an overview of the work carried out to meet the objectives of the study, and is organized as follows:

- Chapter 2 summarizes the HVS test structure location, design, and construction.
- Chapter 3 details the HVS test plan, test section layout, instrumentation plan, and HVS test criteria.
- Chapter 4 provides a summary of the HVS test data collected.
- Chapter 5 provides conclusions from the study.

1.5 Measurement Units

Although Caltrans has recently returned to the use of U.S. standard measurement units, metric units have always been used by the UCPRC in the design and layout of HVS test tracks, and for laboratory and field measurements and data storage, to facilitate comparisons of data between accelerated pavement testing studies worldwide. In this report, metric and English units (provided in parentheses after the metric units) are provided in general discussion. In keeping with convention, only metric units are used in HVS data analyses and reporting. A conversion table is provided on Page xiii at the beginning of this report.

2. TEST STRUCTURE LOCATION, DESIGN, AND CONSTRUCTION

2.1 Test Structure Location

The HVS test site was located on a temporarily vacant area close to the bridge construction offices at the Port of Oakland, California (Figure 2.1 through Figure 2.3).

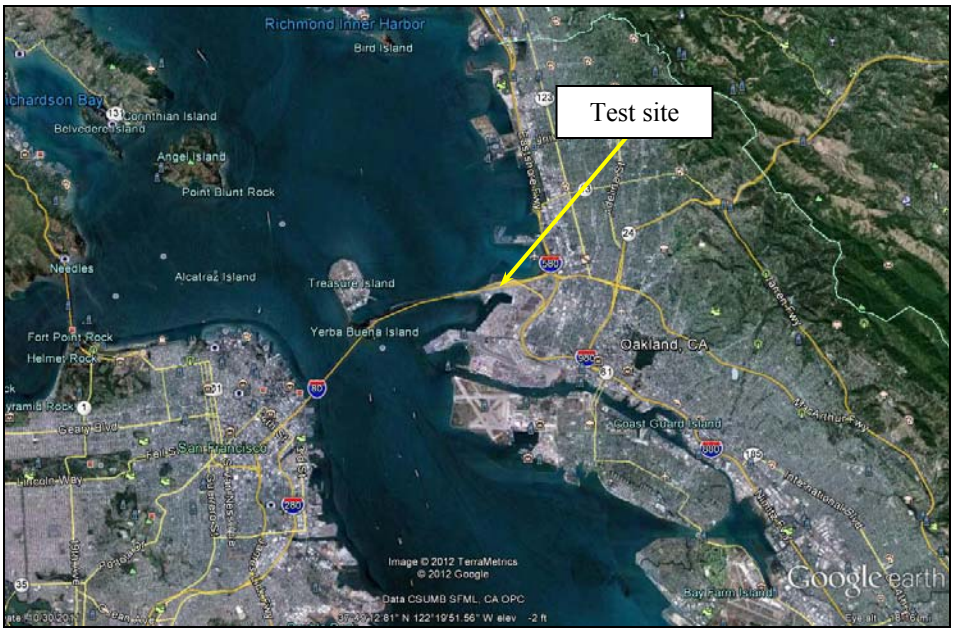

Figure 2.1: Location of HVS test site (regional perspective).

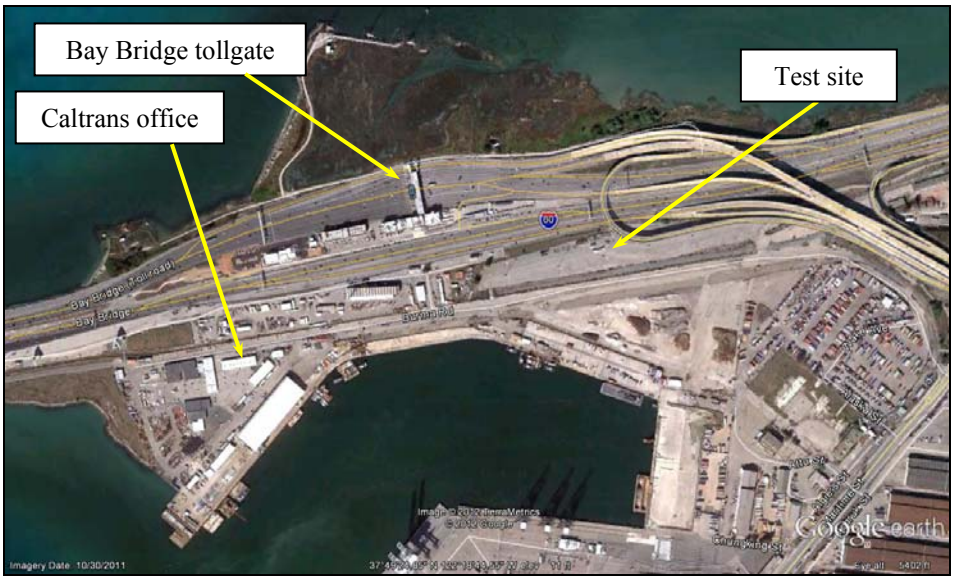

Figure 2.2: Location of HVS test site (local perspective).

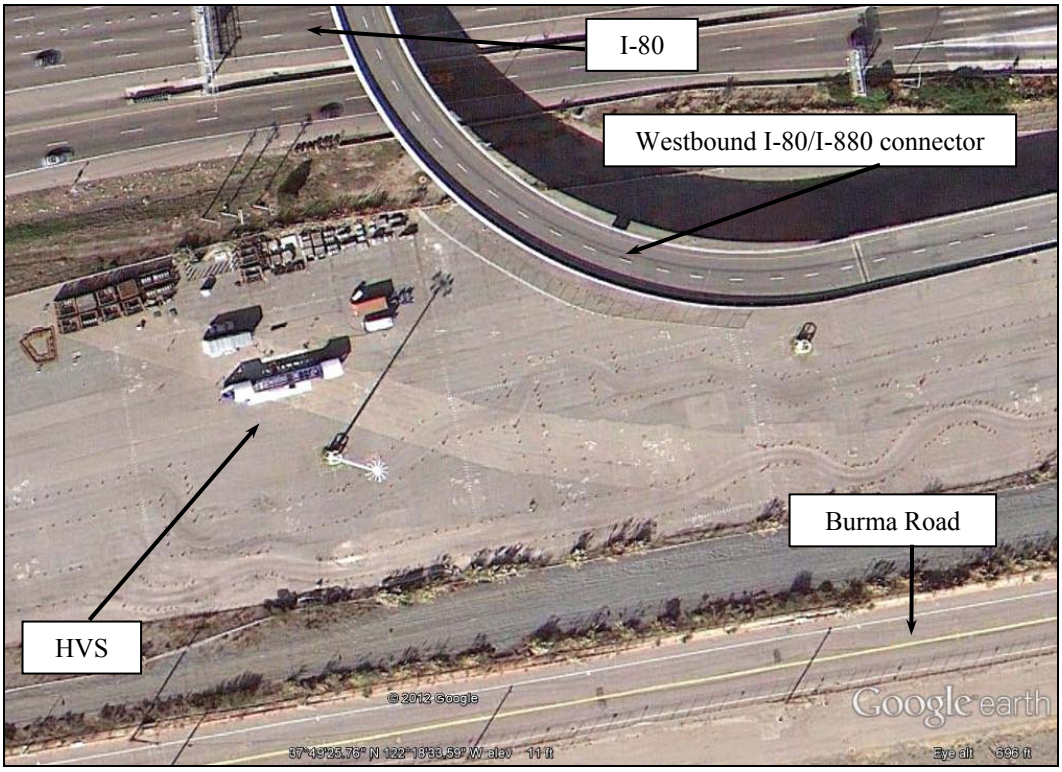

Figure 2.3: Location of HVS test site (site perspective).

2.2 Test Structure Design

The Caltrans seismic expansion joint was designed by T.Y. Lin International Group, who also assisted Caltrans with the design of a structure to house the joint for the accelerated load testing discussed in this report. A copy of the design is provided in Appendix A. The dimensions matched those on the actual bridge. Reinforced concrete approach slabs for the HVS wheels were included in the design.

2.3 Test Structure Construction

The test structure was built by Caltrans. Construction was started in March 2011, and completed in July 2011. Photographs of the construction are provided in Figure 2.4 through Figure 2.9. Problems were encountered with the concrete pour around the channel assembly structure (Figure 2.10), but this was repaired prior to installation of the instruments and the start of testing (Figure 2.11). However, this problem resulted in a gap between the steel plate and the channel assembly on the west side of the structure (Figure 2.11). This gap could not be repaired without dismantling and reconstruction, which prevented testing on this edge of the steel plate, since loading would have led to unrealistic responses being recorded. The completed project with the HVS in place is shown in Figure 2.12.

Figure 2.4: Initial excavation.

Figure 2.5: Formwork for test structure.

Figure 2.6: Trelleborg installation.

Figure 2.7: Steel plate installation.

Figure 2.8: Completed steel plate installation.

Figure 2.9: Completed structure.

Figure 2.10: Concrete pour problem on channel assembly structure.

(Concrete was repaired prior to HVS testing.)

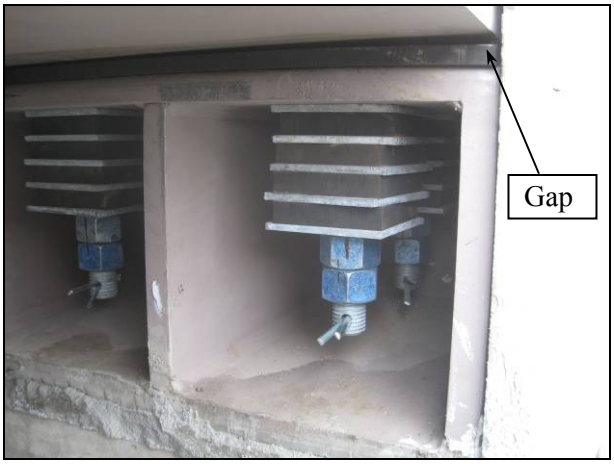

Figure 2.11: Gap between steel plate and channel assembly (note concrete repair).

Figure 2.12: HVS on test structure prior to start of testing.

3. HVS TEST PLAN, INSTRUMENTATION, AND TEST CRITERIA

3.1 HVS Test Protocols

Heavy Vehicle Simulator (HVS) test section layout, test setup, trafficking, and measurements followed standard University of California Pavement Research Center (UCPRC) protocols *(1)*.

3.2 Test Plan

Two main tasks were identified for this accelerated load study:

- Identify any fatal flaws in the seismic expansion joint design related to vehicle trafficking
- Determine how the seismic expansion joint will fail under vehicle trafficking

A review of the literature found no published reference to any similar studies and given a testing period limitation of three months, best use of this time was taken into consideration in preparing a test plan to meet the study objectives. A phased approach was followed, starting with normal truck loads in the center of the joint to identify any fatal flaws (Task 1), followed by incremental changes in loading and wheel position to determine how the joint was likely to fail (Task 2). A test plan summary is provided in Table 3.1.

Table 3.1: HVS Test Plan Summary

Phase No.	Test Section Location	Duration (days)	Wheel Loads (kN)	Repetitions Applied
1.1	Center	30	1 day at 25, then 29 days at 40	518,000
1.2	Center	6	1 day each at 25, 40, 60, 80, and 100, then back to 40	120,000
1.3	Center + Edge	7	1 day each at 40, 100, and 80, then 4 days at 60	120,000
2.1	Edge	11	2 days at 40, 1 day each at 60, 80 and 100, then 6 days at 80	189,000
3.1	Edge	3	60, with impact load*	23,000
3.2	Edge	15	5 days each at 60, 80, and 100, all with impact load	240,000
3.3	Edge	15	1 day at 100, then 14 days at 150	150,000
-	-	3	No test days	0
Total	-	90	-	1,360,000

Test Section Numbering	
Phase No	**Test Section No**
1.1	640HC
1.2	640HC
1.3	640HC-A
2.1	640HC-B
3.1	640HC-C
3.2	640HC-D
3.3	640HC-E

* Impact load was applied by forcing the HVS wheel over a step in the wheelpath created by either a 13 mm (1/2 in.) neoprene pad or 19 mm (3/4 in.) hardwood board.

In the first phase (Phase 1.1), testing at standard wheel loads in a channelized trafficking mode for four weeks (i.e., equivalent to an 80 kN [18,000 lb] axle load) was included to identify any potential major

flaws in the design. The following phases would then evaluate the joint response under wandering traffic, increasing wheel load, and different wheelpath (specifically along the edge of the joint). Assuming that no damage was caused in the first two phases, the final phase would investigate impact loads and very high wheel loads and tire pressures with a view to identifying the weakest point of the design.

Load variations on a single day were included in the study to establish relationships between wheel load and structural response, and to identify any nonlinearity that might lead to structural damage.

3.3 Instrumentation Plan and Test Section Layout

The expansion joint was comprehensively instrumented to monitor status and responses under HVS trafficking. Parameters monitored included ambient and steel plate temperatures, vertical deflections at various locations, and longitudinal strain at the bottom of the steel plate. The instruments used and their location on the bridge deck expansion joint are listed in Table 3.2. Layouts of the instrumentation for testing on the center and edge of the joint are shown in Figure 3.1 and Figure 3.2, respectively. Instruments #1 through #9 and Instrument #13 are Linear Variable Differential Transducers (LVDTs), Instruments #10 through #12 are strain gauges, and Instruments #14 through #18 are thermocouples. Location of LVDTs and strain gauges are also on the design drawings in Appendix A.

Standard HVS test sections were used for all testing. These are 8.0 m by 0.6 m (26.3 ft. by 2.0 ft.) for channelized loading and 8.0 m by 1.0 m (26.3 ft. by 3.3 ft.) for loading with wheel wander.

Permanent deformation of the Trelleborg unit was measured with a laser profilometer. Figure 3.3 shows the relative HVS wheel positions and location of profilometer measurements for the different testing configurations. Stations 1 through 6 were inside the HVS wheelpath at some point during each phase while Station 7 and Station 8 were outside the wheelpath at all times for all phases. Station 8 was approximately 300 mm (12 in.) from the edge of the wheelpath and consequently no permanent deformation should have been measured at this location. All surface profiles were measured in a longitudinal direction (i.e., the trafficking direction) at 200 mm intervals in the transverse direction (Figure 3.4). Daily change in surface elevation of the Trelleborg ribs was calculated by subtracting the initial surface elevation from the deformed surface elevation.

Data from all instruments except the profilometer were collected continuously throughout the test. Profilometer measurements were taken once a day while the HVS was stopped.

Photographs of the various instruments are shown in Figure 3.5 through Figure 3.13.

Table 3.2: List of Instrumentation

Instrument Number	Type	Label	Quantity Measured	Location
1	LVDT	LVDT#1	Vertical Deflection	On head of Bolt A5 for Phases 1.1 and 1.2, removed for Phase 1.3. On head of Bolt A3 for Phases 2 and 3.
2	LVDT	LVDT#2	Vertical Deflection	On head of Bolt B5 for Phases 1.1 and 1.2, removed for Phase 1.3. On head of Bolt B3 for Phases 2 and 3.
3	LVDT	LVDT#3	Vertical Deflection	Bottom washer under Bolt A4
4	LVDT	LVDT#4	Vertical Deflection	Bottom washer under Bolt B4
5	LVDT	LVDT#5	Vertical Deflection	Top of steel plate at outside edge
6	LVDT	LVDT#6	Vertical Deflection	Top of steel plate at inside edge for Phases 1.1 and 1.2, removed for Phase 1.3. Bottom of steel plate in the same horizontal location for Phases 2 and 3.
7	LVDT	LVDT#7	Vertical Deflection	Bottom of steel plate at midwidth
8	LVDT	LVDT#8	Vertical Deflection	On head of bolt at the connection between steel plate and Trelleborg; on head of Bolt 2 for Phases 1.1, 1.2, and 1.3; on head of Bolt 4 for Phases 2 and 3.
9	LVDT	LVDT#9	Vertical Deflection	On head of bolt at the connection between steel plate and Trelleborg; on head of Bolt 6 for Phases 1.1 and 1.2; removed for remaining phases.
10	Strain Gauge	SG#10	Longitudinal Strain	Bottom of steel plate at outside edge
11	Strain Gauge	SG#11	Longitudinal Strain	Bottom of steel plate at midwidth
12	Strain Gauge	SG#12	Longitudinal Strain	Bottom of steel plate at inside edge
13	LVDT	LVDT#13	Vertical Deflection	Bottom of steel plate at midwidth and midspan of the tunnel
14	Thermocouple	TC-SG#10	Temperature	Bottom of steel plate next to SG#10
15	Thermocouple	TC-SG#11	Temperature	Bottom of steel plate next to SG#11
16	Thermocouple	TC-SG#12	Temperature	Bottom of steel plate next to SG#12
17	Thermocouple	TC-SG#10-S	Temperature	Surface of steel plate on top of SG#10
18	Thermocouple	TC-Ambient	Temperature	Ambient air temperature next to steel plate

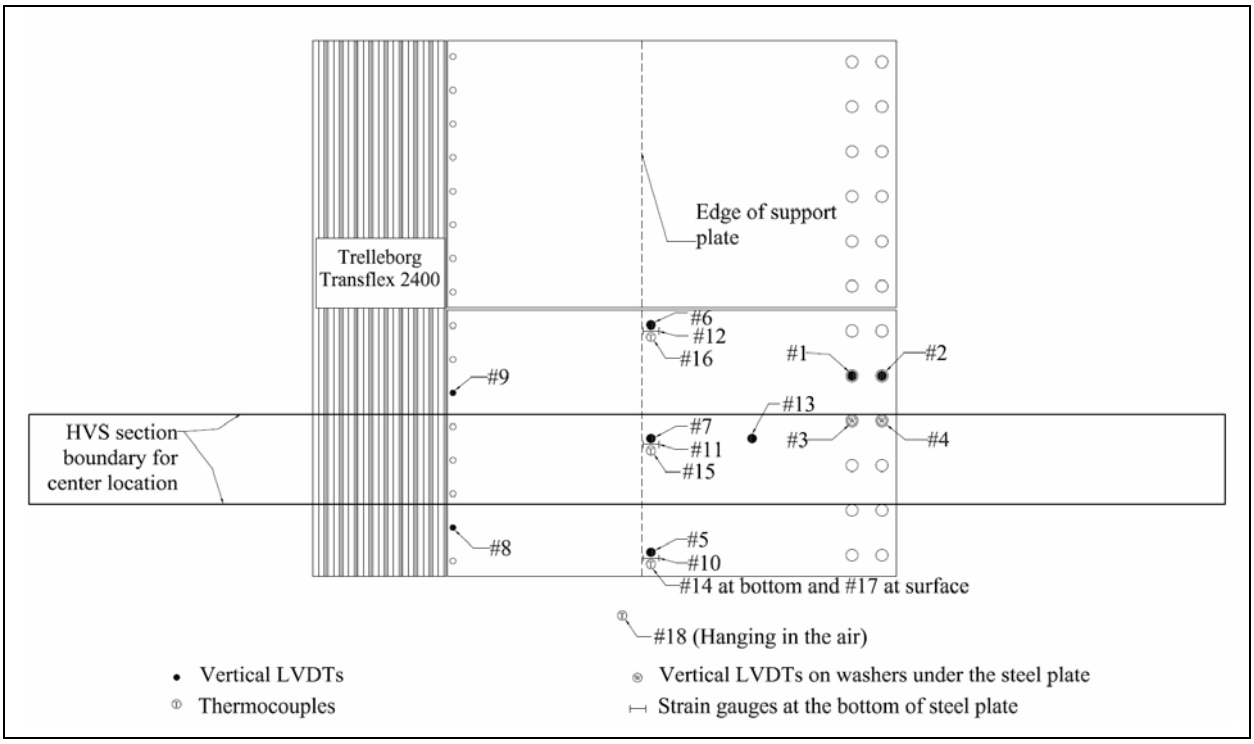

Figure 3.1: Layout of instrumentation for testing on the center of the expansion joint.

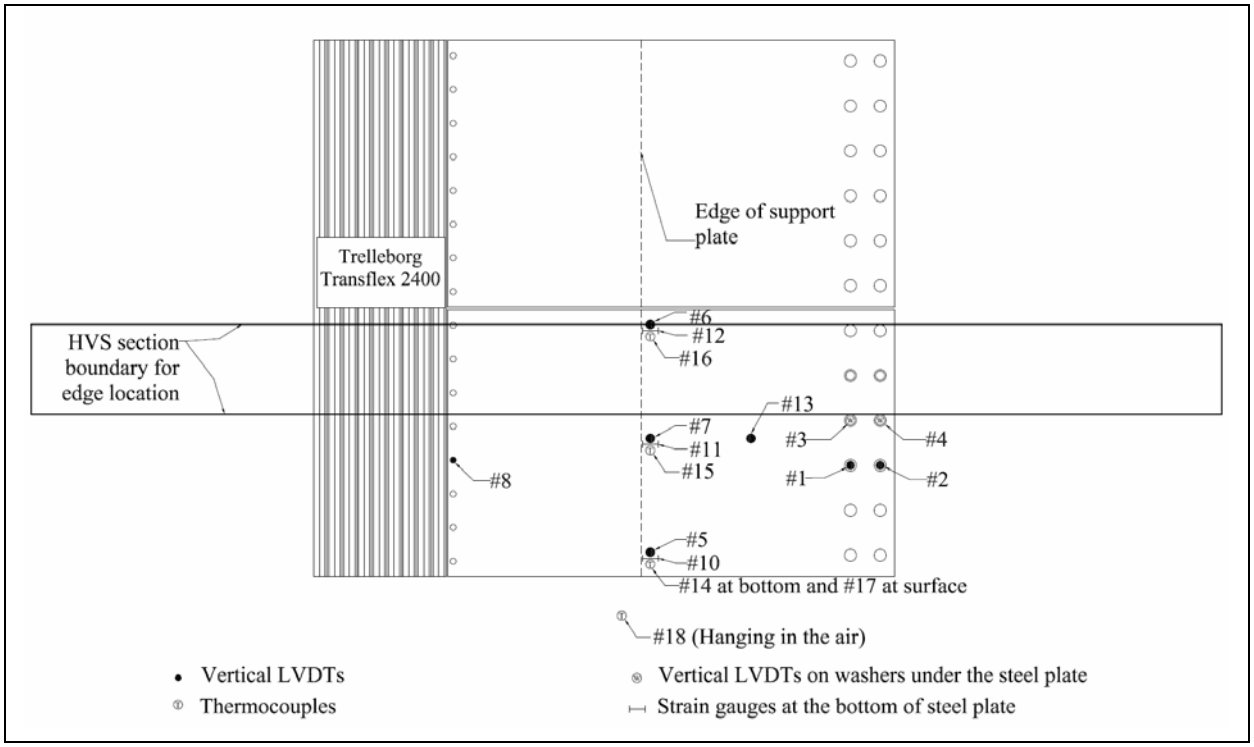

Figure 3.2: Layout of instrumentation for testing on the edge of the expansion joint.

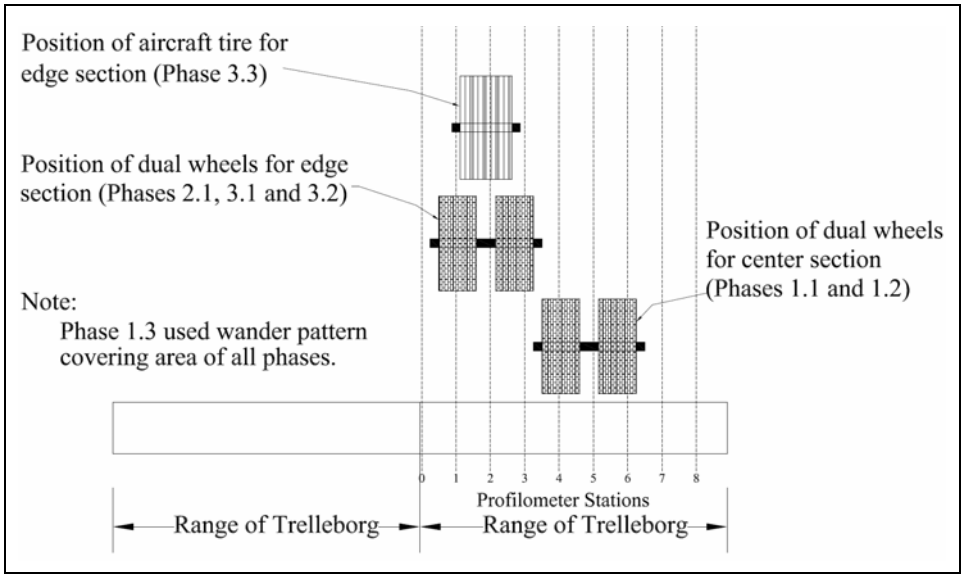

Figure 3.3: Relative location of HVS wheels for phases with channelized traffic.

Figure 3.4: Laser profilometer recording surface profile of the Trelleborg unit.

Figure 3.5: General view of instruments on top of structure.

Figure 3.6: LVDTs on channel assembly bolts.

(Instruments #1 and #2)

Figure 3.7: LVDTs on edge of steel plate.

(Instrument #5)

Figure 3.8: LVDTs on edge of steel plate.

(Instrument #6)

Figure 3.9: LVDTs on Trelleborg unit.

(Instruments #8 and #9)

Figure 3.10: General view of instruments underneath steel plate.

Figure 3.11: LVDT on bottom of steel plate.

(Instrument #13)

Figure 3.12: LVDT, strain gauge, and thermocouple on midpoint under steel plate.

(Instruments #7, #11, and #15)

Figure 3.13: LVDTs on channel assembly bolt washers.

(Instruments #3 and #4)

3.4 Visual Assessments

Visual assessments of the Trelleborg unit, steel plate, channel assembly, bolts, and instruments were undertaken on an hourly basis. Bolts and washers in the channel assembly were marked prior to the start of testing and were checked for rotation on a daily basis.

3.5 HVS Test Criteria

3.5.1 Test Section Failure Criteria

No failure criteria were set for this study. Instead, all instrument data and profile measurements were reviewed on a daily basis throughout the study and any unexpected distress/deformation/deflection discussed with the design consultant.

3.5.2 Environmental Conditions

All testing was carried out under ambient conditions. Temperatures are summarized in Chapter 4.

3.5.3 Loading Program

The HVS loading program for each section is summarized in Table 3.3. Wheel loads applied are half axle (i.e., the load applied by a 40 kN [9,000 lb] half axle is the same as that applied by an 80 kN [18,000 lb] full-axle). Equivalent Standard Axle Loads (ESALs) were determined using the following Caltrans pavement design conversion (Equation 3.1):

$$ESALs = (\text{full axle load}/80\ kN)^{4.2} \quad \textbf{(3.1)}$$

Most trafficking was applied in a channelized, bidirectional mode using dual wheel truck tires (Goodyear G159 - 11R22.5- steel belt radial inflated to 720 kPa [104 psi]) with these exceptions:

- Phase 1.3, which assessed the effects of bidirectional traffic wander using the dual tires (Figure 3.14),
- Phase 3.1, which assessed the effects of an impact load in a unidirectional mode, and
- Phase 3.3, which assessed the effects of very high bidirectional loads using an aircraft tire (Boeing 737, Figure 3.15) inflated to 1,380 kPa (200 psi).

Load was checked with a portable weigh-in-motion pad at the beginning of each test (Figure 3.14) and after each load change.

All testing was carried out at a wheel speed of 9.5 km/h (5.9 mph).

Table 3.3: Summary of HVS Loading Program

Phase No.	Wheel Load		Repetitions Applied	ESALs*
	kN	lbs		
1.1	25	5,625	20,000	3,000
	40	9,000	498,000	498,000
1.2	25	5,625	20,000	3,000
	40	9,000	20,000	20,000
	60	13,500	20,000	110,000
	80	18,000	20,000	368,000
	100	22,500	20,000	938,000
	40	9,000	20,000	20,000
1.3	40	9,000	20,000	20,000
	100	22,500	20,000	938,000
	80	18,000	20,000	368,000
	60	13,500	60,000	329,000
2.1	40	9,000	36,000	36,000
	60	13,500	20,000	110,000
	80	18,000	20,000	368,000
	100	22,500	19,000	891,000
	80	18,000	94,000	1,728,000
3.1	60	13,500	23,000	126,000
3.2	60	13,500	91,000	500,000
	80	18,000	69,000	1,268,000
	100	22,500	80,000	3,754,000
3.3	100	22,500	20,000	938,000
	150	33,750	130,000	33,489,000
Total			1,360,000	46,821,000
* Equivalent Standard Axle Load using Caltrans pavement design formula				

Figure 3.14: Dual truck tire configuration (note load calibration pad).

Figure 3.15: Aircraft tire (Boeing 737) configuration.

4. HVS TEST DATA

4.1 Introduction

This chapter summarizes the data collected during the different phases of accelerated pavement testing. Each phase is covered separately and includes discussion on temperature (measured with thermocouples at various locations on and next to the test structure), vertical deflection (measured with LVDTs), longitudinal strain (measured with strain gauges), visual observations, and a phase summary. Static response and permanent deformation (measured with a laser profilometer) for all phases are discussed in separate sections. Where appropriate, data plots are presented on the same scale for all phases to facilitate comparisons.

4.2 Phase 1.1: Fatal Flaw Assessment

4.2.1 Introduction

The main tasks of this phase were identification of any major flaws in the seismic expansion joint design, and evaluation of the strain and deflections caused by a small increase in wheel load. The test ran for 30 days. Test load on the first day was set at 25 kN (5,625 lbs) and thereafter at 40 kN (9,000 lbs). All loading was applied to the center of the expansion joint in a bidirectional channelized mode.

4.2.2 Temperature

The average (daily, minimum, and maximum), lowest, and highest temperatures measured during Phase 1.1 are summarized in Table 4.1. Daily average temperatures are plotted in Figure 4.1, with error bars indicating minimum and maximum temperatures for the thermocouple located next to Strain Gauge #11 (TC-SG#11). Average ambient temperatures were typical for the area and had a relatively small diurnal range. Average daily maximum temperatures recorded on the steel plate were considerably higher than the ambient temperatures (4°C to 6°C [7°F to 11°F]), but average daily minimum temperatures were only slightly higher. This was attributed to heat absorption by the steel. There was some difference between the temperatures recorded at the different strain gauges, with variation attributed to partial shading or different/restricted air flow movements, especially for those thermocouples underneath the structure. No extreme temperature events were recorded. It is unlikely that temperature had any significant influence on the way that the bridge deck expansion joint components functioned during this phase of testing.

Table 4.1: Phase 1.1: Temperature Summary

Thermocouple	Temperature (°C)				
	Average of Daily Average	Average of Daily Minimum	Average of Daily Maximum	Lowest	Highest
Ambient	18	15	22	15	26
TC-SG#10	21	17	27	16	33
TC-SG#10-S	20	17	27	16	33
TC-SG#11	21	17	26	16	31
TC-SG#12	21	17	28	16	33
Thermocouple	**Temperature (°F)**				
Ambient	64	59	72	58	79
TC-SG#10	69	63	81	61	91
TC-SG#10-S	69	62	81	60	92
TC-SG#11	69	63	79	61	87
TC-SG#12	71	63	83	61	91

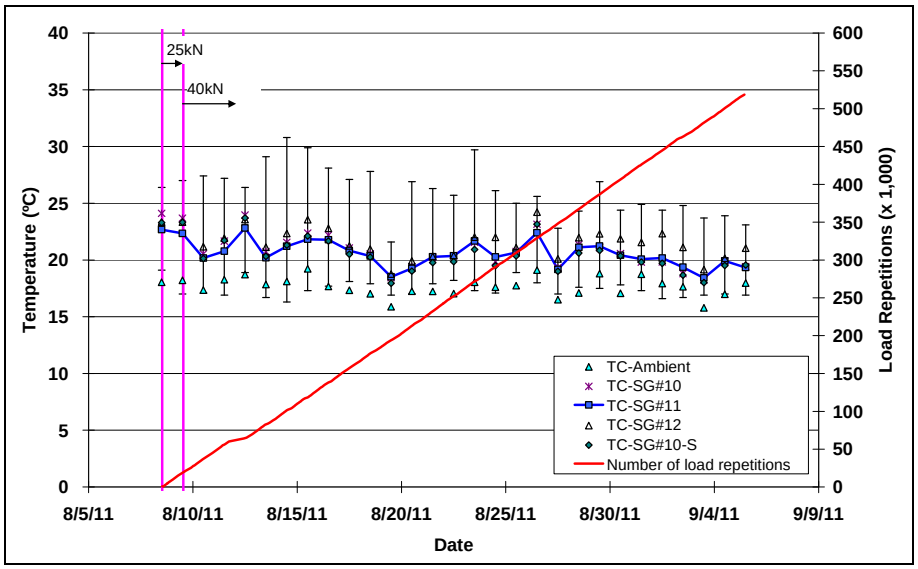

Figure 4.1: Phase 1.1: Daily average temperatures and HVS testing schedule.

4.2.3 Vertical Deflection

Influence lines (or deflection bowls) from a single pass of the 40 kN wheel load for the LVDTs on the bolts, washers, and steel plate are shown in Figure 4.2 through Figure 4.4, respectively. Vertical deflections on the bolts and washers were very small (between zero and 0.05 mm) with deflection increasing with proximity to the load wheels, as expected. Deflections measured on the washers were slightly higher than those measured on the bolts. Deflections on the steel plate were higher than those on the bolts and washers and ranged between 0.6 mm and 0.9 mm depending on location, with highest deflections on the midpoints of edges of the steel plate and the midpoint of the steel plate.

Plots of the peak deflections measured on bolts, washers, and the steel plate for the duration of the phase are shown in Figure 4.5 through Figure 4.7. Deflections increased with the change in wheel load as expected. Thereafter, deflections recorded by each of the LVDTs remained constant, with no evidence of damage accumulation with increasing load repetitions. Deflection did not appear to be influenced by temperature, with variation attributed to slight variation in the actual load applied, which was always well within the acceptable range for the hydraulic loading system on the HVS.

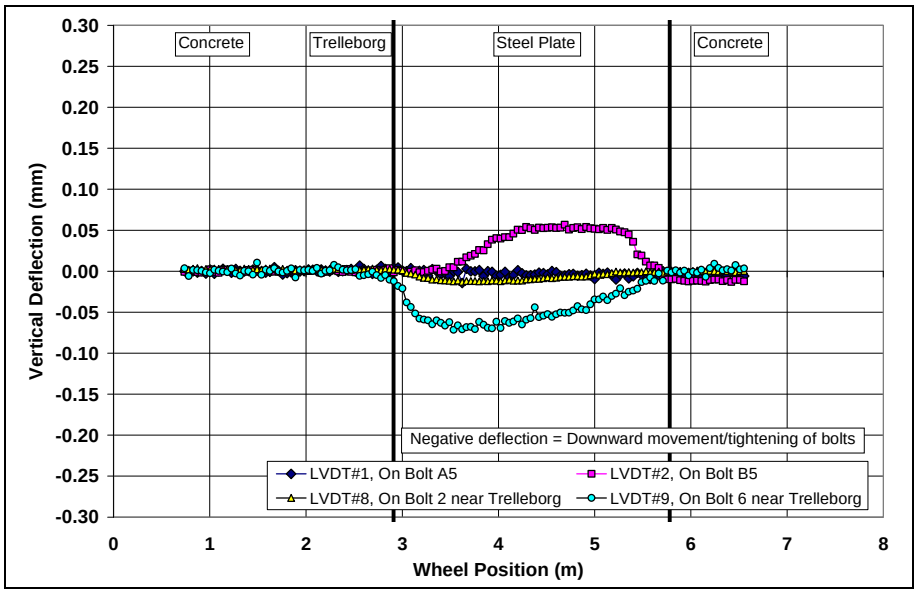

Figure 4.2: Phase 1.1: Influence lines of vertical deflection for LVDTs on bolts.

(Repetition #500,000, wheel load at 40 kN)

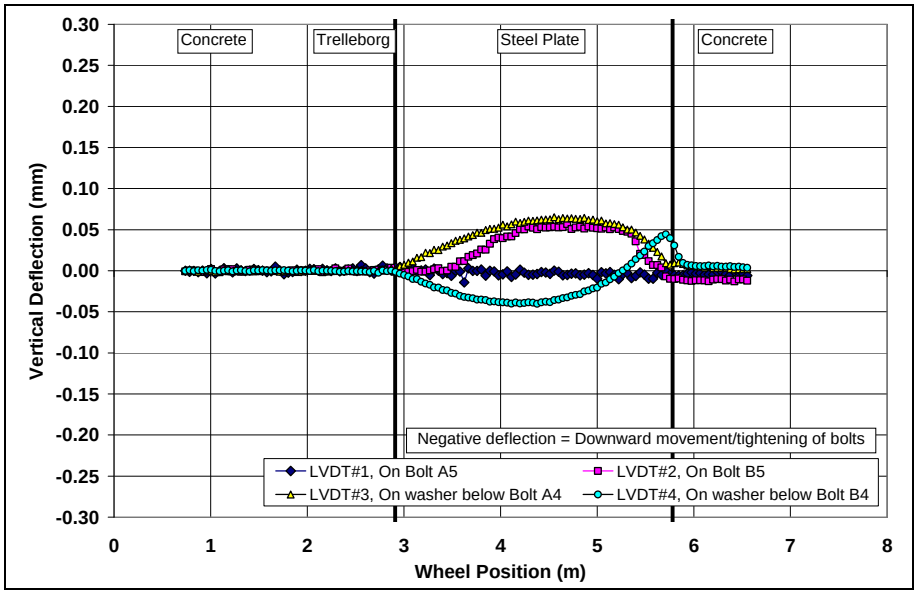

Figure 4.3: Phase 1.1: Influence lines of vertical deflection for LVDTs on bolts and washers.

(Repetition #500,000, wheel load at 40 kN)

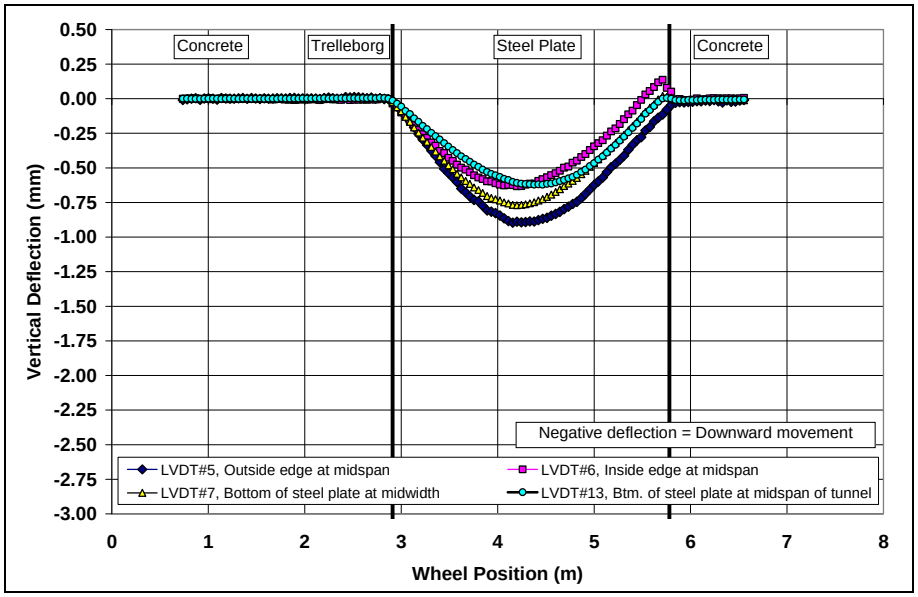

Figure 4.4: Phase 1.1: Influence lines of vertical deflection for LVDTs on steel plate.

(Repetition #500,000, wheel load at 40 kN)

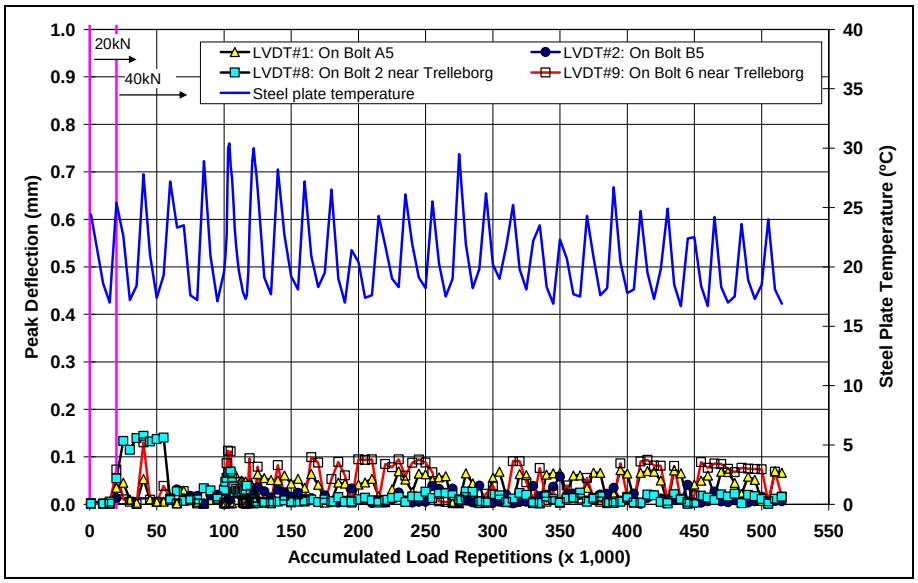

Figure 4.5: Phase 1.1: History of peak deflections on bolts.

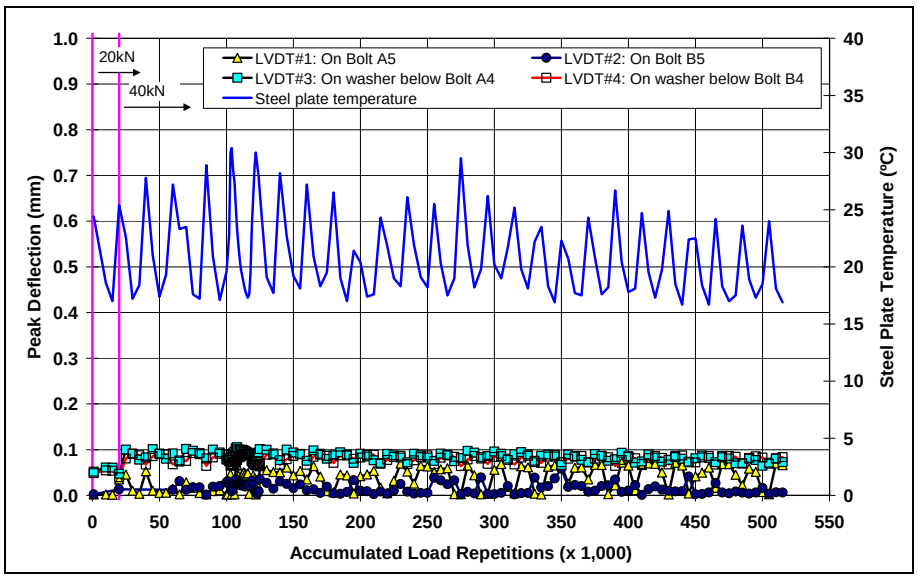

Figure 4.6: Phase 1.1: History of peak deflections on bolts and washers.

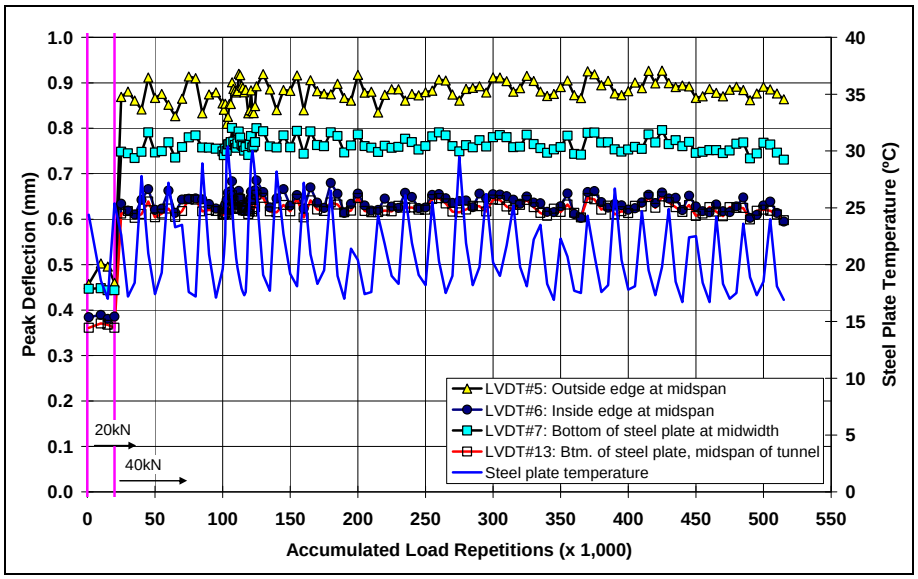

Figure 4.7: Phase 1.1: History of peak deflections on steel plate.

4.2.4 Longitudinal Strain

Influence lines (or strain bowls) from a single pass of the 40 kN wheel load (repetition #500,000) for the strain gauges at the midpoints of the inside and outside edge and midpoint of the steel plate are shown in Figure 4.8. Strains were very similar and ranged between 40 and 60 microstrain, with highest strain recorded at the midpoint of the steel plate.

A plot of the peak strains for the three strain gauges for the duration of the phase is shown in Figure 4.9. Peak strain increased with the change in wheel load as expected. After the load change, peak strain recorded by each of the gauges remained constant, with no evidence of damage accumulation with increasing load repetitions. There was no correlation between temperature and elastic response, although some very small daily variation (~3 με to 5 με) between early morning and early afternoon was observed in the plots.

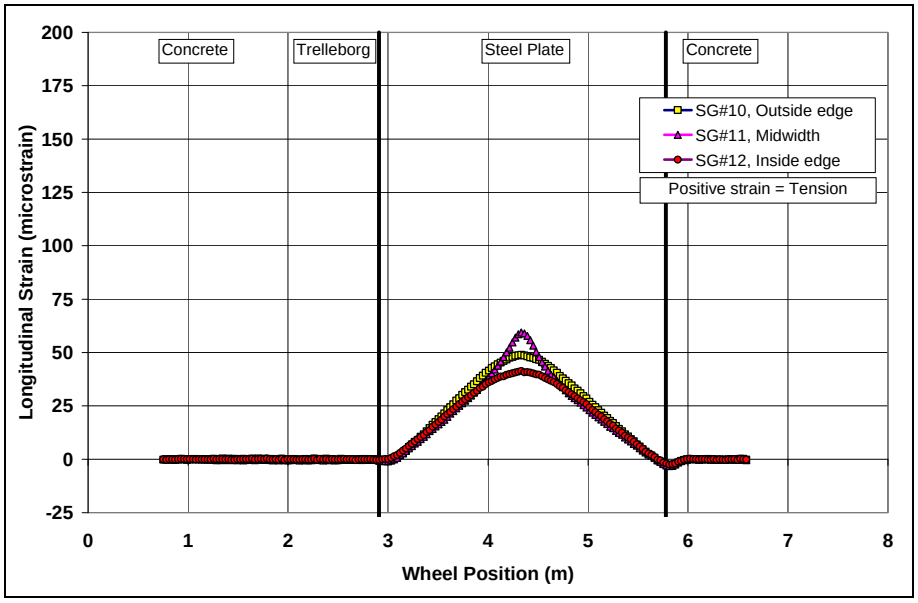

Figure 4.8: Phase 1.1: Influence lines of longitudinal strain at bottom of steel plate.

(Repetition #500,000, wheel load at 40 kN)

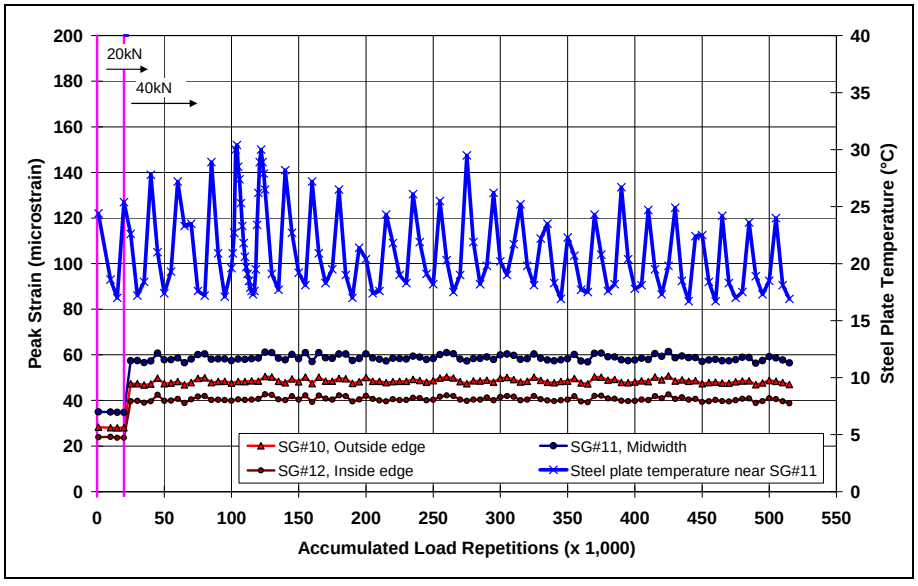

Figure 4.9: Phase 1.1: History of peak longitudinal strains at bottom of steel plate.

4.2.5 Visual Damage

No visual damage was observed on the concrete structure, steel plate, bolts, or washers. However, some wear, in the form of tire abrasion on the rubber sections, was observed on the Trelleborg unit after about 100,000 load repetitions. Small rubber particles started to accumulate on the steel ribs and in the bolt recesses (Figure 4.10). Apart from some slight deformation (< 2.0 mm) on the rubber in the wheelpaths, no other damage was observed on the Trelleborg unit. No rotation of the bolts or washers was observed.

Figure 4.10: Phase 1.1: Rubber abrasion on Trelleborg unit after 100,000 load repetitions.

4.2.6 Phase Summary

No apparent damage was observed at the end of Phase 1.1. The permanent vertical settlement of the structure after testing was 0.2 mm, which was considered minimal and unlikely to influence joint performance. No permanent deformation in the steel plate occurred during this phase, based on the strain data recorded. Deflections and longitudinal strains induced by the 80 kN standard axle load (40 kN half axle) at midspan of the steel plate were approximately 0.9 mm and 60 microstrain, respectively, and remained constant throughout the phase (i.e., deflections and strains did not increase with increasing load repetitions). The vertical deflections at the bolts and washers were less than 0.1 mm, with washers deflecting a little more than the bolts. There was no distinct correlation between temperature and elastic response in the steel plate; however, very small changes in peak strain between the coldest and warmest periods each day were observed on the data plots on most days. Minor fluctuations in strain and deflection measurements were most likely caused by very small fluctuations in the actual load applied by the HVS. No fatal flaws in the expansion joint design were identified.

4.3 Phase 1.2: Load Response on the Center of the Steel Plate

4.3.1 Introduction

Phase 1.2 assessed load response on the center of the steel plate by evaluating changes in strain and deflection induced by increases in wheel load. The test ran for six days, with a load increase each day for the first five days. Loads applied were 25 kN, 40 kN, 60 kN, 80 kN, and 100 kN, respectively. On the sixth day, the load was changed back to 40 kN to assess recovery after the very high loads. All loading was applied to the center of the expansion joint in a bidirectional channelized mode.

4.3.2 Temperature

The average (daily, minimum, and maximum), lowest, and highest temperatures measured during Phase 1.2 are summarized in Table 4.2. Daily average temperatures are plotted in Figure 4.11, with error bars indicating minimum and maximum temperatures for the thermocouple located next to Strain Gauge #11 (TC-SG#11). Average ambient temperatures were again typical for the area and had a relatively small diurnal range. Average daily minimum and maximum temperatures recorded on the steel plate were similar to the ambient temperatures, except for the thermocouple at Strain Gauge #12, which indicated a higher average daily maximum than the other measurement points (4°C [7°F]). This was attributed to different/restricted air flow movements around the thermocouple (positioned underneath the structure, furthest away from the opening). No extreme temperature events were recorded. It is unlikely that temperature had any significant influence on the way that the bridge deck expansion joint components functioned during this phase of testing.

Table 4.2: Phase 1.2: Temperature Summary

Thermocouple	Temperature (°C)				
	Average of Daily Average	Average of Daily Minimum	Average of Daily Maximum	Lowest	Highest
Ambient	18	15	22	14	27
TC-SG#10	19	17	23	15	26
TC-SG#10-S	19	16	23	15	27
TC-SG#11	20	17	23	16	26
TC-SG#12	21	17	27	16	35
Thermocouple	**Temperature (°F)**				
Ambient	64	59	71	56	81
TC-SG#10	66	62	74	59	80
TC-SG#10-S	66	62	74	58	81
TC-SG#11	67	63	74	60	79
TC-SG#12	69	63	81	60	95

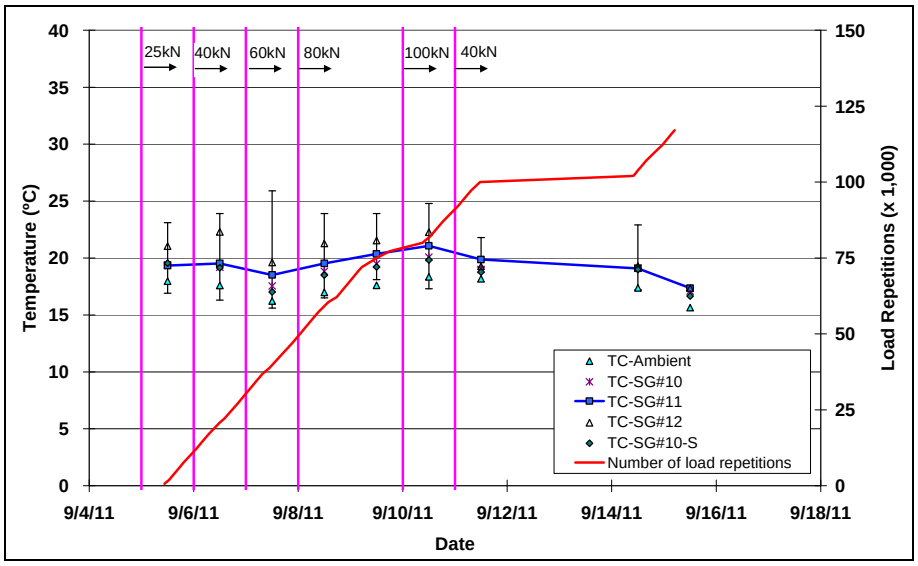

Figure 4.11: Phase 1.2: Daily average temperatures and HVS testing schedule.

4.3.3 Vertical Deflection

Plots of the peak deflections measured on bolts, washers, and the steel plate for the duration of Phase 1.2 are shown in Figure 4.12 through Figure 4.14. Deflections increased with the change in wheel load as expected, but were still very small, with deflection on the bolts, washers, and steel plate ranging between zero and 0.25 mm, zero and 0.15 mm, and 0.4 mm and 2.2 mm, respectively depending on load and sensor location. The relationship between peak deflection and load was linear for loads between 20 kN and 80 kN, but showed marginal non-linearity for the 100 kN load (example for LVDT #5 in Figure 4.15). The reason for this was not investigated given the very small difference and that the bridge deck expansion joints would not be subjected to loads of this magnitude. After each load change, deflections recorded by each of the LVDTs remained constant until the next load change. There was no evidence of damage accumulation with increasing load repetitions. Deflections recorded during the 40 kN loading on the second and sixth days were essentially the same (0.01 mm lower on the sixth day), indicating that no permanent damage was caused by the very high wheel loads. Daily temperature change appeared to result in very small daily variations in deflection (<0.01 mm on the bolts and washers and 0.1 mm on the steel plate), especially at the lower loads.

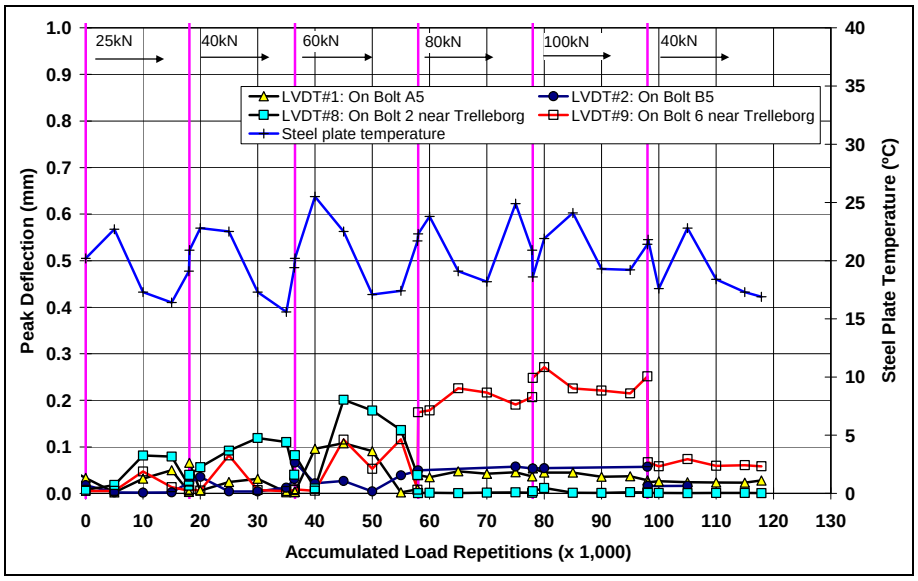

Figure 4.12: Phase 1.2: History of peak deflections on bolts.

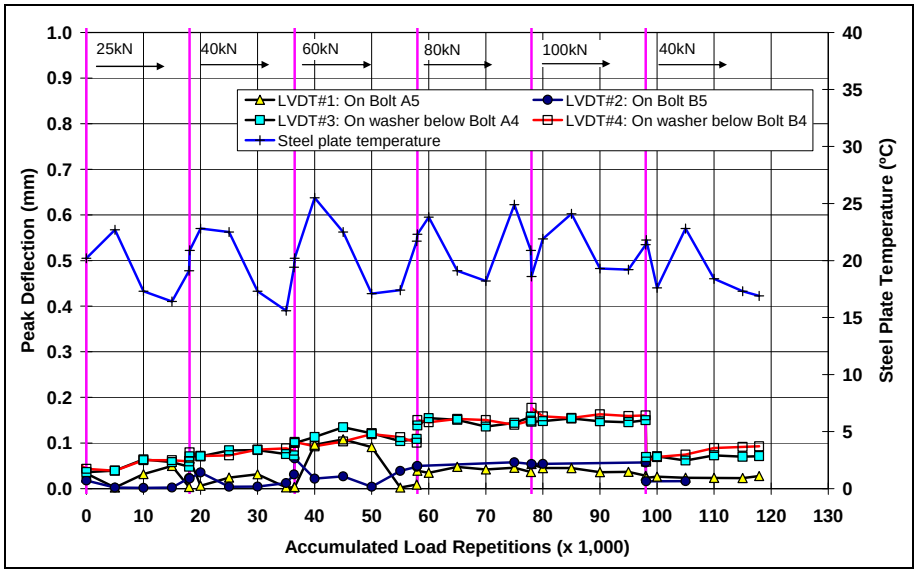

Figure 4.13: Phase 1.2: History of peak deflections on bolts and washers.

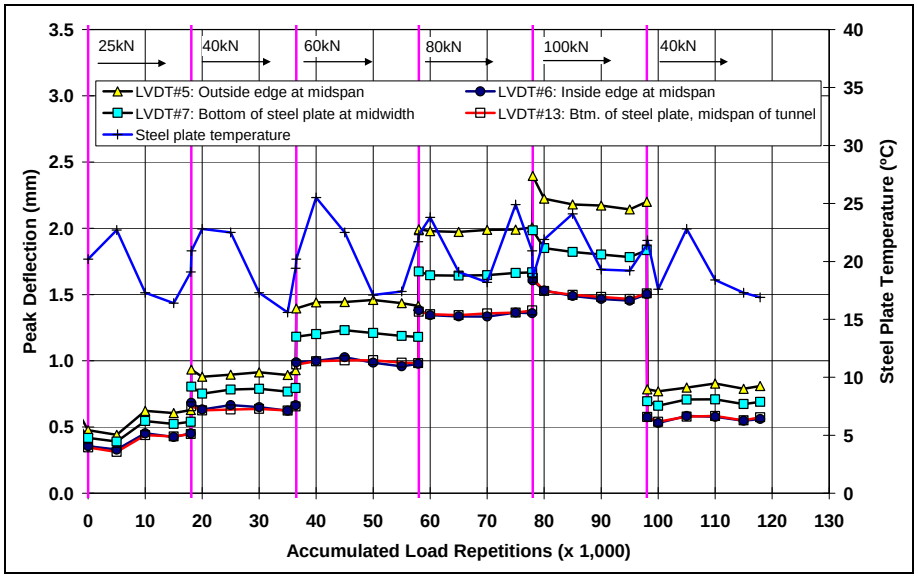

Figure 4.14: Phase 1.2: History of peak deflections on steel plate.

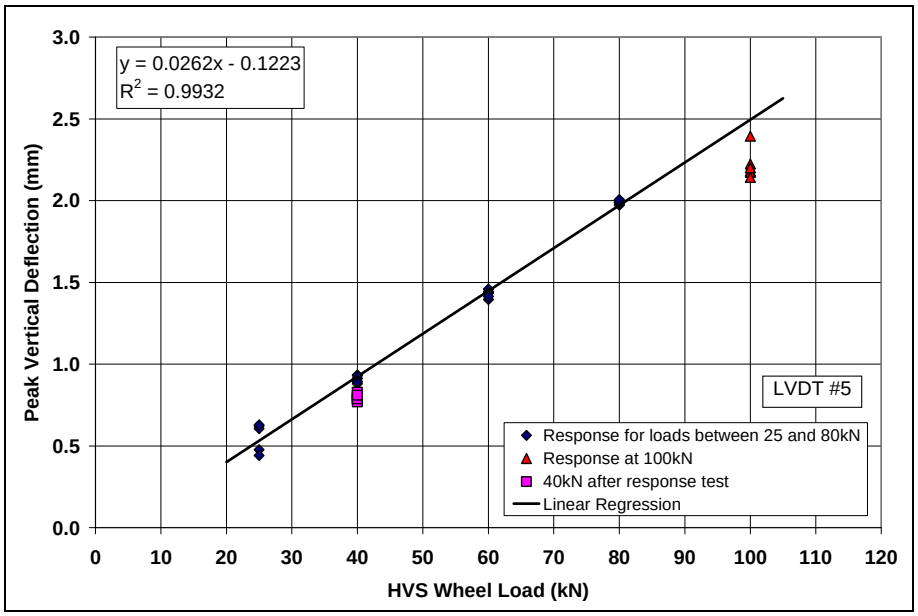

Figure 4.15: Phase 1.2: Relationship between peak deflection and wheel load.

(LVDT #5, midspan, outside edge of steel plate)

4.3.4 Longitudinal Strain

A plot of the peak strains for the three strain gauges for the duration of the phase is shown in Figure 4.16. Peak strain increased with the change in wheel load as expected, with highest strains recorded at the midpoint of the steel plate. Strains measured at the midpoint of the inside edge of the steel plate were slightly higher than those measured at the midpoint of the outside edge. This was attributed to the

wheelpath being closer to the sensor on the inside edge. The difference in strain between the three sensors increased with increasing wheel load, as expected, showing a general linear trend. After each load change, peak strain recorded by each of the gauges remained constant, with no evidence of damage accumulation with increasing load repetitions. The relationship between peak strain and load was linear for all three strain gauges for loads between 20 kN and 80 kN, but again showed marginal non-linearity for the 100 kN load (Figure 4.17 through Figure 4.19 for the three strain gauges). The reason for this was not investigated given the very small difference and that the bridge deck expansion joints would not be subjected to loads of this magnitude. Strains recorded during the 40 kN loading on the sixth day were slightly lower (approximately 5 με) than those recorded on the second day, indicating that no permanent damage was caused by the very high loads. Daily variation in peak strain followed daily temperature change, similar to the earlier phases.

4.3.5 Visual Damage

No visual damage was observed on the concrete structure, steel plate, bolts, or washers at the end of this phase. Tire abrasion wear on the Trelleborg unit, discussed in Section 4.2.5, continued with additional accumulations of rubber particles. No further deformation or other damage was observed on the Trelleborg unit. No rotation of the bolts or washers was observed.

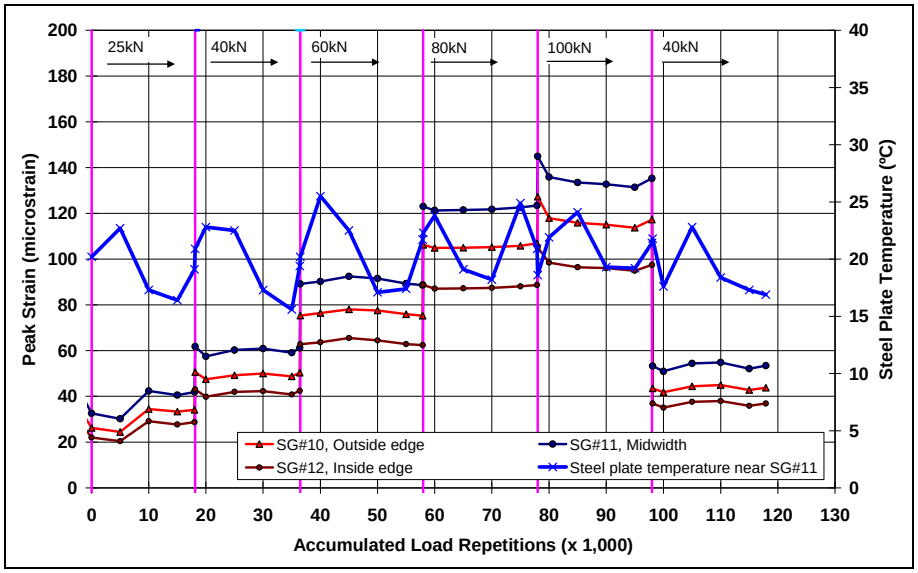

Figure 4.16: Phase 1.2: History of longitudinal strains at bottom of steel plate.

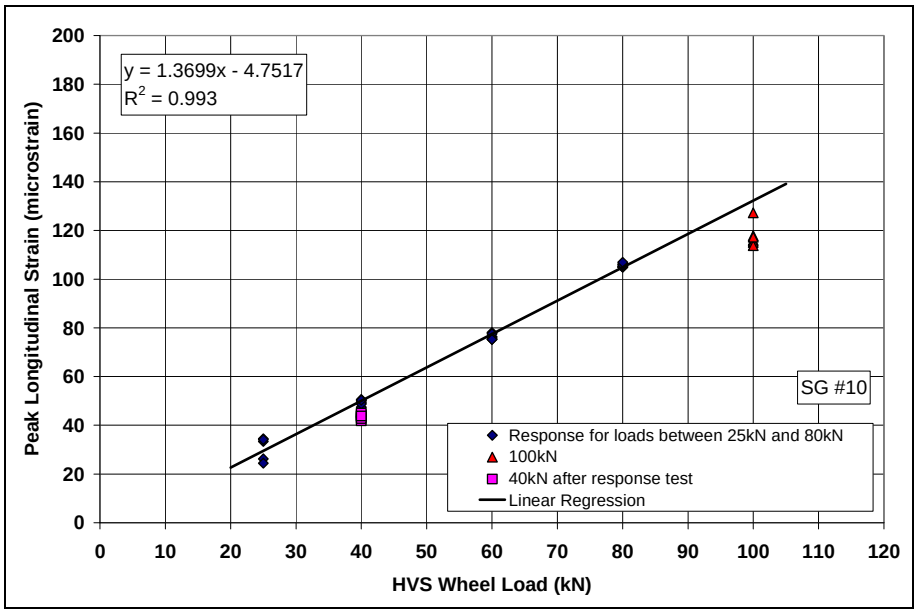

Figure 4.17: Phase 1.2: Relationship between peak strain and wheel load for SG #10.

(SG #10, outside edge of steel plate)

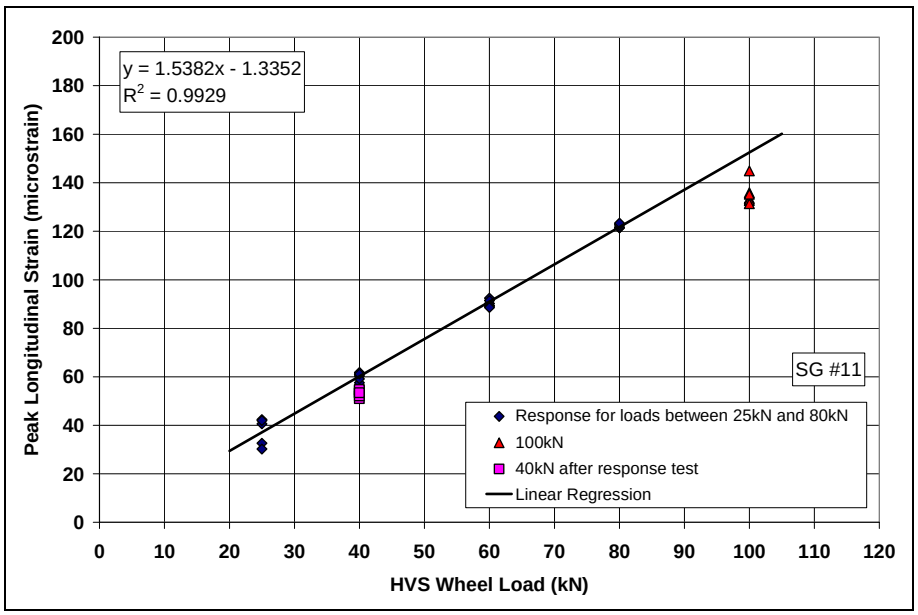

Figure 4.18: Phase 1.2: Relationship between peak strain and wheel load for SG #11.

(SG #11, midspan, outside edge of steel plate)

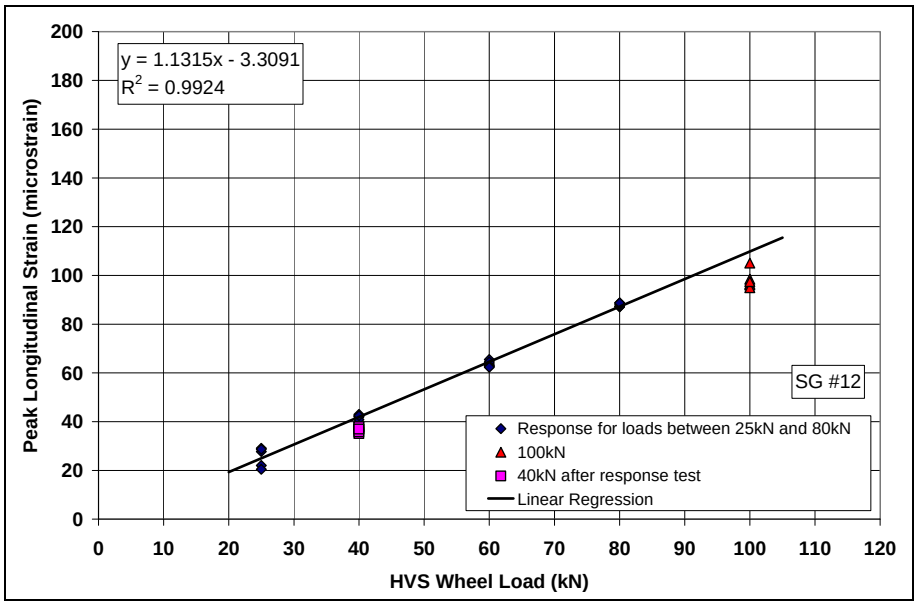

Figure 4.19: Phase 1.2: Relationship between peak strain and wheel load for SG #12.

(SG #12, outside edge of steel plate)

4.3.6 Phase Summary

No damage was observed at the end of Phase 1.2. No permanent deformation in the steel plate occurred during this phase, based on the strain data recorded. Increases in peak deflection and peak strain showed a linear relationship with increasing load. The maximum deflection and maximum strain recorded was 2.3 mm and 135 με respectively, both at the midpoint of the steel plate, under the 100 kN wheel load. Changes in deflection and strain with increasing wheel load showed similar trends. Very small daily variations in peak deflection and peak strain were consistent with daily temperature change on the data plots. Minor fluctuations in strain and deflection measurements were again likely caused by very small fluctuations in the actual load applied by the HVS.

4.4 Phase 1.3: Load Response Comparison at Center and Edge of the Steel Plate

4.4.1 Introduction

Phase 1.3 compared load response at the center and edge of the steel plate during traffic wander by evaluating changes in strain and deflection induced by increases in wheel load. The test ran for seven days, with a load change each day for the first three days (40 kN, 100 kN and 80 kN), followed by four days at 60 kN. All loading was applied in a bidirectional mode using a stepwise normally distributed wander pattern over a 1.0 m wide test track.

4.4.2 Temperature

The average (daily, minimum, and maximum), lowest, and highest temperatures measured during Phase 1.3 are summarized in Table 4.3. Daily average temperatures are plotted in Figure 4.20, with error bars indicating minimum and maximum temperatures for the thermocouple located next to Strain Gauge #11 (TC-SG#11). Average ambient temperatures were again typical for the area and had a relatively small diurnal range. Average daily minimum and maximum temperatures recorded on the steel plate were similar to the ambient temperatures, except for the thermocouple at Strain Gauge #12, which again indicated a higher average daily maximum than the other measurement points. No extreme temperature events were recorded. It is unlikely that temperature had any significant influence on the way that the bridge deck expansion joint components functioned during this phase of testing.

Table 4.3: Phase 1.3: Temperature Summary

Thermocouple	Temperature (°C)				
	Average of Daily Average	Average of Daily Minimum	Average of Daily Maximum	Lowest	Highest
Ambient	21	16	25	15	29
TC-SG#10	22	17	26	16	29
TC-SG#10-S	22	17	27	16	29
TC-SG#11	22	18	25	17	28
TC-SG#12	26	18	31	17	36
Thermocouple	**Temperature (°F)**				
Ambient	69	60	78	59	84
TC-SG#10	72	63	79	61	83
TC-SG#10-S	72	62	81	60	85
TC-SG#11	72	64	77	62	82
TC-SG#12	78	65	89	62	96

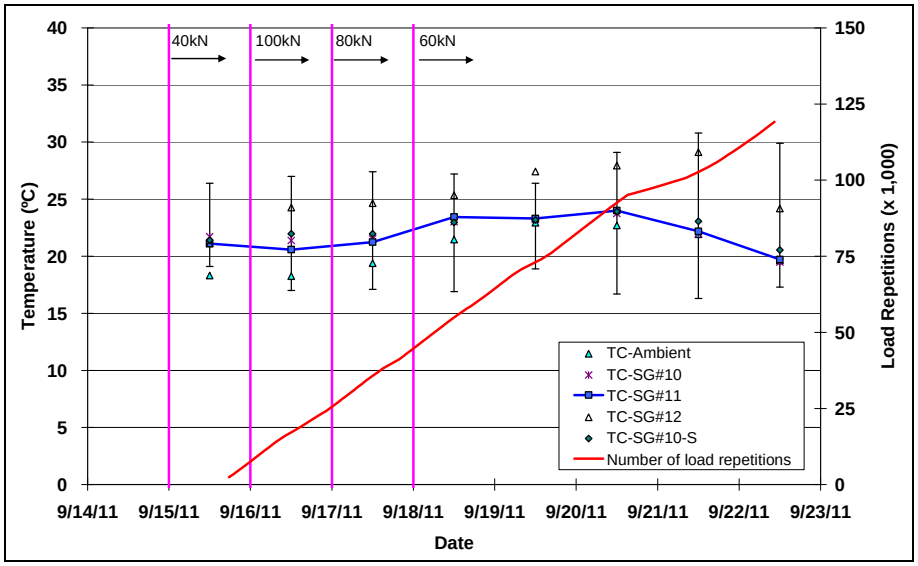

Figure 4.20: Phase 1.3: Daily average temperatures and HVS testing schedule.

4.4.3 Vertical Deflection

Plots of the lowest (wheel wander point furthest from the sensor) and highest (wheel wander point closest to the sensor) peak deflections measured on washers and the steel plate for the duration of Phase 1.3 are shown in Figure 4.21 through Figure 4.24, respectively. Plots for deflection on the bolts are not shown given the very small movements that were measured on them (<0.02 mm). Average deflections for the sensors on the steel plate are also summarized in Table 4.4 together with a ratio between the highest and lowest deflection recorded on each sensor. The difference in deflection on the washers during traffic wander with a 40 kN wheel load was very small (~0.01 mm), with the washer closest to the outside edge of the channel assembly having a slightly higher deflection than the one on the inside edge of the assembly. It increased slightly with the 60 kN wheel load (~0.02 mm) and a little more for the 80 kN load (~0.04 mm). At 100 kN, the difference between the lowest and highest deflections measured was a little more noticeable at about 0.08 mm; however, the difference between the two washers for the same traffic pass was about 0.2 mm at the higher load.

Deflections on the steel plate were a little higher, with bigger differences and larger variation between the different sensor locations. The sensor furthest away from the wheel was most affected by wheel position. At the 40 kN wheel load, differences in deflection ranged between 0.1 mm (LVDT #7 at the midpoint on the bottom of the steel plate and LVDT #13 on the bottom of the steel plate in the midspan of the tunnel) to 0.5 mm on the outside edge at the midspan (LVDT #5). The effect of increasing wheel load was similar to that observed for the LVDTs on the washers, except that the deflections were higher. The effect of wheel wander was most noticeable on the outside edge of the steel plate, with a variation of about 2.3 mm (or 2.75 times higher) at the 100 kN wheel load, between the time that the wheel was closest to the sensor and the time that it was furthest away. By comparison, variation in the middle of the steel plate during the two extremes of wheel position was about 0.35 mm. This difference in deflection range was also partially attributed to there being less support under the outside edge of the steel plate, compared to the midpoint and inside edge, resulting from a construction problem (see Section 2.3).

Table 4.4: Average Peak Deflections for Different Lateral Wheel Positions on the Steel Plate

Test Load (kN)	Lowest Peak Deflection (mm)			Highest Peak Deflection (mm)			Ratio of Highest to Lowest		
	LVDT #5	LVDT #7	LVDT #13	LVDT #5	LVDT #7	LVDT #13	LVDT #5	LVDT #7	LVDT #13
40	0.31	0.63	0.51	0.80	0.72	0.58	2.58	1.14	1.14
60	0.45	0.91	0.74	1.25	1.10	0.89	2.81	1.21	1.20
80	0.64	1.25	1.00	1.79	1.52	1.25	2.80	1.22	1.24
100	0.83	1.57	1.27	2.29	1.94	1.59	2.75	1.23	1.25

The trends in deflection at different wheel loads showed similar linearity to that observed during Phase 1.2. After each load change, deflections recorded by each of the LVDTs remained constant until

the next load change. There was no evidence of damage accumulation with increasing load repetitions and the deflections recorded during wander, even at the high wheel load, were not considered to be detrimental to the longer-term performance of the steel plate. Daily temperature change appeared to result in very small daily variations in deflection (<0.01 mm), especially at the lower loads.

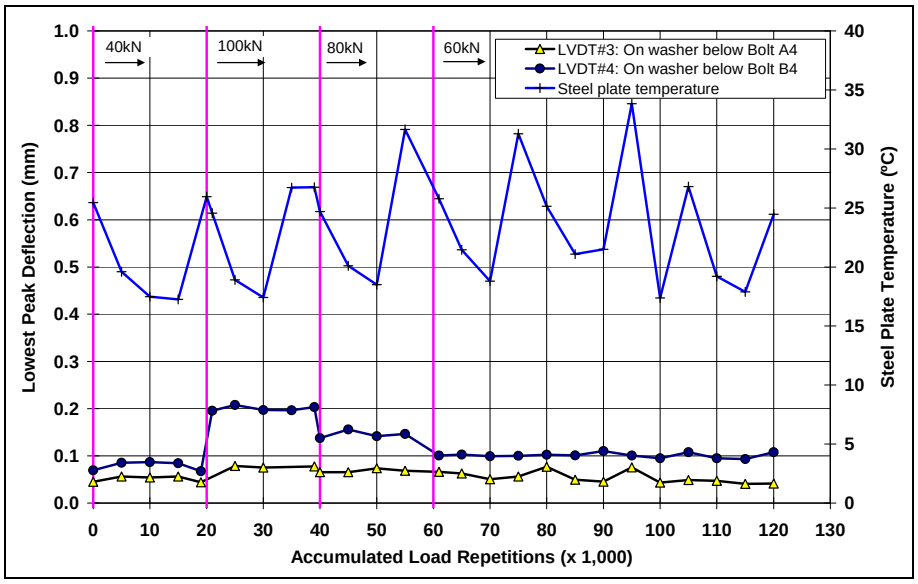

Figure 4.21: Phase 1.3: Lowest peak deflections recorded on washers during traffic wander.

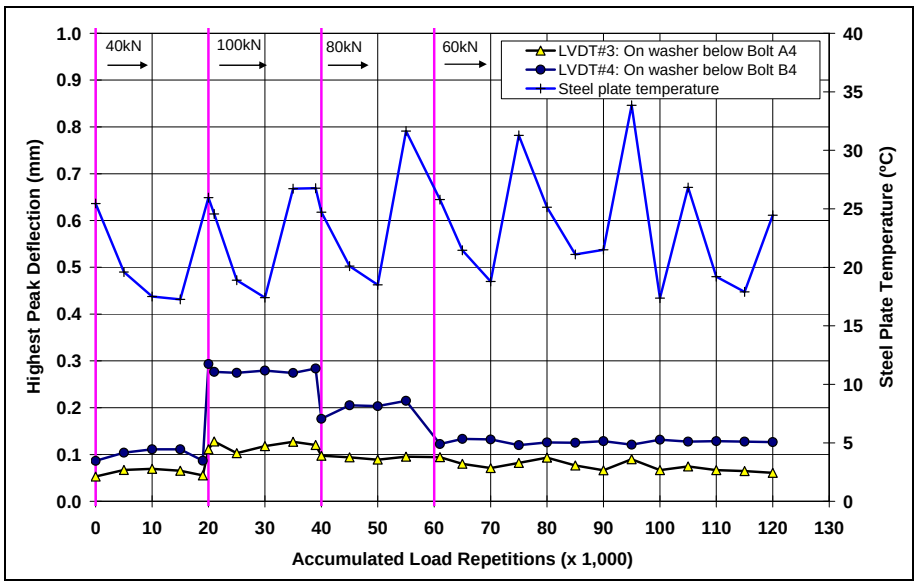

Figure 4.22: Phase 1.3: Highest peak deflections recorded on washers during traffic wander.

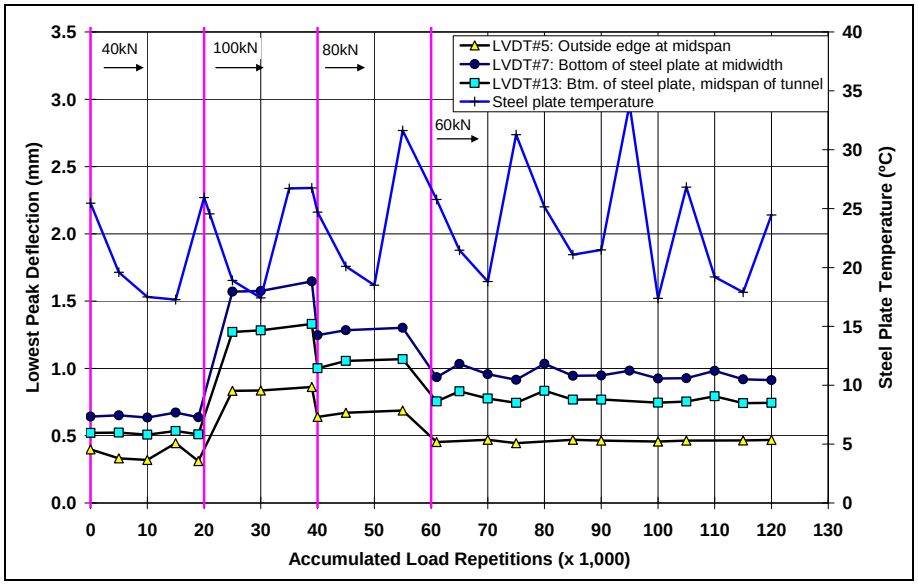

Figure 4.23: Phase 1.3: Lowest peak deflections on steel plate during traffic wander.

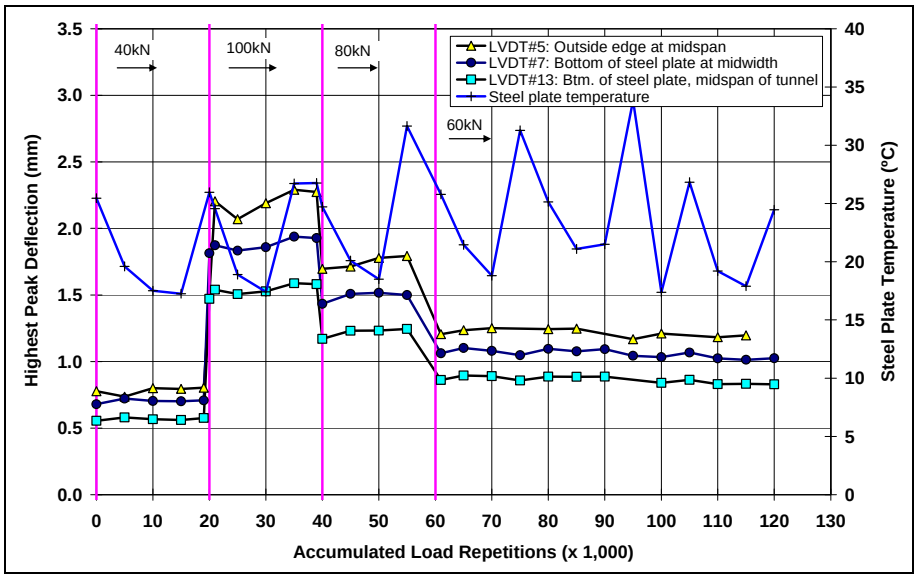

Figure 4.24: Phase 1.3: Highest peak deflections on steel plate during traffic wander.

4.4.4 Longitudinal Strain

Plots of the lowest (wheel wander point furthest from the sensor) and highest (wheel wander point closest to the sensor) peak strains measured on the steel plate for the duration of Phase 1.3 are shown in Figure 4.25 and Figure 4.26, respectively. Average strains are also summarized in Table 4.5 together with a ratio between the highest and lowest peak strain recorded on each sensor at each wheel load. Changes in strain at different wheel loads and different wheel positions were consistent with the changes observed in

deflection (discussed in Section 4.4.3). Differences in strains measured by the sensors on the edges of the steel plate varied significantly more with changing wheel position than the sensor at the midpoint (ratio of highest to lowest strain of between 2.1 and 2.5 for the outside edge compared to between 1.4 and 1.5 for the midpoint).

Table 4.5: Average Peak Strains for Different Lateral Wheel Positions on the Steel Plate

Test Load (kN)	Lowest Peak Strain (με)			Highest Peak Strain (με)			Ratio of Highest to Lowest		
	SG#10	SG#11	SG#12	SG#10	SG#11	SG#12	SG#10	SG#11	SG#12
40	23	38	35	46	55	89	2.0	1.5	2.5
60	33	55	52	71	84	129	2.1	1.5	2.5
80	48	78	74	97	112	174	2.0	1.4	2.3
100	62	99	97	127	143	216	2.1	1.4	2.2

The trends in peak strain at different wheel loads showed similar linearity to that observed during Phase 1.2. After each load change, peak strains recorded at each of the strain gauges remained constant until the next load change. There was no evidence of damage accumulation with increasing load repetitions and the peak strains recorded during wander, even at the high wheel load, were not considered to be detrimental to the longer-term performance of the steel plate. Daily temperature cycles appeared to result in very small daily variations in peak strain (~ 8 με), especially at the lower wheel loads.

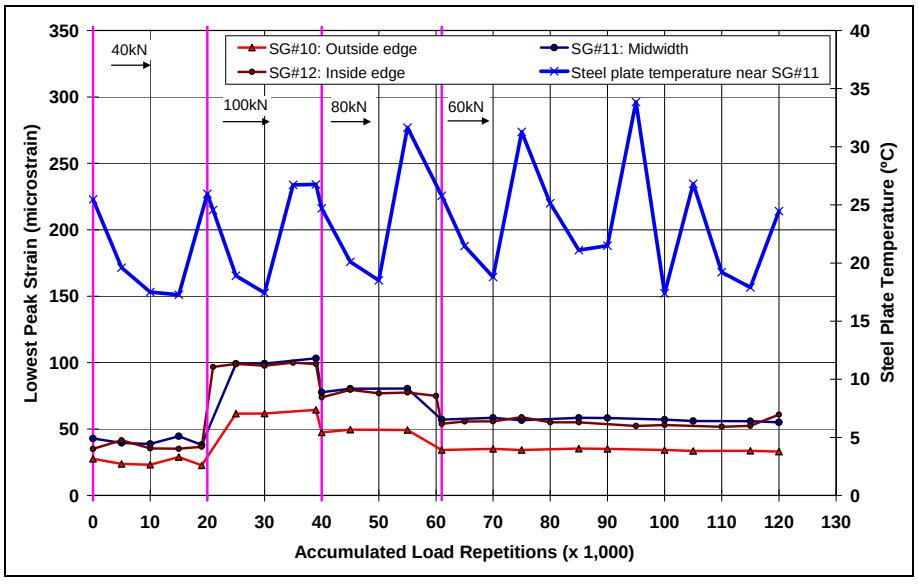

Figure 4.25: Phase 1.3: Lowest peak longitudinal strains on steel plate during traffic wander.

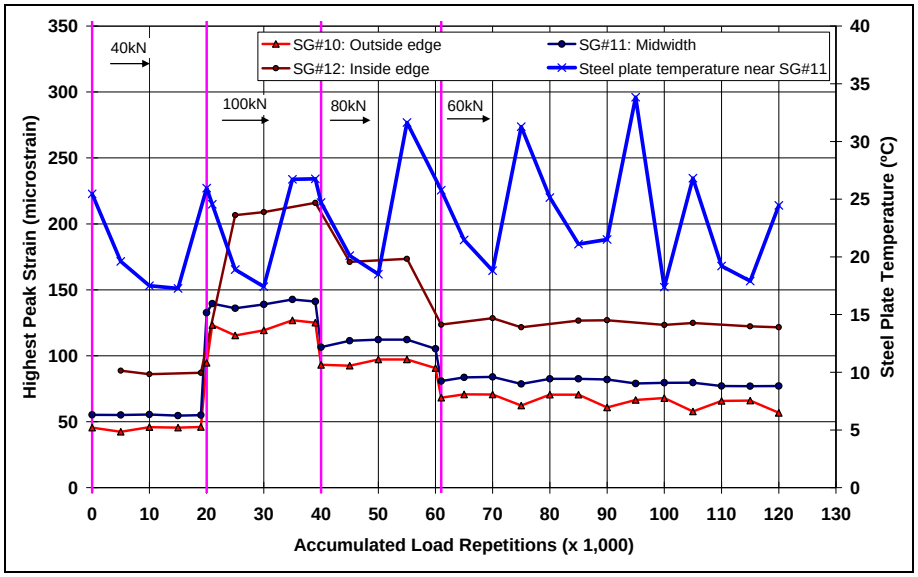

Figure 4.26: Phase 1.3: Highest peak longitudinal strains on steel plate during traffic wander.

4.4.5 Visual Damage

No visual damage was observed on the concrete structure, steel plate, bolts, or washers at the end of this phase. Tire abrasion wear on the Trelleborg unit continued with additional accumulations of rubber particles (Figure 4.27). No further deformation or other damage was observed on the Trelleborg unit. No rotation of the bolts or washers was observed.

Figure 4.27: Phase 1.3: Rubber particle accumulation on Trelleborg unit after 740,000 repetitions.

4.4.6 Phase Summary

No damage was observed at the end of Phase 1.3 and based on the deflection and strain data recorded, no permanent deformation in the steel plate occurred. Peak strain and deflection at any time was influenced by the position of the wheels in the wander pattern, as expected. Sensors furthest away from the wheels

(i.e., on the edge of the steel plate) had larger differences between the lowest and highest deflection and strain (ratio of ~2.5) compared to the sensors inside the wheelpath (i.e., at the midpoint of the steel plate), which had highest strain to lowest strain ratios of about 1.5. Increases in peak deflection and peak strain continued to show a linear relationship with increasing load. Very small daily variations in peak deflection and peak strain were consistent with daily temperature change on the data plots. Minor fluctuations in strain and deflection measurements were again likely caused by very small fluctuations in the actual load applied by the HVS. Based on the results and observations in this phase, it was concluded that there was no significant difference in the measurements recorded during traffic wander compared to those recorded during channelized traffic, and that wander had very little effect on the behavior of the expansion joint. Consequently all further testing was carried out in a channelized mode as this was considered more likely to induce damage given the concentrated nature of the loading.

4.5 Phase 2.1: Edge Loading Test

4.5.1 Introduction

During Phase 2.1, testing was carried out on the edge of one of the expansion joints as shown in Figure 3.3. The term "edge" is used because the wheelpath for this phase was closer to the edge of one of the two steel plates, despite being closer to the center of the entire lane width. Normal trafficking on the actual bridge would not occur in this way except when vehicles change lanes. The objective in this phase was to assess whether trafficking at higher loads on the edge of the steel plate would cause the expansion joint to behave differently compared to the central loading in Phases 1.1 and 1.2, and to determine if any new damage was caused. The test ran for 11 days with a range of wheel loads (2 days at 40 kN, 1 day each at 60 kN, 80 kN and 100 kN, then 6 days at 80 kN) to allow monitoring of changes in response. The longer period of testing at the end of the phase was conducted at a higher wheel load than previous phases to further explore likely modes of failure. All loading was applied in a bidirectional channelized mode.

4.5.2 Temperature

The average (daily, minimum, and maximum), lowest, and highest temperatures measured during Phase 2.1 are summarized in Table 4.6. Daily average temperatures are plotted in Figure 4.28, with error bars indicating minimum and maximum temperatures for the thermocouple located next to Strain Gauge #11 (TC-SG#11). Average ambient temperatures were again typical for the area and had a relatively small diurnal range. Average daily minimum and maximum temperatures recorded on the steel plate were similar to the ambient temperatures, except for the thermocouple at Strain Gauge #12, which again indicated a higher average daily maximum than the other measurement points. No extreme temperature events were recorded. It is unlikely that temperature had any significant influence on the way that the bridge deck expansion joint components functioned during this phase of testing.

Table 4.6: Phase 2.1: Temperature Summary

Thermocouple	Temperature (°C)				
	Average of Daily Average	Average of Daily Minimum	Average of Daily Maximum	Lowest	Highest
Ambient	19	16	25	15	33
TC-SG#10	20	17	24	16	29
TC-SG#10-S	20	17	25	15	30
TC-SG#11	21	18	24	16	29
TC-SG#12	23	19	30	17	38
Thermocouple	**Temperature (°F)**				
Ambient	66	61	76	59	91
TC-SG#10	68	63	76	60	85
TC-SG#10-S	68	62	77	60	87
TC-SG#11	69	64	75	61	84
TC-SG#12	73	66	85	62	100

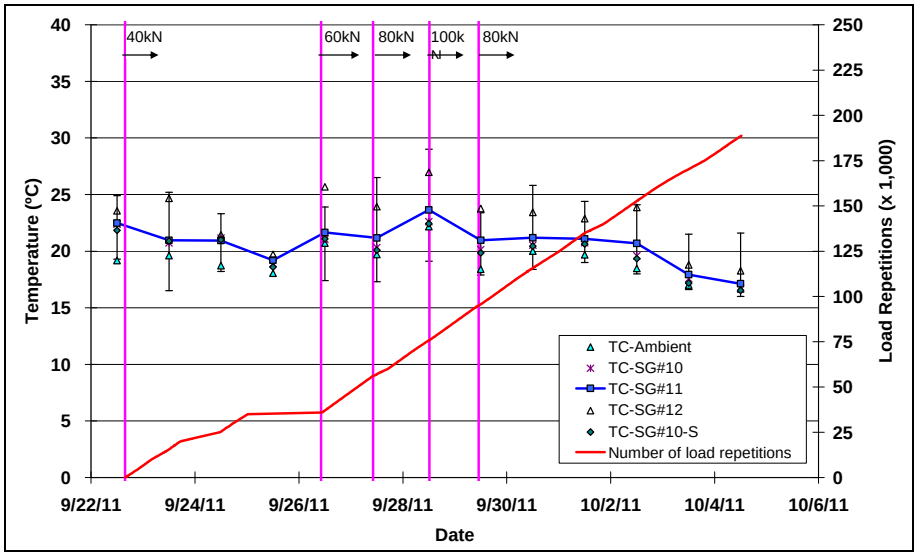

Figure 4.28: Phase 2.1: Daily average temperatures and HVS testing schedule.

4.5.3 Vertical Deflection

Influence lines (or deflection bowls) from a single pass of the 80 kN wheel load for the LVDTs on the bolts, washers, and steel plate are shown in Figure 4.29 through Figure 4.31, respectively. Vertical deflections on the bolts and washers were higher than those recorded in a similar test in Phase 1.1 at 40 kN, as expected because of the higher load. Deflections showed similar trends to those observed in Phase 1.1 and were still considered to be very small (between 0.02 mm and 0.12 mm) with deflection increasing or decreasing with proximity to the wheel, as expected. Deflections measured on the washers were similar to those measured on the bolts. Deflections on the steel plate were again significantly higher than those on the bolts and washers, ranging between 0.75 mm and 2.0 mm depending on location of the sensor, with highest deflections on the midpoint of the inside edge of the steel plate (closest sensor to the wheel) and midpoint of the steel plate. The deflections on the bolts and washers on the channel assembly

and on the steel plate briefly changed from a negative deflection to a positive deflection and then back to a zero deflection when the wheels moved from the steel plate to the concrete, indicating a small recovery "bounce" after the load was removed. The movement was very small (total of 0.025 mm, 0.06 mm, and 0.08 mm on the bolts, washers, and steel plate respectively) and was not considered to be of any consequence in terms of long-term performance.

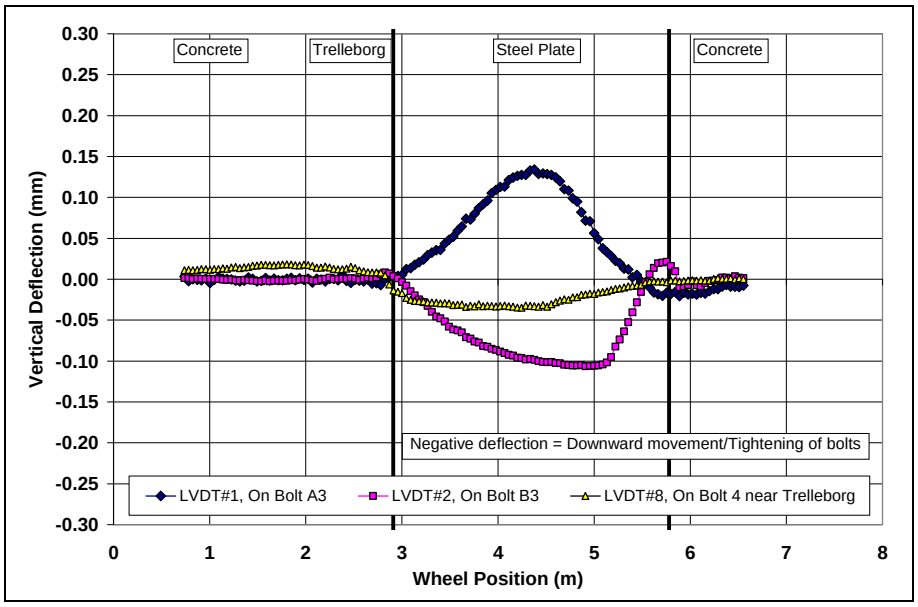

Figure 4.29: Phase 2.1: Influence lines of vertical deflection for LVDTs on bolts.

(Repetition #938,000, wheel load at 80 kN)

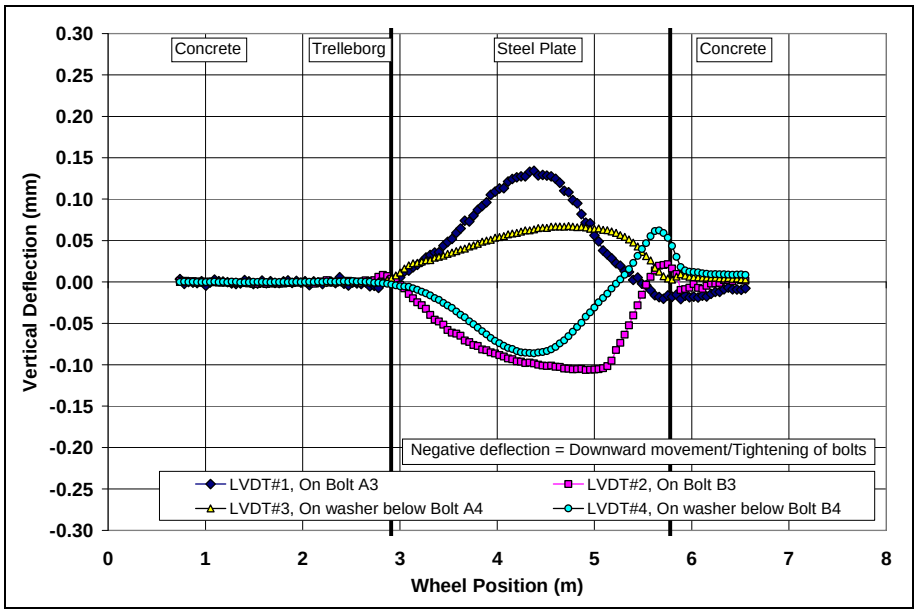

Figure 4.30: Phase 2.1: Influence lines of vertical deflection for LVDTs on bolts and washers.

(Repetition #938,000, wheel load at 80 kN)

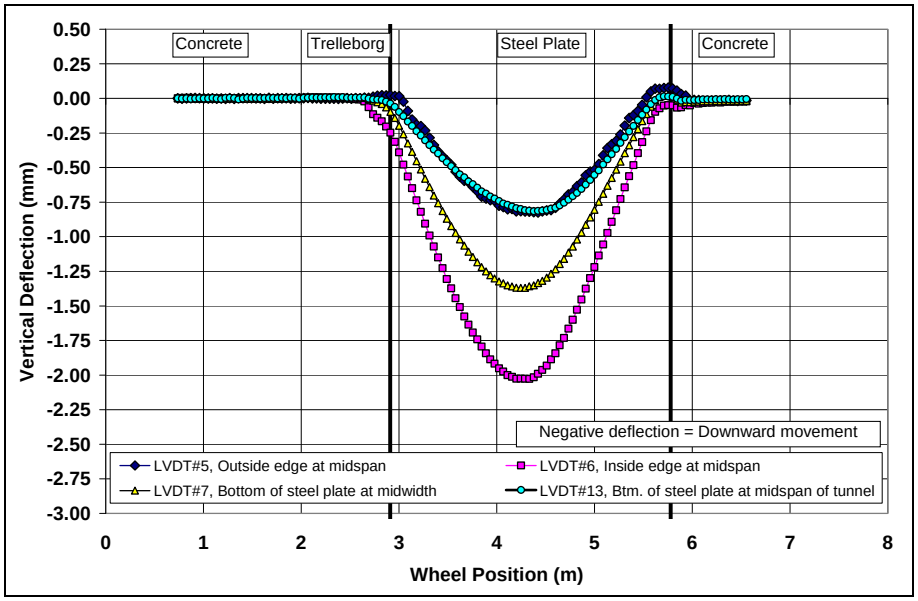

Figure 4.31: Phase 2.1: Influence lines of vertical deflection for LVDTs on steel plate.

(Repetition #938,000, wheel load at 80 kN)

Plots of the peak deflections measured on bolts, washers, and the steel plate for the duration of Phase 1.3 are shown in Figure 4.32 through Figure 4.34, respectively. Deflections increased with the change in wheel load as expected, and were consistent with observations from previous phases. The relationship between peak deflection and load was linear for all loads (example for LVDT #5 in Figure 4.35). After the load change, deflections recorded by each of the LVDTs remained constant, with no evidence of damage accumulation with increasing load repetitions. Deflection did not appear to be influenced by temperature.

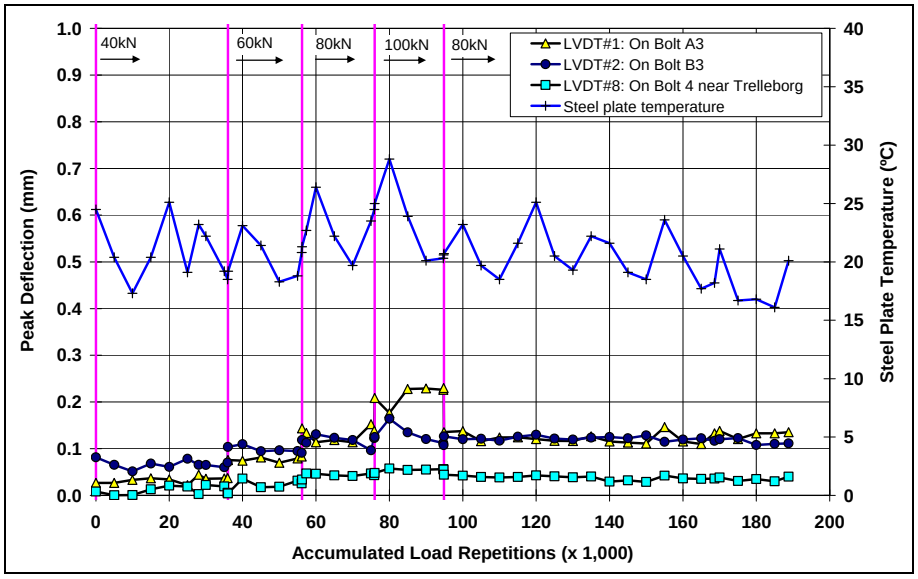

Figure 4.32: Phase 2.1: History of peak deflections on bolts.

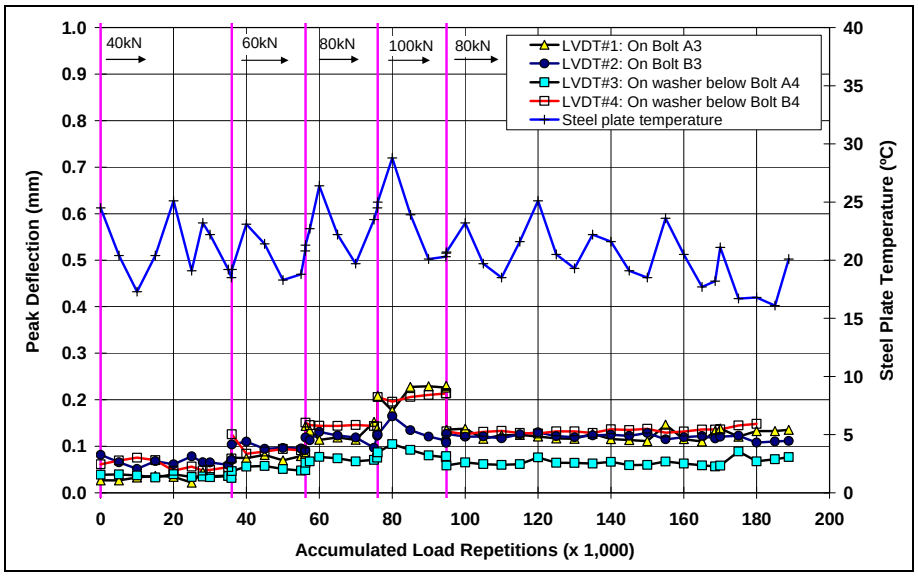

Figure 4.33: Phase 2.1: History of peak deflections on bolts and washers.

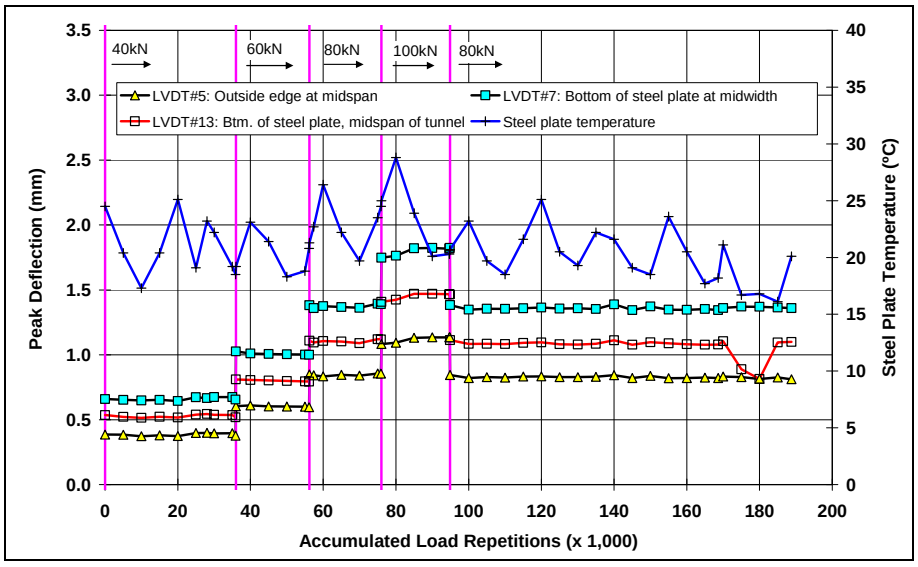

Figure 4.34: Phase 2.1: History of peak deflections at bottom of steel plate.

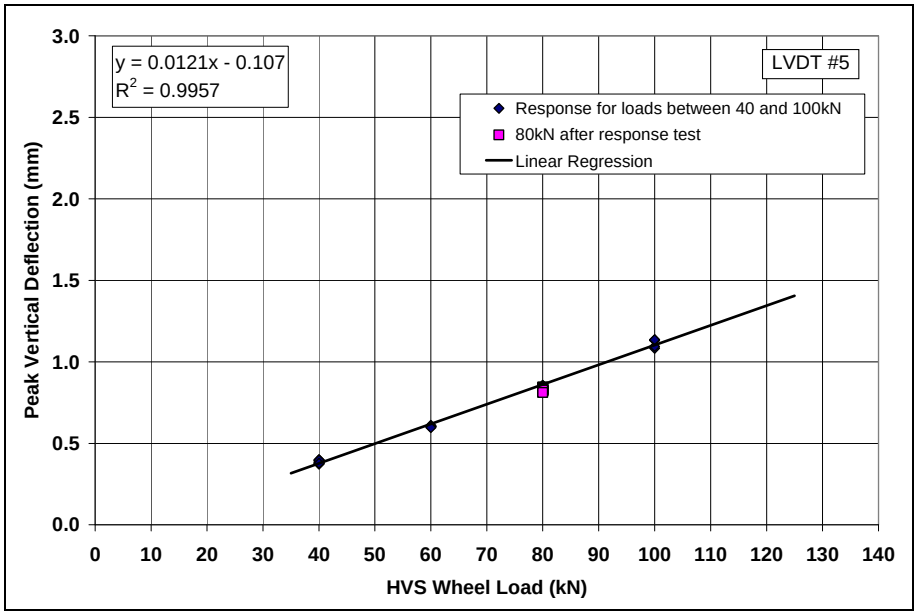

Figure 4.35: Phase 2.1: Relationship between peak deflection and wheel load.

(LVDT #5, midspan, outside edge of steel plate)

4.5.4 Longitudinal Strain

A plot of the peak strains for the three strain gauges for the duration of the phase is shown in Figure 4.36. Peak strain increased with the change in wheel load as expected, and showed similar trends to earlier phases. Highest strains were recorded on the sensor closest to the wheelpath. After each load change, peak strain recorded by each of the gauges remained constant, with no evidence of damage accumulation with increasing load repetitions. The relationship between peak strain and load in this phase was linear for all three strain gauges for all loads (Figure 4.37 through Figure 4.39 for the three strain gauges). Strain measurements did not appear to be influenced by temperature in this phase.

4.5.5 Visual Damage

No visual damage was observed on the concrete structure, steel plate, bolts, or washers at the end of this phase. Tire abrasion wear on the Trelleborg unit continued with additional accumulations of rubber particles (Figure 4.40). Apart from some deformation (approximately 4.0 mm) on the rubber, no damage was observed on the Trelleborg unit. Permanent deformation is discussed in Section 4.10. No rotation of the bolts or washers was observed.

4.5.6 Phase Summary

No damage was observed at the end of Phase 2.1 and based on the deflection and strain data recorded, no permanent deformation in the steel plate occurred. Responses were similar to those recorded in earlier phases during loading on the center of the expansion joint. Increases in peak deflection and peak strain

continued to show a linear relationship with increasing load. Based on the results and observations in this phase, it was concluded that there was no significant difference in the trends of measurements recorded during trafficking on the edge compared to those recorded during trafficking on the center. However, since higher deflections and strains were measured in this phase for the same loads, it was decided to undertake all further testing on the edge of the bridge deck expansion joint as this was considered more likely to induce damage.

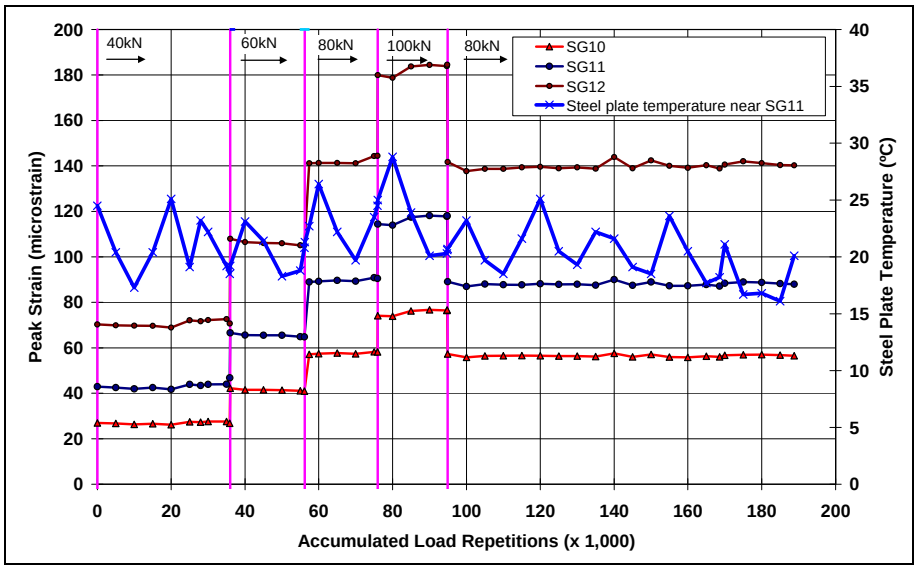

Figure 4.36: Phase 2.1: History of longitudinal strains at bottom of steel plate.

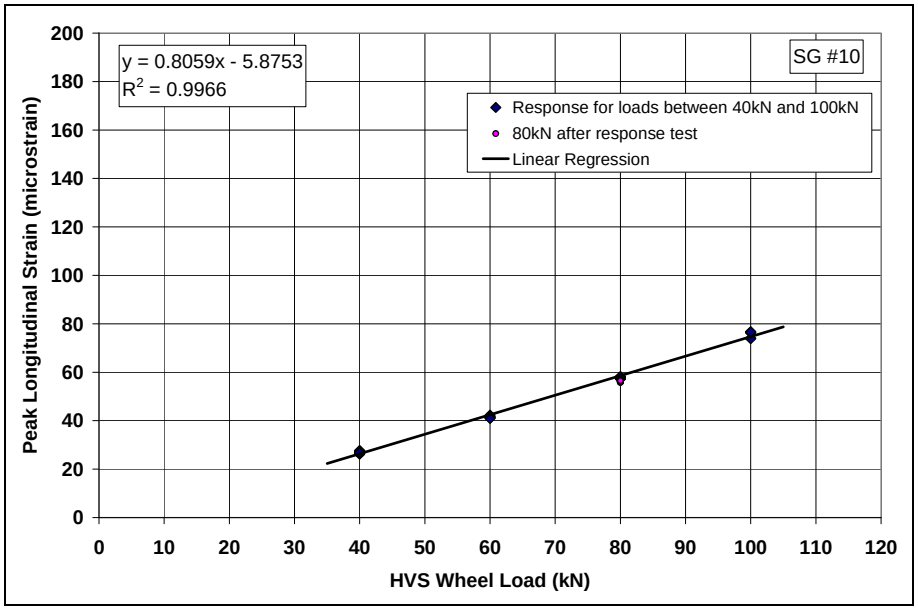

Figure 4.37: Phase 2.1: Relationship between peak strains and wheel load for SG #10.

(SG #10, outside edge of steel plate)

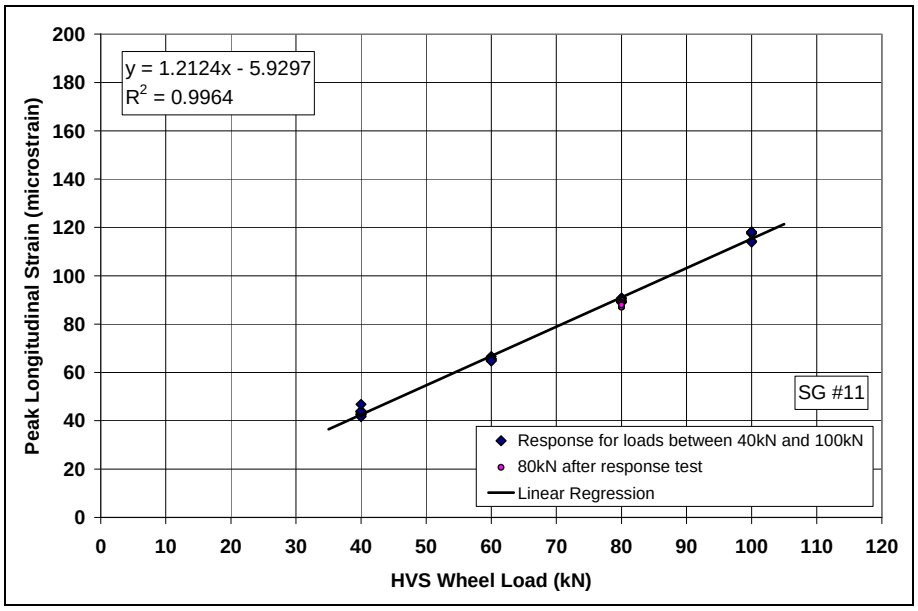

Figure 4.38: Phase 2.1: Relationship between peak strains and wheel load for SG #11.

(SG #11, midspan, outside edge of steel plate)

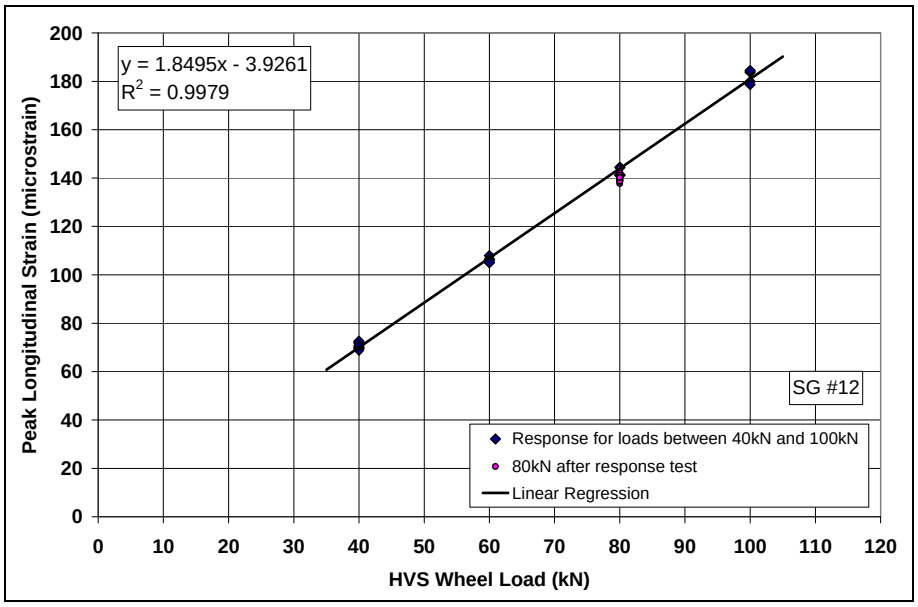

Figure 4.39: Phase 2.1: Relationship between peak strains and wheel load for SG #12.

(SG #12, outside edge of steel plate)

Figure 4.40: Phase 2.1: Rubber particle accumulation on Trelleborg unit after 928,000 repetitions.

4.6 Phase 3.1: Edge Test with Impact Load and Unidirectional Traffic

4.6.1 Introduction

After reviewing the Phase 1 and Phase 2 results, it was concluded that continued trafficking at 80 kN and 100 kN was unlikely to cause any significant structural damage to the seismic joint in the time available. The study therefore proceeded to Phase 3 of the test plan, which required impact loading—caused by including a "step" in the wheelpath—and was followed by significantly heavier wheel loads (using an aircraft tire).

The objective of Phase 3.1 was to determine whether impact loads on the steel plate had any influence on the response trends observed during earlier phases. Testing was carried out on the edge of the expansion joints in the same wheelpath used in Phase 2.1. On the first day, a 13 mm (0.5 in.) neoprene mat (Figure 4.41) was used to cause the impact and thereafter a 19 mm (0.75 in.) hardwood board (Figure 4.42). Larger steps could not be used as these would have caused a system error and consequent shut down of the HVS hydraulic operating unit. The test ran for three days with a 60 kN wheel load in a unidirectional (i.e., one-way traffic only) channelized mode. Wheel direction travelled from the channel assembly toward the Trelleborg unit, with impact applied to the channel assembly on the first day (i.e., from the 13 mm neoprene mat) and then the midpoint of the steel plate thereafter (i.e., from the 19 mm hardwood board. See Figure 4.41 and Figure 4.42 for relative positions of the steps). The influence of the two steps on actual load applied to the steel plate was not determined.

Figure 4.41: Phase 3.1: Impact load from neoprene step.

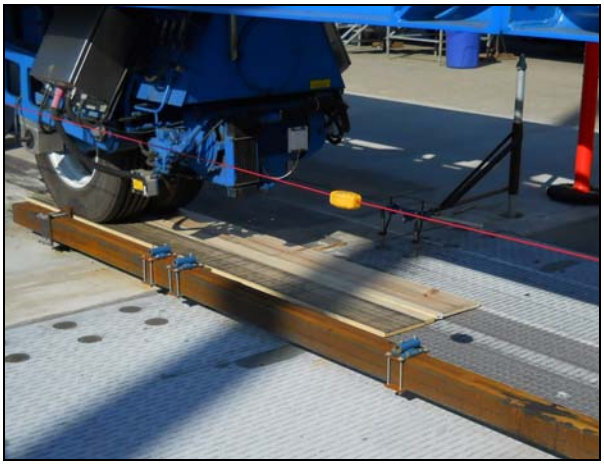

Figure 4.42: Phase 3.1: Impact load from wooden step.

4.6.2 Temperature

The average (daily, minimum, and maximum), lowest, and highest temperatures measured during Phase 3.1 are summarized in Table 4.7. Daily average temperatures are plotted in Figure 4.43, with error bars indicating minimum and maximum temperatures for the thermocouple located next to Strain Gauge #11 (TC-SG#11). Average ambient temperatures were again typical for the area, had a relatively small diurnal range, but showed a definite cooling trend compared to the other phases. Average daily minimum and maximum temperatures recorded on the steel plate were similar to the ambient temperatures, except for Strain Gauge #12, which again indicated a higher average daily maximum than the other measurement points, but with a smaller difference compared to the previous phases. No extreme temperature events were recorded. It is unlikely that temperature had any significant influence on the way that the bridge deck expansion joint components functioned during this phase of testing.

Table 4.7: Phase 3.1: Temperature Summary

Thermocouple	Temperature (°C)				
	Average of Daily Average	Average of Daily Minimum	Average of Daily Maximum	Lowest	Highest
Ambient	15	13	19	11	22
TC-SG#10	16	14	18	12	23
TC-SG#10-S	15	13	18	12	23
TC-SG#11	16	14	19	13	24
TC-SG#12	18	14	22	13	26
Thermocouple	**Temperature (°F)**				
Ambient	60	56	66	53	71
TC-SG#10	60	57	65	54	74
TC-SG#10-S	60	56	65	53	74
TC-SG#11	62	57	66	55	74
TC-SG#12	64	58	72	56	79

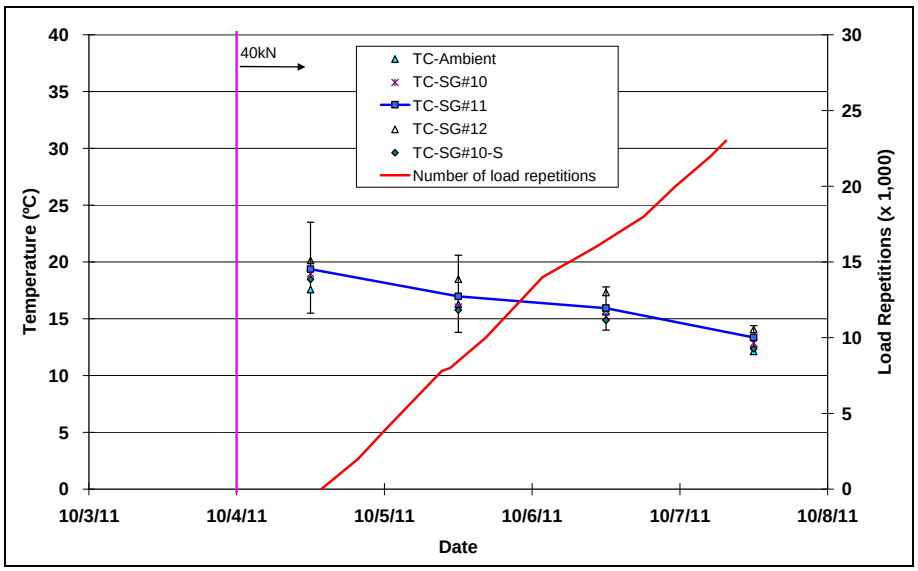

Figure 4.43: Phase 3.1: Daily average temperatures and HVS testing schedule.

4.6.3 Vertical Deflection

Plots of the peak deflections measured on bolts, washers, and the steel plate for the duration of Phase 3.1 are shown in Figure 4.44 through Figure 4.46, respectively. Deflections remained constant for all sensors throughout the phase, with actual deflection dependent on sensor location in relation to the wheelpath. Minor fluctuations (~0.01 mm) in deflection for each load were attributed to changes in temperature and/or load. Based on the data recorded, the impact loads applied did not appear to influence deflection of the expansion joint at the sensor locations.

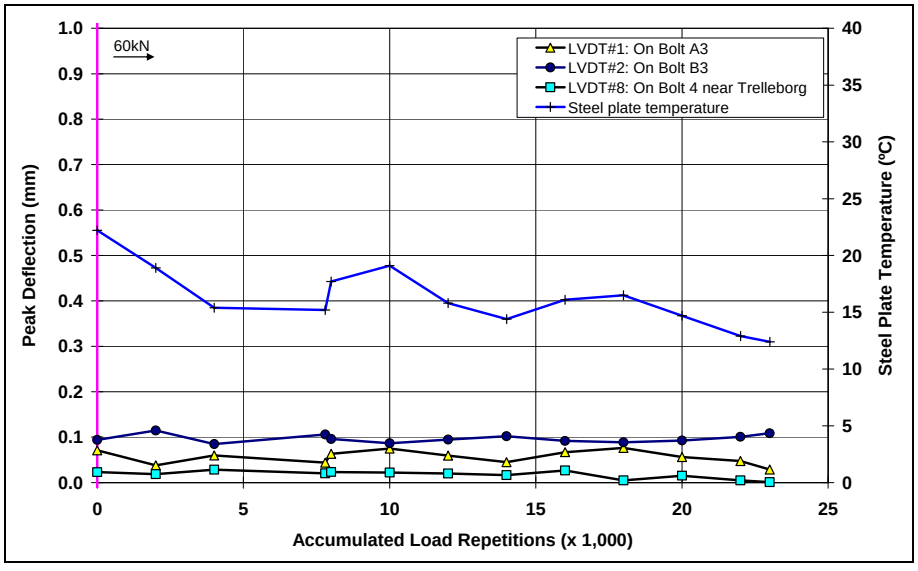

Figure 4.44: Phase 3.1: History of peak deflections on bolts.

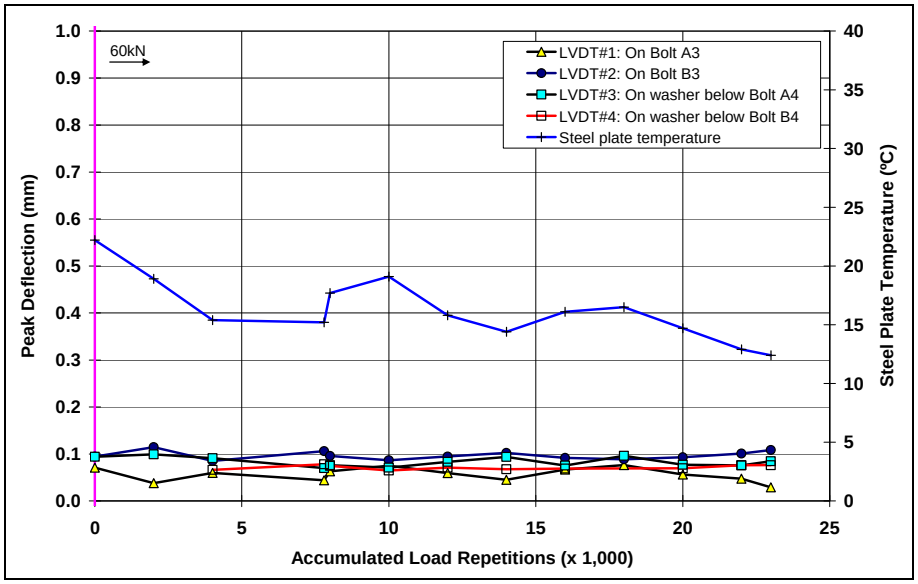

Figure 4.45: Phase 3.1: History of peak deflections on bolts and washers.

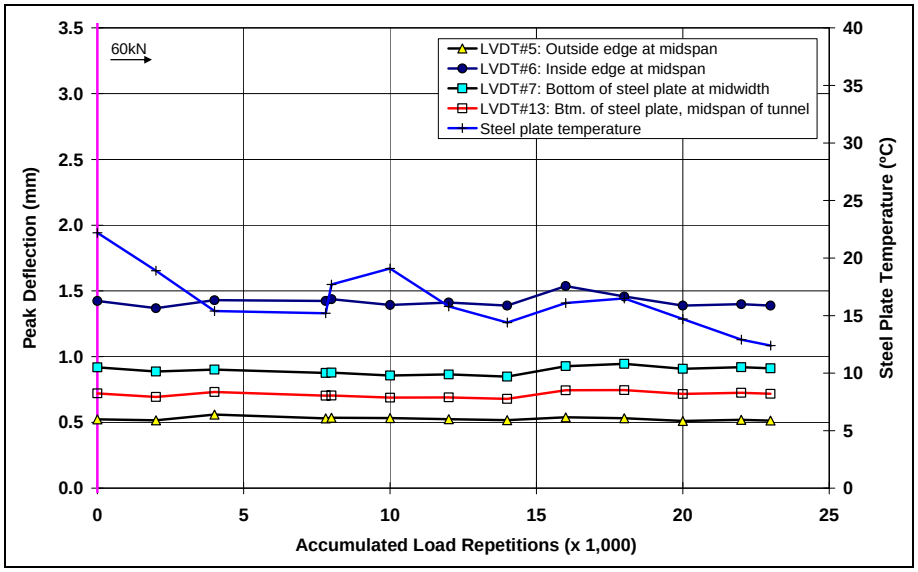

Figure 4.46: Phase 3.1: History of peak deflections at bottom of steel plate.

4.6.4 Longitudinal Strain

Plots of the peak longitudinal strains measured by the three strain gauges for the duration of this phase are shown in Figure 4.47. Peak strains remained constant for all sensors throughout the phase, with actual strain dependent on sensor location in relation to the wheelpath. Minor fluctuations (~2 με) were attributed to changes in temperature and/or load. Based on the data recorded, the impact loads applied did not appear to influence strain in the steel plate at the sensor locations.

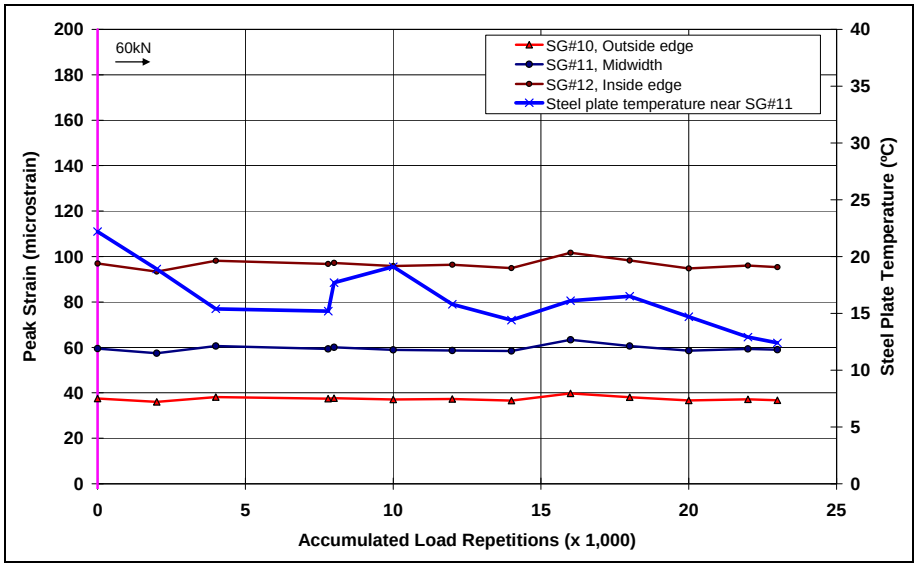

Figure 4.47: Phase 3.1: History of peak longitudinal strains at bottom of steel plate.

4.6.5 Visual Damage

No damage was observed to any part of the expansion joint or structure after completion of this phase of testing. No rotation of the bolts or washers was observed.

4.6.6 Phase Summary

A 60 kN impact load did not appear to influence response in the expansion joint at the sensor locations, and no damage was observed on completion of this short phase. Responses were similar to those recorded in earlier phases. There was also no difference observed between unidirectional and bidirectional trafficking and consequently all further testing was carried out in a bidirectional mode, which applies more wheel loads than unidirectional trafficking in a given period of time.

4.7 Phase 3.2: Load Response with Impact Load

4.7.1 Introduction

Phase 3.2 assessed load response with impact load by evaluating changes in strain and deflection induced by increases in wheel load. The test ran for 15 days with five days each at loads of 60 kN, 80 kN, and 100 kN, respectively. All loading was applied to the edge of the expansion joint in a bidirectional channelized mode. The impact load, which was applied on every alternate pass of the bidirectional trafficking, was induced with the 19 mm (0.75 in.) hardwood board used in Phase 3.1.

4.7.2 Temperature

Temperatures were not recorded during this phase due to a data acquisition system malfunction, which was repaired while testing continued. Given the limited time available to complete the testing and that temperature appeared to have little or no influence on the behavior of the bridge deck expansion joint, the project team agreed to continue testing in this phase without temperature data.

4.7.3 Vertical Deflection

Influence lines (or deflection bowls) from a single pass of the 100 kN wheel load (repetition #240,000 for the phase or #1,210,000 for the test) for the LVDTs on the bolts, washers, and steel plate are shown in Figure 4.48 through Figure 4.50, respectively. The impact load had a very small effect (wheel position 4.5 in the figures) on response. Plots of the peak deflections measured on bolts, washers, and the steel plate for the duration of Phase 3.2 are shown in Figure 4.51 through Figure 4.53, respectively. No differences in behavior to that recorded in Phase 2.1 (edge testing without impact load) were observed, with deflections remaining constant for each load for all sensors throughout the phase. The relationship between load and response was linear and consistent with previous phases (Figure 4.54). Based on the data recorded, the impact applied at any of the wheel loads did not appear to influence deflection of the expansion joint at the sensor locations.

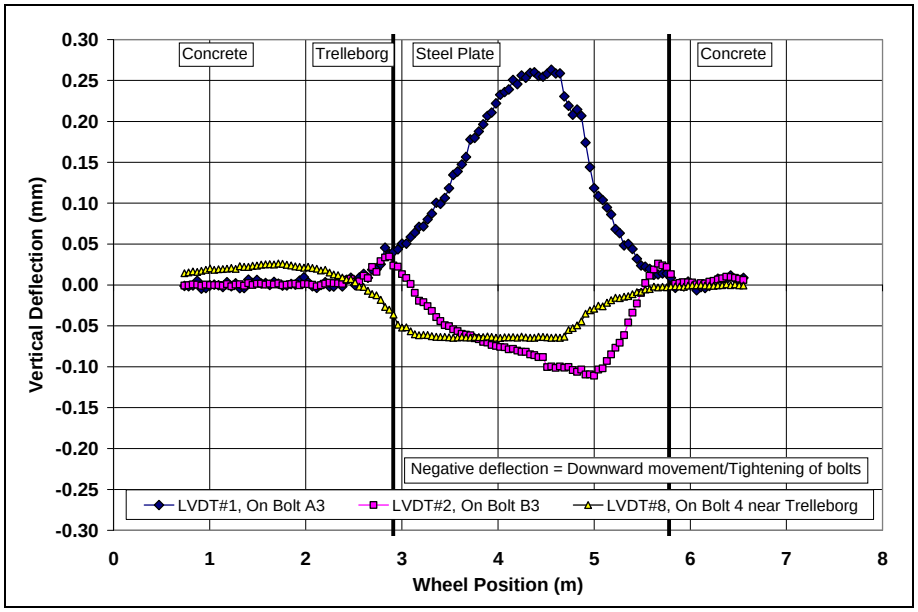

Figure 4.48: Phase 3.2: Influence lines of vertical deflection for LVDTs on bolts.

(Repetition #1,210,000, wheel load at 100 kN)

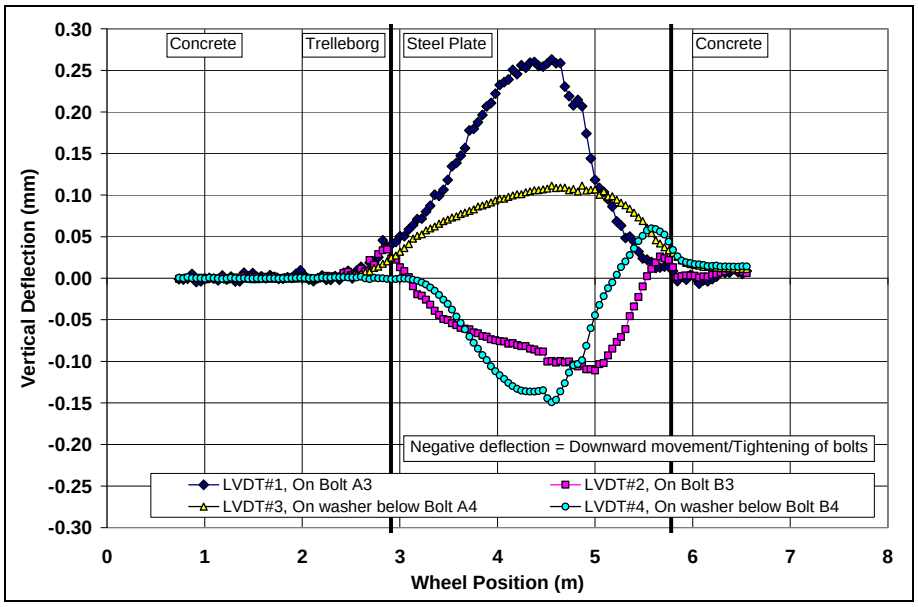

Figure 4.49: Phase 3.2: Influence lines of vertical deflection for LVDTs on bolts and washers.

(Repetition #1,210,000, wheel load at 100 kN)

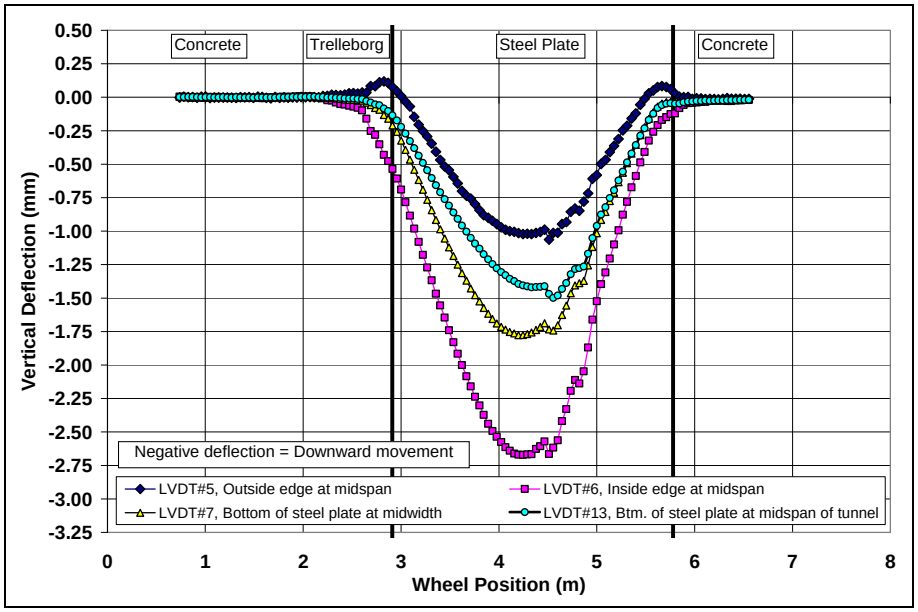

Figure 4.50: Phase 3.2: Influence lines of vertical deflection for LVDTs on steel plate.

(Repetition #1,210,000, wheel load at 100 kN)

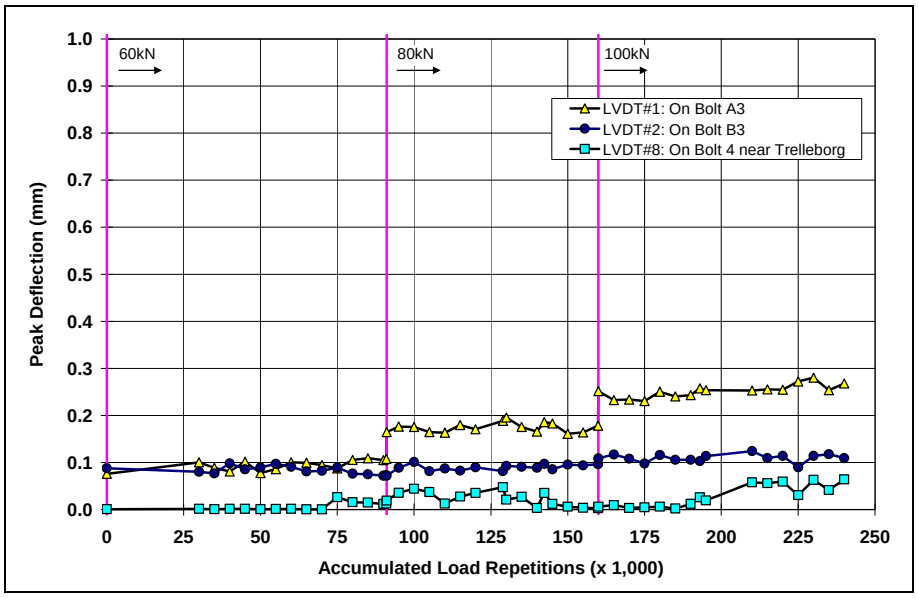

Figure 4.51: Phase 3.2: History of peak deflections on bolts.

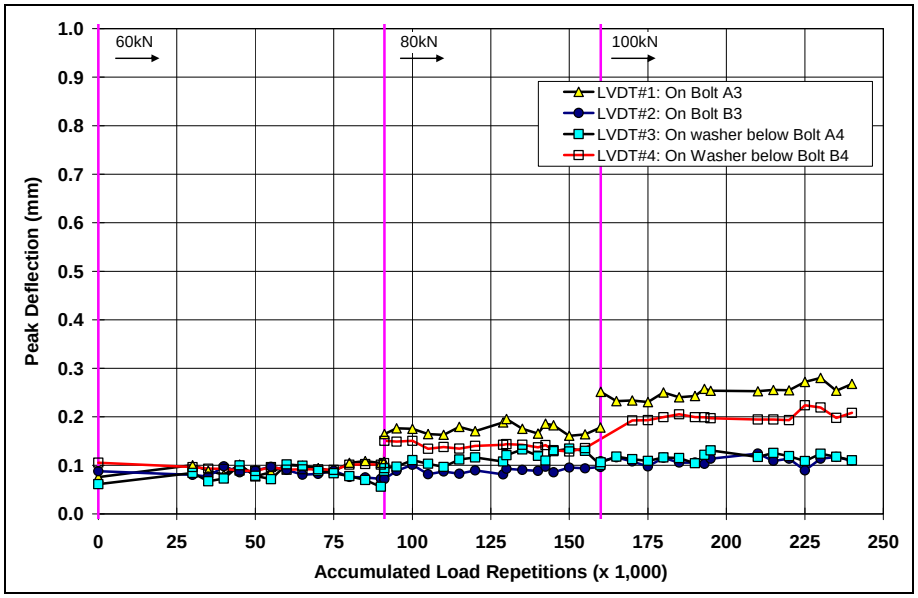

Figure 4.52: Phase 3.2: History of peak deflections on bolts and washers.

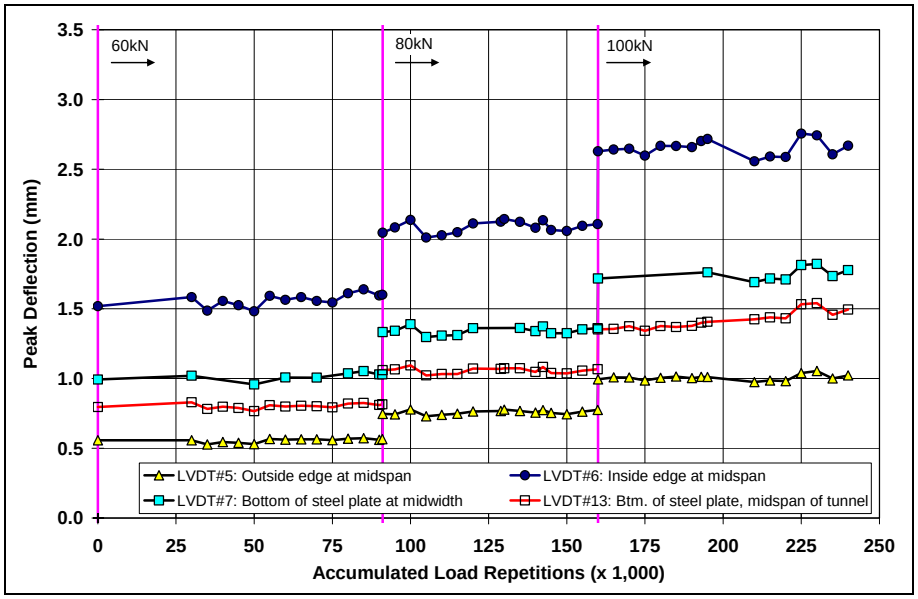

Figure 4.53: Phase 3.2: History of peak deflections at bottom of steel plate.

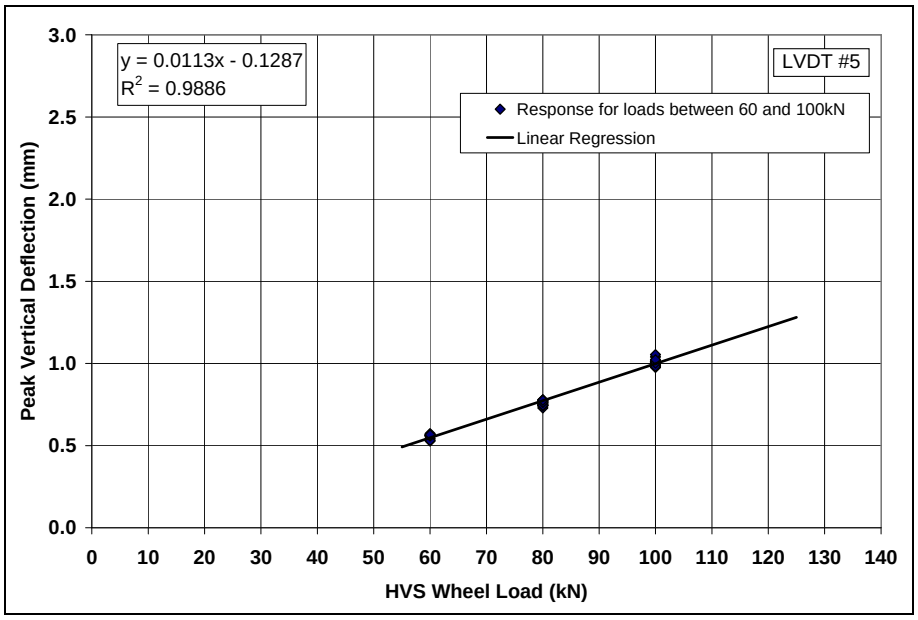

Figure 4.54: Phase 3.2: Relationship between peak deflection and wheel load.

(LVDT #5, midspan, outside edge of steel plate)

4.7.4 Longitudinal Strain

Influence lines (or deflection bowls) from a single pass of the 100 kN wheel load (Repetition #240,000 for the phase and #1,210,000 for the test) for the three strain gauges is shown in Figure 4.55. The impact load had a very small effect (wheel position 4.5 in the figure) on response. A plot of the peak strains measured

on bolts, washers, and the steel plate for the duration of Phase 3.2 are shown in Figure 4.56. No differences in behavior to that recorded in Phase 2.1 were observed, with strains remaining constant for each load for all sensors throughout the phase. The relationship between load and response was linear and consistent with previous phases for all three sensors (Figure 4.57 through Figure 4.59). Based on the data recorded, the impact applied at any of the wheel loads did not appear to influence longitudinal strain on the steel plate at the sensor locations.

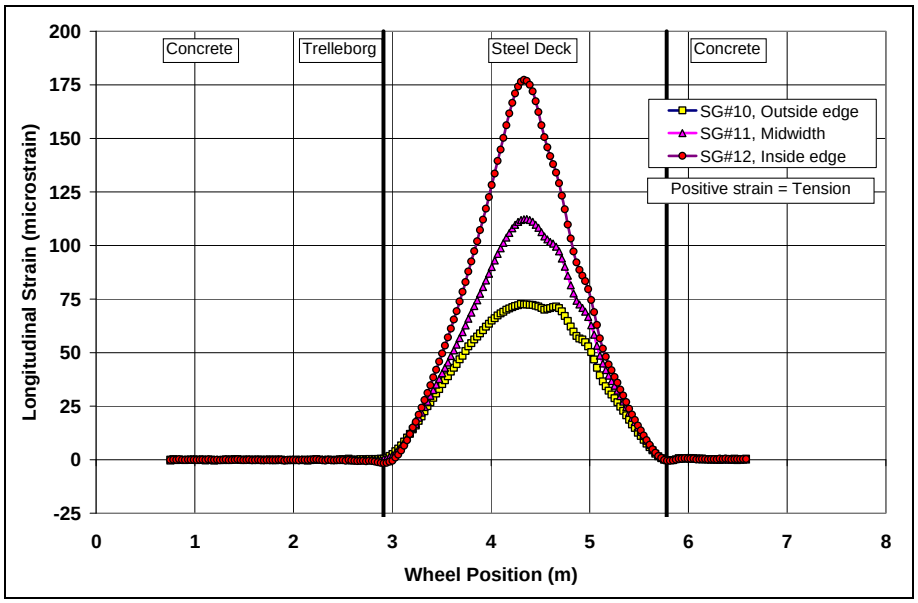

Figure 4.55: Phase 3.2: Influence lines for longitudinal strains at bottom of steel plate.

(Repetition #1,210,000, wheel load at 100 kN)

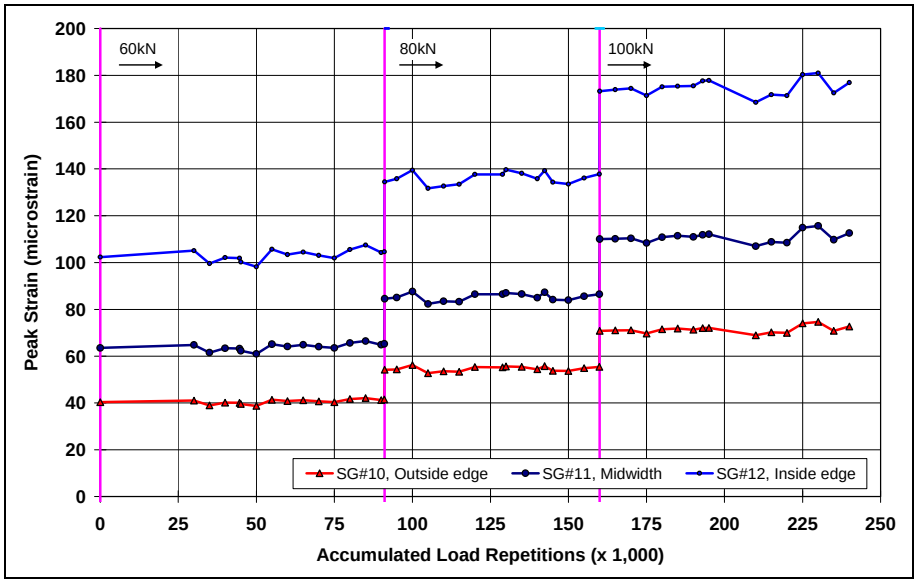

Figure 4.56: Phase 3.2: History of peak longitudinal strains at bottom of steel plate.

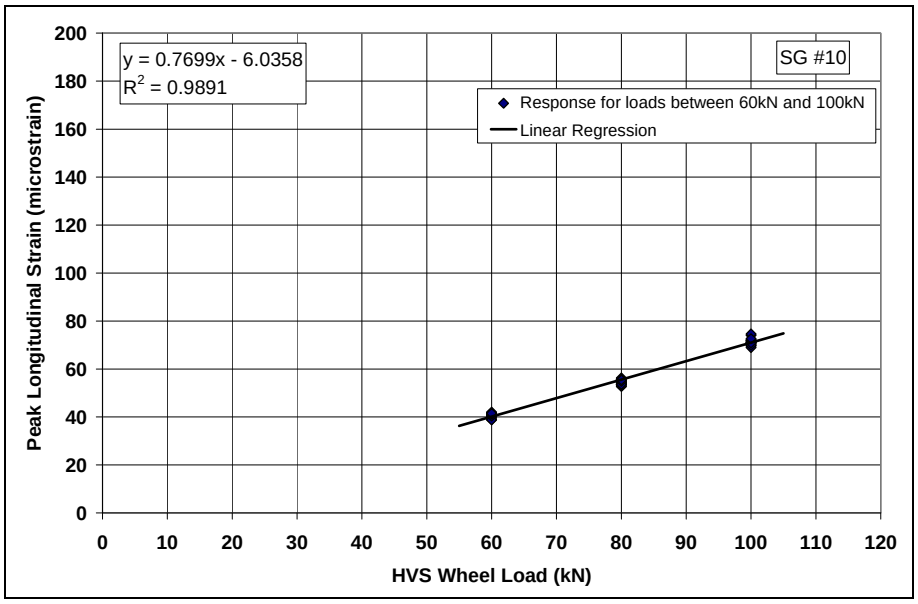

Figure 4.57: Phase 3.2: Relationship between peak strains and wheel load for SG #10.

(SG #10, outside edge of steel plate)

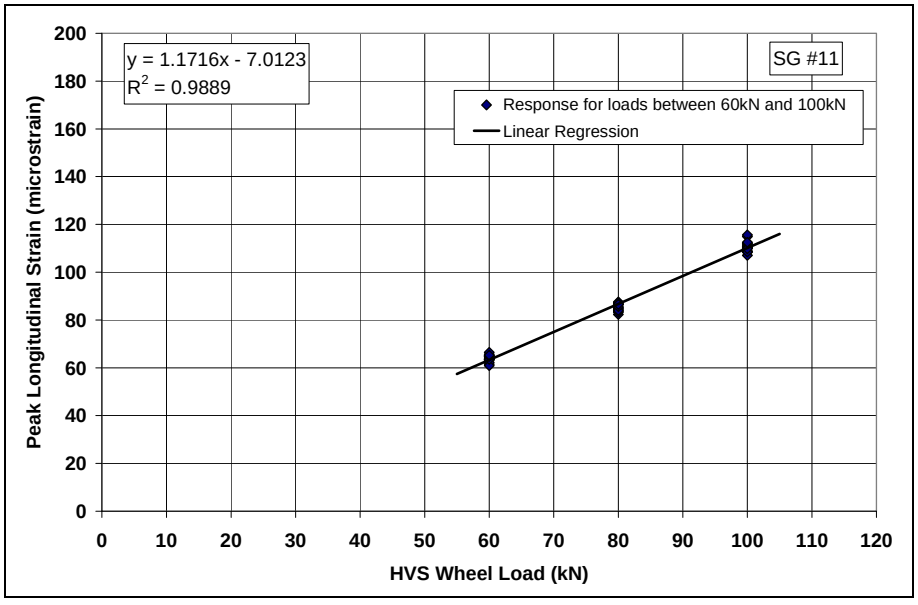

Figure 4.58: Phase 3.2: Relationship between peak strains and wheel load for SG #11.

(SG #11, midspan, outside edge of steel plate)

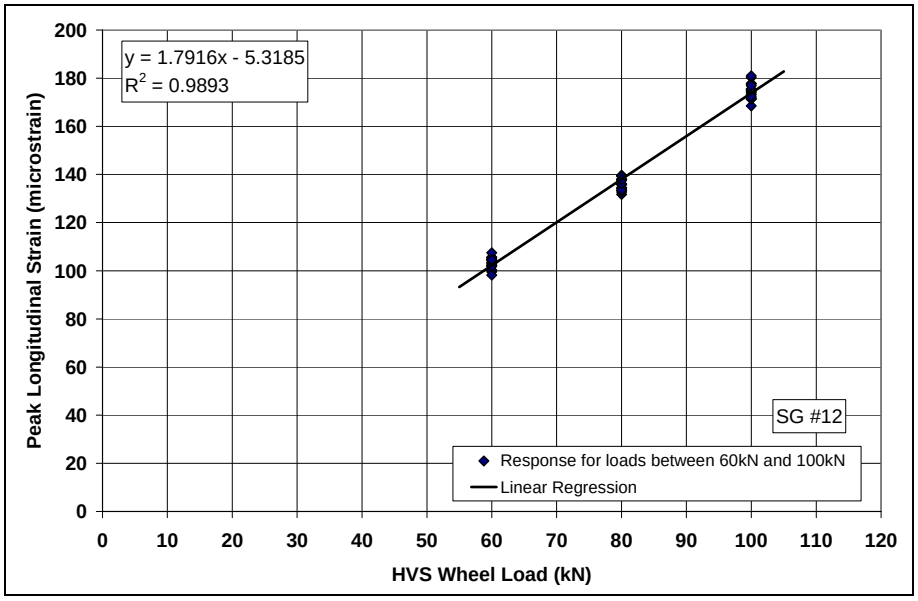

Figure 4.59: Phase 3.2: Relationship between peak strains and wheel load for SG #12.

(SG #12, outside edge of steel plate)

4.7.5 Visual Damage

No visual damage was observed on the concrete structure, steel plate, bolts, or washers at the end of this phase. Tire abrasion wear on the Trelleborg unit continued with additional accumulations of rubber particles (Figure 4.60). Apart from some additional deformation on the rubber, no new damage was observed on the Trelleborg unit. No rotation of the bolts or washers was observed.

Figure 4.60: Phase 3.2: Rubber accumulation on Trelleborg unit after 1,191,000 repetitions.

4.7.6 Phase Summary

No damage was observed at the end of Phase 3.2 and based on the deflection and strain data recorded, no permanent deformation in the steel plate occurred. Responses continued to be the same as those recorded

in earlier phases and increases in peak deflection and peak strain continued to show a linear relationship with increasing load. Based on the results and observations in this phase, it was concluded that the impact loading applied did not significantly influence performance.

4.8 Phase 3.3: Edge Test with High Load

4.8.1 Introduction

The objective of Phase 3.3 was to cause as much damage to the joint as possible to identify the weakest part of the design. The test ran for 15 days using an aircraft tire, with one day of half-axle loading at 100 kN and 14 days at 150 kN. All loading was applied to the edge of the expansion joint in a bidirectional channelized mode.

4.8.2 Temperature

The average (daily, minimum, and maximum), lowest, and highest temperatures measured during Phase 3.3 are summarized in Table 4.8. Daily average temperatures are plotted in Figure 4.61, with error bars indicating minimum and maximum temperatures for the thermocouple located next to Strain Gauge #11 (TC-SG#11). Average ambient temperatures were again typical for the area, had a relatively small diurnal range, and continued to show the cooling trend observed in Phase 3.1, but with a number of unseasonably warm days. Average daily minimum and maximum temperatures recorded on the steel plate were similar to the ambient temperatures, except for the thermocouple on Strain Gauge #12, which again indicated a higher average daily maximum than the other measurement points. No extreme temperature events were recorded. It is unlikely that temperature had any significant influence on the way that the bridge deck expansion joint components functioned during this phase of testing.

Table 4.8: Phase 3.3: Temperature Summary

Thermocouple	Temperature (°C)				
	Average of Daily Average	Average of Daily Minimum	Average of Daily Maximum	Lowest	Highest
Ambient	18	14	22	11	28
TC-SG#10	19	16	21	13	23
TC-SG#10-S	18	15	21	12	23
TC-SG#11	21	17	25	15	27
TC-SG#12	26	20	33	18	37
Thermocouple	**Temperature (°F)**				
Ambient	64	58	72	52	83
TC-SG#10	65	61	70	55	74
TC-SG#10-S	65	59	69	54	73
TC-SG#11	70	63	76	58	81
TC-SG#12	78	68	91	64	98

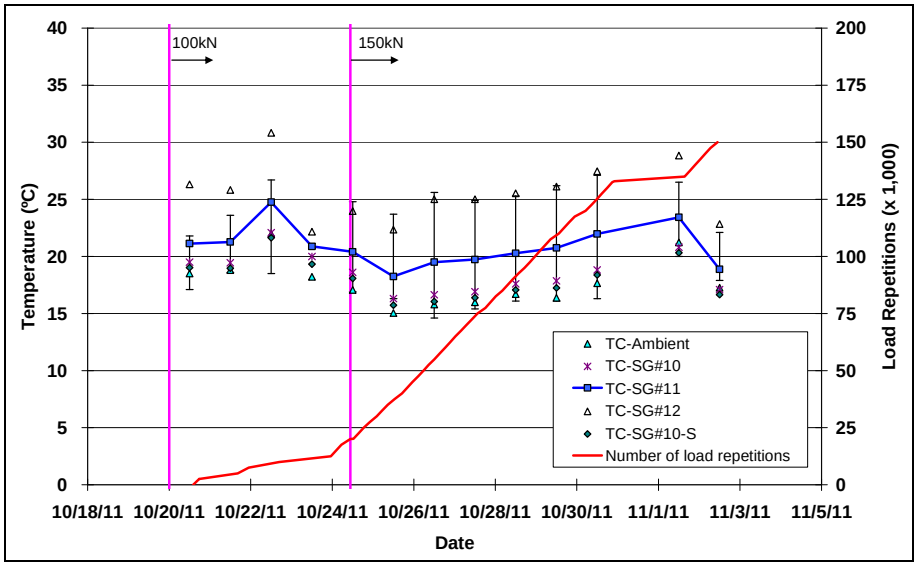

Figure 4.61: Phase 3.3: Daily average temperatures and HVS testing schedule.

4.8.3 Vertical Deflection

Plots of the peak deflections measured on bolts, washers, and the steel plate for the duration of Phase 3.3 are shown in Figure 4.62 through Figure 4.64, respectively. Deflections remained constant for all sensors throughout the phase, with actual deflection dependent on sensor location in relation to the wheelpath. Minor fluctuations (~0.01 mm) in deflection were attributed to changes in temperature and/or load and were consistent with previous test phases. Based on the data recorded, the very high loads applied did not appear to influence deflection of the expansion joint at the sensor locations and there was no evidence of any accumulated damage.

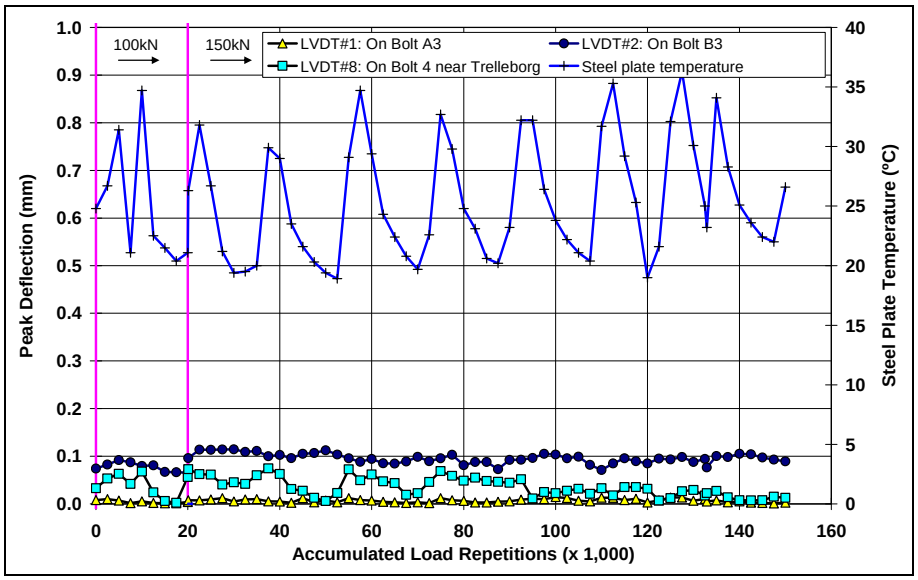

Figure 4.62: Phase 3.3: History of peak deflections on bolts.

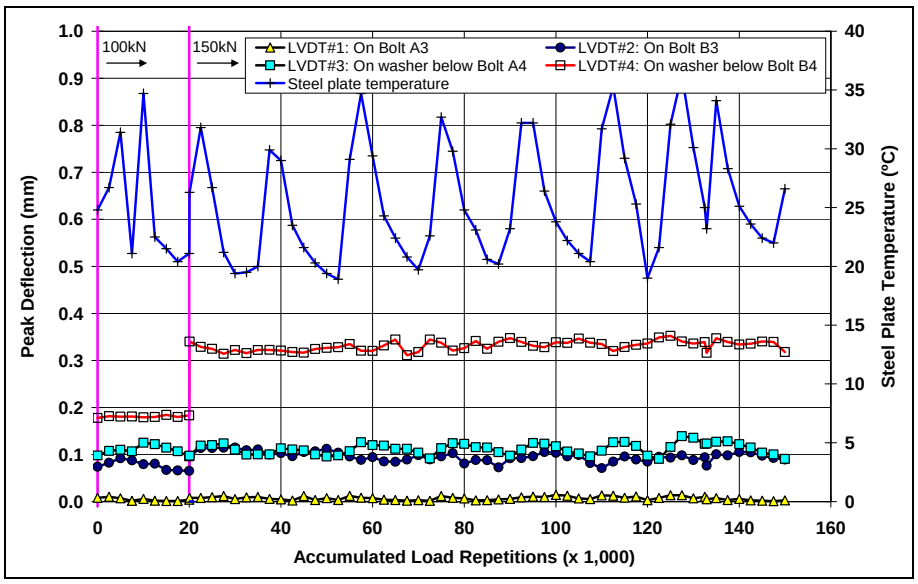

Figure 4.63: Phase 3.3: History of peak deflections on bolts and washers.

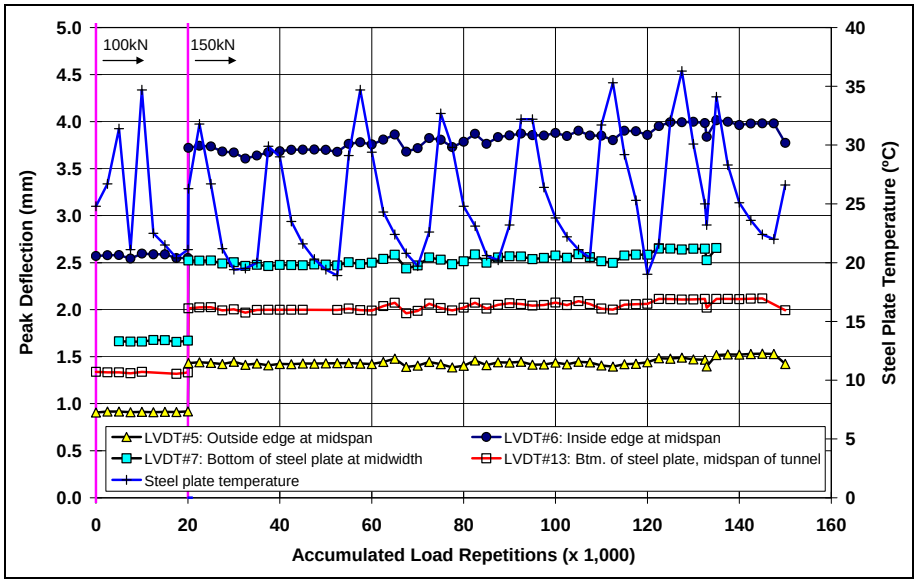

Figure 4.64: Phase 3.3: History of peak deflections at bottom of steel plate.

4.8.4 Longitudinal Strain

A plot of the peak strains measured on the steel plate for the duration of Phase 3.3 is shown in Figure 4.65. Strains remained constant for all sensors throughout the phase and were consistent with those measured in previous phases. Increasing the load to 150 kN resulted in a linear increase in strain recorded at the various sensors. Minor fluctuations (<5 με) in longitudinal strain were again attributed to changes in temperature and/or load and were consistent with previous phases. Based on the data recorded, the very

high loads applied did not appear to influence longitudinal strain in the steel plate at the sensor locations and there was no evidence of any accumulated damage.

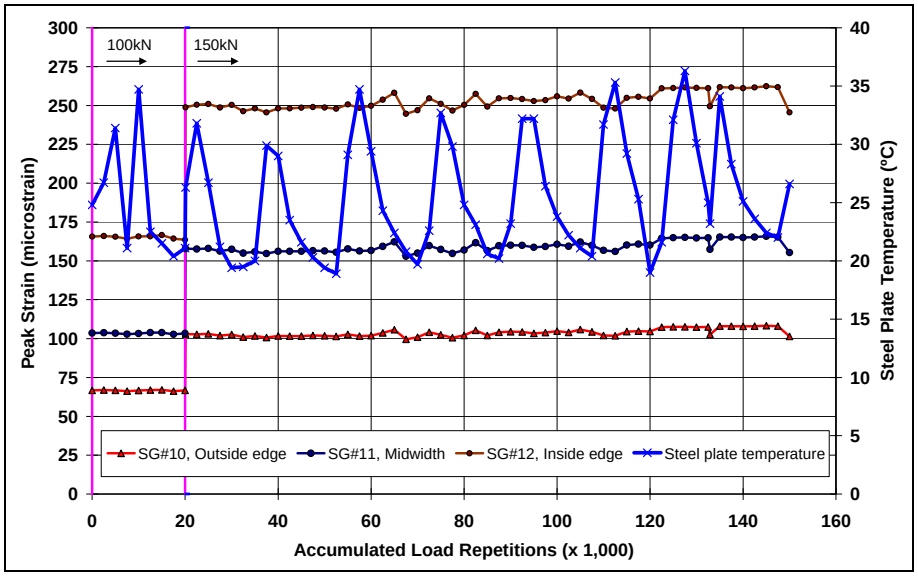

Figure 4.65: Phase 3.3: History of peak longitudinal strains at bottom of steel plate.

4.8.5 Visual Damage

No visual damage was observed on the steel plate, bolts, or washers at the end of this phase. However, isolated damage was caused by the very high wheel load to the steel ribs of the Trelleborg unit directly under the wheelpath (Figure 4.66). Damage to these ribs then resulted in severe deformation/shoving (Figure 4.67) and then tearing of the rubber (Figure 4.68). Large quantities of accumulated rubber particles were observed between the ribs and in other depressions. The concrete approach slab also cracked under the very heavy loading, but this did not influence the behavior of the expansion joint in any way. No rotation of the bolts or washers was observed. Photographs of the structure and Trelleborg unit on completion of all testing are provided in Figure 4.69.

4.8.6 Phase Summary

On completion of this phase of testing, the measured data from the LVDTs and strain gauges indicated that there was still no structural damage on any steel parts of the expansion joint. Observed damage was limited to the wheelpath over the Trelleborg unit only, and consisted of significant wear and deformation on the rubber sections of the Trelleborg unit and deformation and shearing in one of the steel ribs supporting these rubber sections. The distress observed to the Trelleborg unit under the very high loads (almost four times the legal limit) applied in this last phase of testing is unlikely to occur under normal traffic on the Bay Bridge.

Figure 4.66: Phase 3.3: Damage to steel rib of Trelleborg unit.

Figure 4.67: Phase 3.3: Deformation and shoving of rubber on Trelleborg unit.

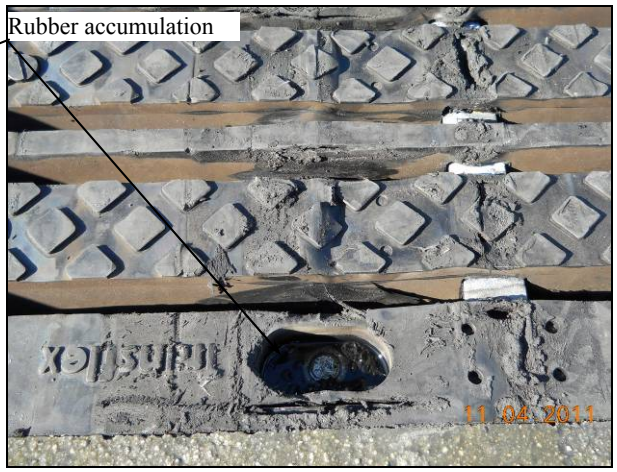

Figure 4.68: Phase 3.3: Tearing of rubber and accumulation of rubber particles in Trelleborg unit.

Figure 4.69: Phase 3.3: Structure and Trelleborg unit after completion of testing.

4.9 Static Responses for All Phases

Static responses are those deflections and strains measured on the bolts, washers, and steel plate caused by either temperature change or plastic deformation induced by wheel loading. They are termed "static" because their rate of change is much slower compared to the dynamic responses of the moving wheels discussed in Section 4.2 through Section 4.8 above.

4.9.1 Vertical Deflections

Example daily variation in vertical deflections measured during Phase 1.1 (representative of all phases) is shown in Figure 4.70. Deflection increased with increasing temperature and generally followed daily temperature change. However, the amount of change in any day was miniscule (~0.03 mm) and was not considered significant to the study.

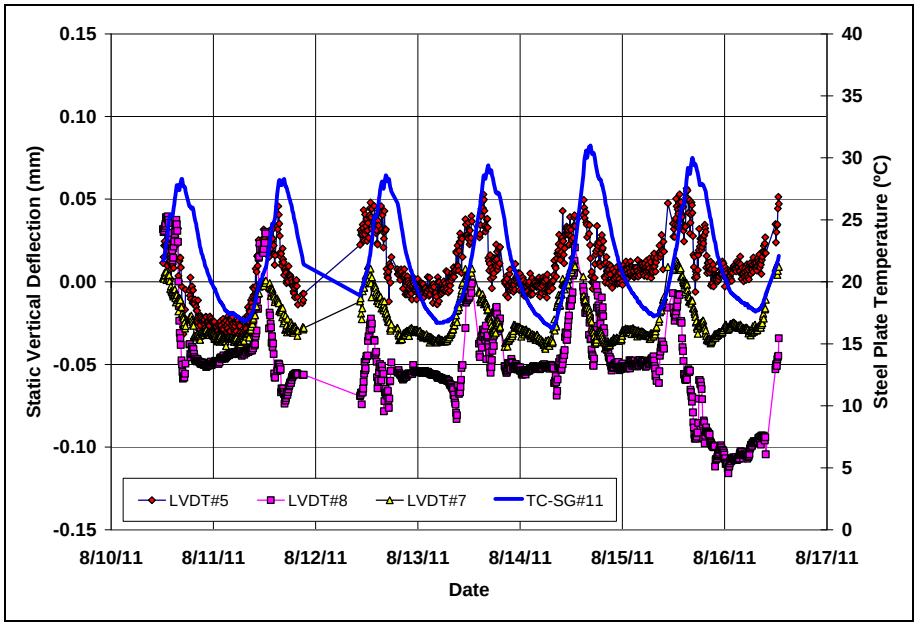

Figure 4.70: Example daily variation for vertical deflections during Phase 1.1.

The history of daily maximum static vertical deflections measured on the steel plate and daily maximum steel plate temperature is shown in Figure 4.71. Deflections did not show strong correlation with temperature. However, some very small change in daily maximum static vertical deflection is evident over the duration of the study (between 0.1 mm and 0.3 mm). It is not clear whether this could be attributed to settlement of the structure on the soft clay subgrade or to permanent deformation caused by the very heavy wheel loads. The amount of change in vertical deflection did not warrant further investigation and was not considered significant to the study.

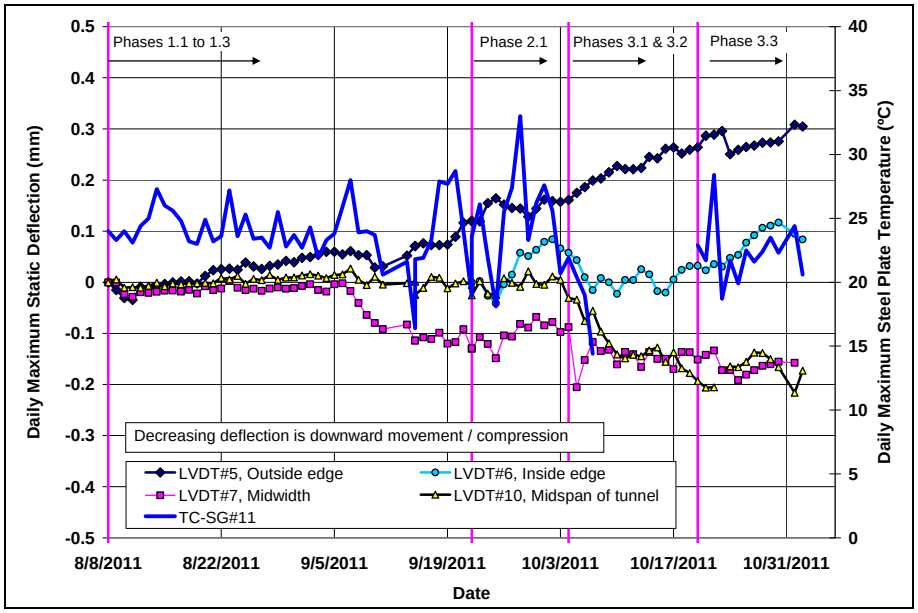

Figure 4.71: History of daily maximum static vertical deflections on steel plate.

4.9.2 Longitudinal Strain

Example daily variations in longitudinal strain for the three strain gauges, measured during Phase 1.1 (representative of all phases), are shown in Figure 4.72 through Figure 4.74. Strain increased with increasing temperature and generally followed (with a lag) daily temperature change. However, the amount of change in any day was very small (~30 με to 70 με) and was not considered significant to the study.

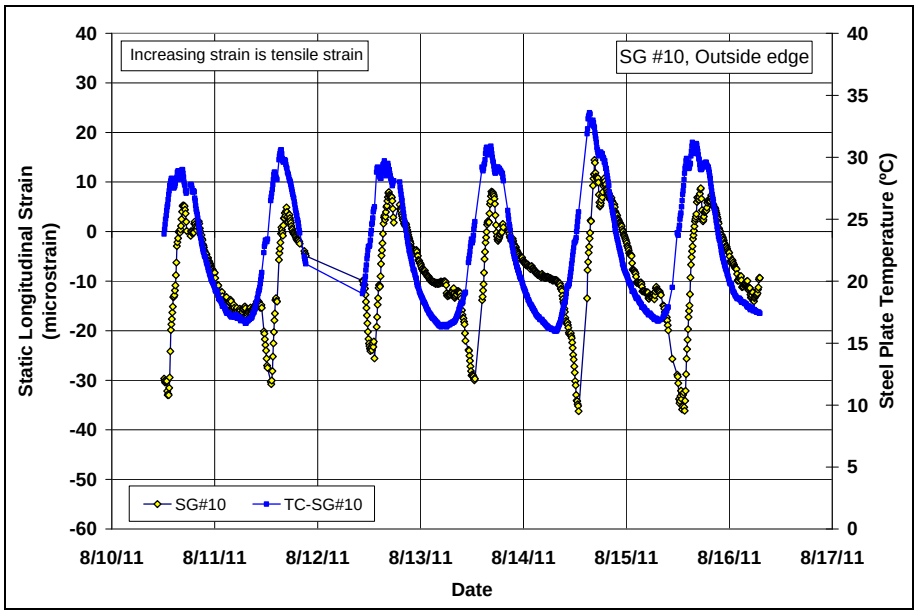

Figure 4.72: Example daily variation for longitudinal strain at SG #10 during Phase 1.1.

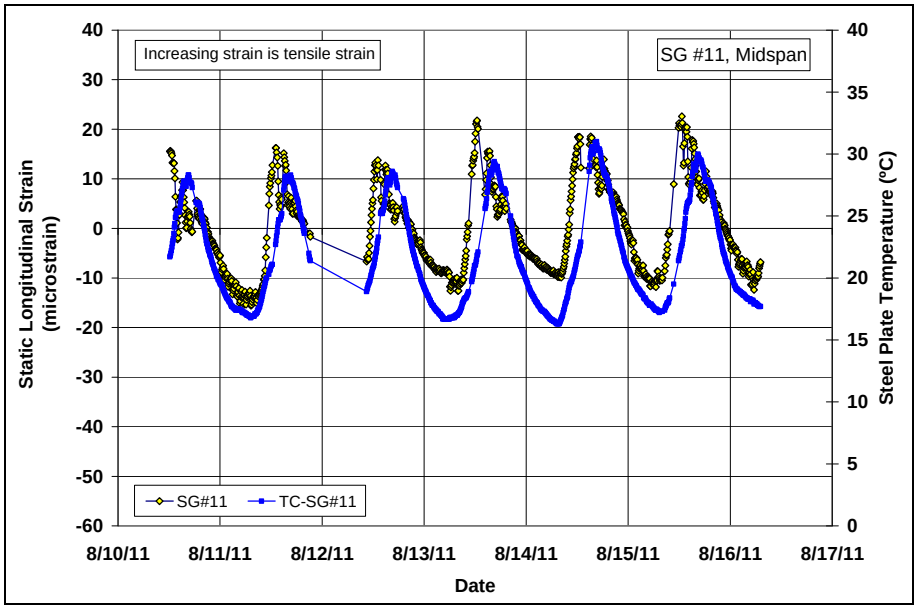

Figure 4.73: Example daily variation for longitudinal strain at SG #11 during Phase 1.1.

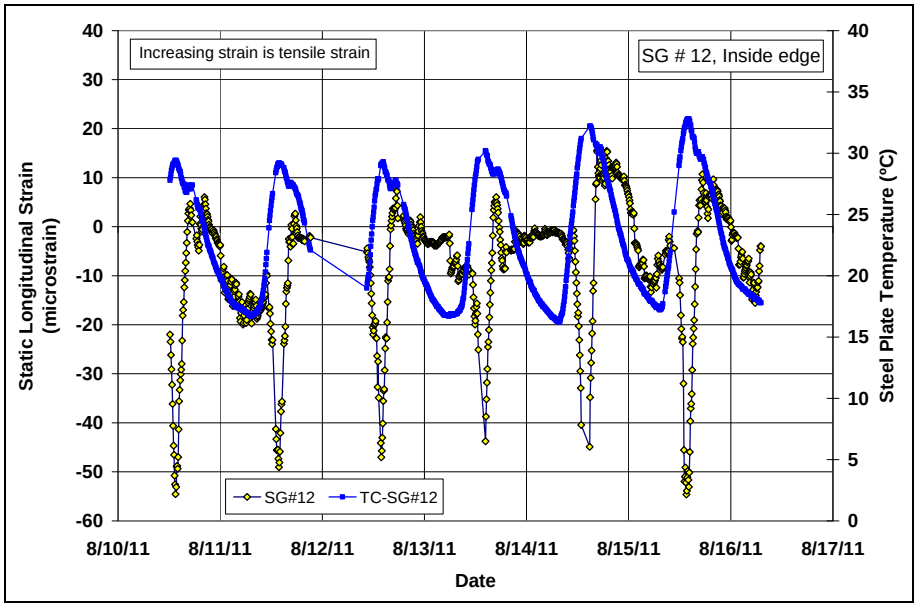

Figure 4.74: Example daily variation for longitudinal strain at SG #12 during Phase 1.1.

Figure 4.75 shows the history of daily maximum static longitudinal strains as well as daily maximum steel plate temperatures for all phases of HVS testing. Changes in daily maximum longitudinal strain generally followed changes in temperature, and any permanent strain caused by the wheel loading is considered to be insignificant.

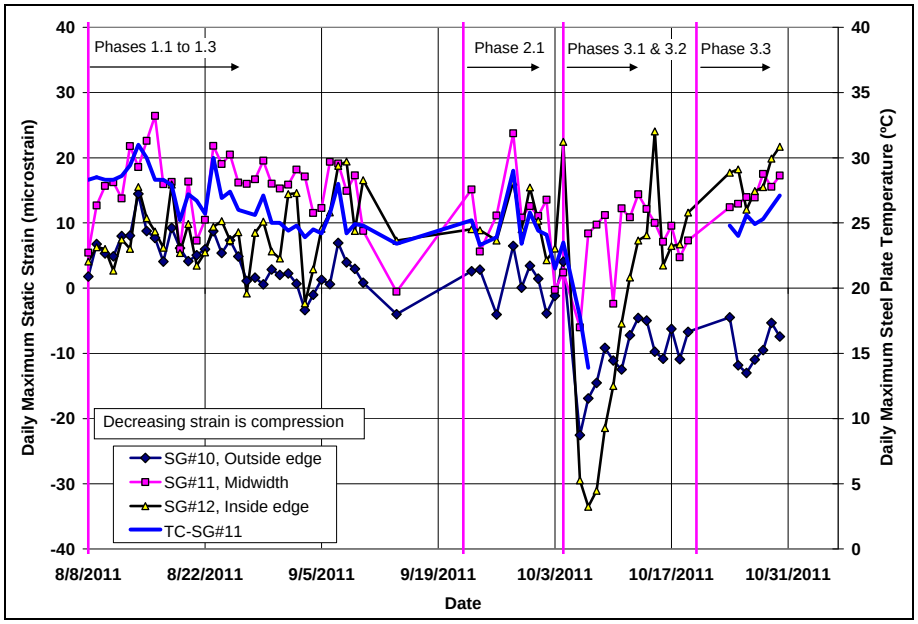

Figure 4.75: History of daily maximum static longitudinal strains.

4.10 Permanent Deformation on Trelleborg Unit

The history of maximum downward permanent deformation on the Trelleborg unit at different profilometer measurement stations is shown in Figure 4.76. Scatter on the figure is attributed to the irregular surface of the Trelleborg unit, the resilient properties of the material from which it is constructed, and constant changes to the shape of the rubber caused by tire load and accumulating damage. Permanent deformations of about 1.0 mm were recorded at Station 8 even though this station was approximately 300 mm (12 in.) from the edge of the wheelpath, where no actual deformation should have been recorded. This implies that the accuracy of the laser profilometer measurements on the Trelleborg unit is about 1.0 mm (0.04 in.).

Figure 4.77 shows the history of average maximum downward permanent deformation of the Trelleborg unit for all stations (Station 1 through Station 8). The permanent deformation increased to approximately 2.5 mm (0.1 in.) after only 20,000 repetitions (which were applied with a 25 kN load), then recovered to approximately 1.0 mm (0.04 in.) after 60,000 repetitions with a 40 kN load, and then remained relatively constant until it started steadily increasing again at the end of Phase 1.3. The reason for the initial increase in permanent deformation during Phase 1.1 is unclear but is considered to be insignificant since it recovered under further trafficking.

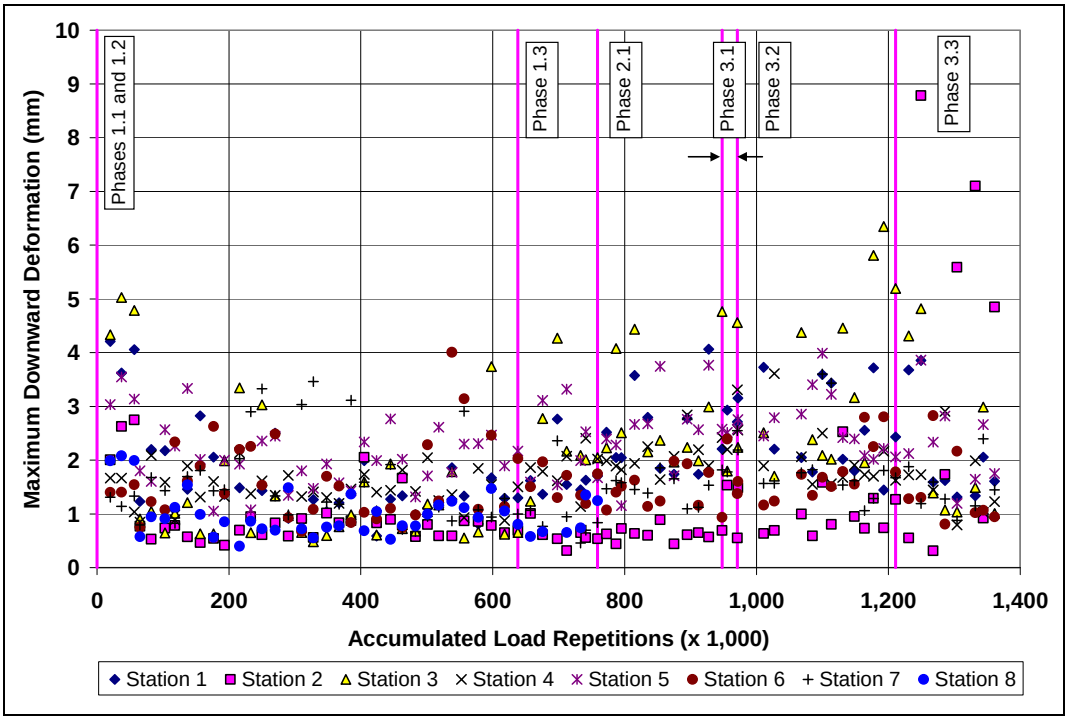

Figure 4.76: Maximum downward permanent deformation of the Trelleborg unit.

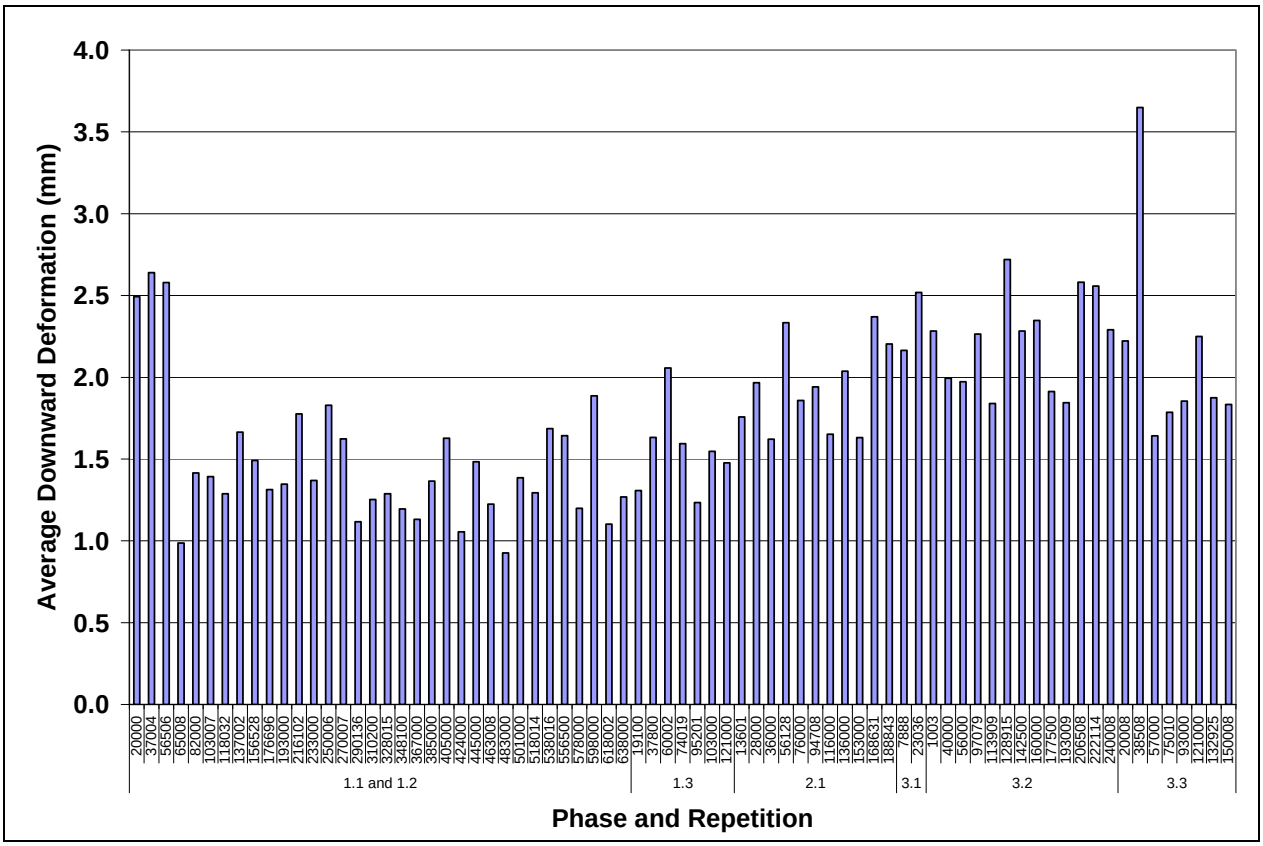

Figure 4.77: Average maximum downward permanent deformation of Trelleborg unit.

Severe damage to the Trelleborg unit was first observed after about 1,230,000 load repetitions, or after about 20,000 load repetitions into Phase 3.3 testing with the aircraft tire (Figure 4.66 through Figure 4.68).

Vertical permanent deformation contour plots at the end of each phase are shown in Figure 4.78 through Figure 4.85. These contour plots show how the surface elevation changed at different profilometer measurement locations. Note that the permanent deformation between profilometer measurement stations is linearly interpolated and that scales are different on each plot.

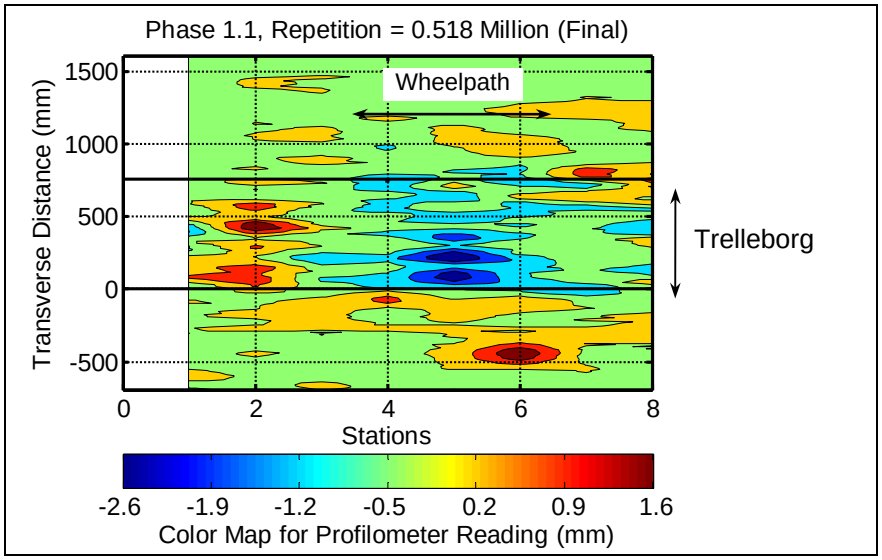

Figure 4.78: Phase 1.1: Contour plot of deformation (dual wheel, channelized on center).

(Max. downward deformation of 2.6 mm [Station 5], max. upward deformation of 1.6 mm [Station 2])

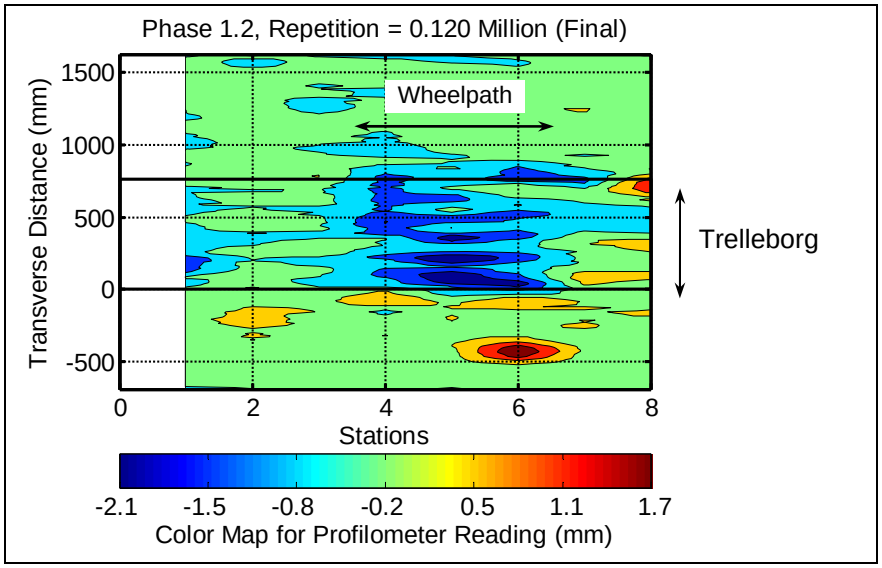

Figure 4.79: Phase 1.2: Contour plot of deformation (dual wheel, channelized on center).

(Max. downward deformation of 2.1 mm [Station 5], max. upward deformation of 1.0 mm [Station 8])

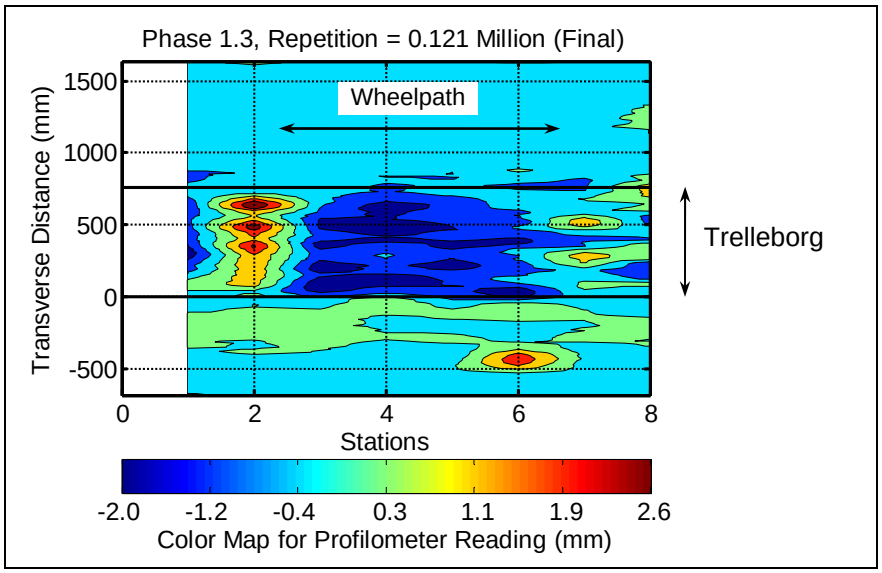

Figure 4.80: Phase 1.3: Contour plot of deformation (dual wheel, wander).

(Max. downward deformation of 2.0 mm [Station 4], max. upward deformation of 2.6 mm [Station 2])

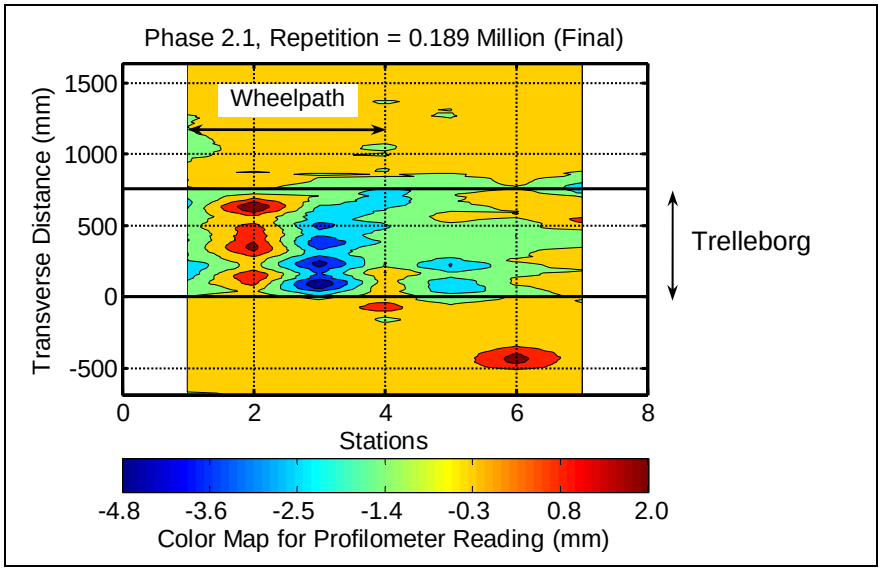

Figure 4.81: Phase 2.1: Contour plot of deformation (dual wheel, channelized on edge).

(Max. downward deformation of 4.8 mm [Station 3], max. upward deformation of 2.0 mm [Station 2])

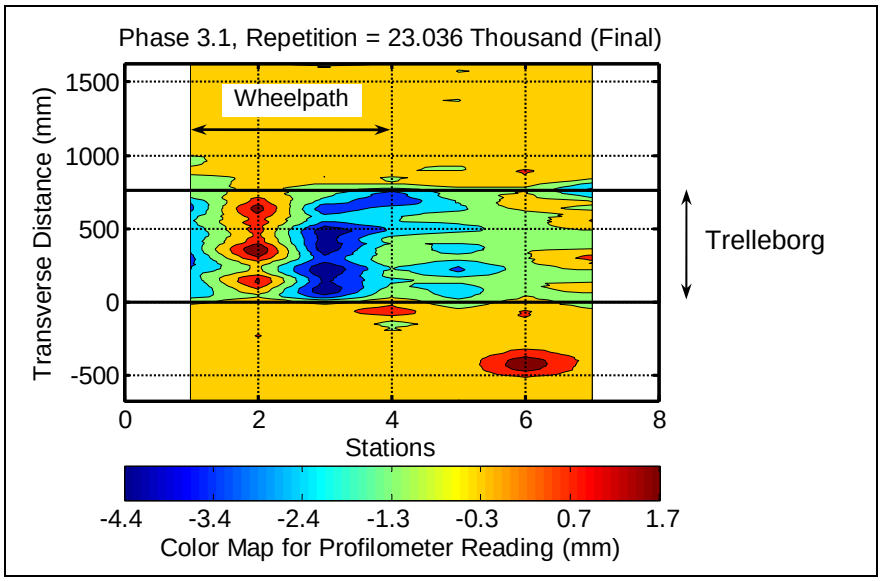

Figure 4.82: Phase 3.1: Contour plot of deformation (dual wheel, channelized on edge).

(Max. downward deformation of 4.4 mm [Station 3], max. upward deformation of 1.7 mm [Station 2])

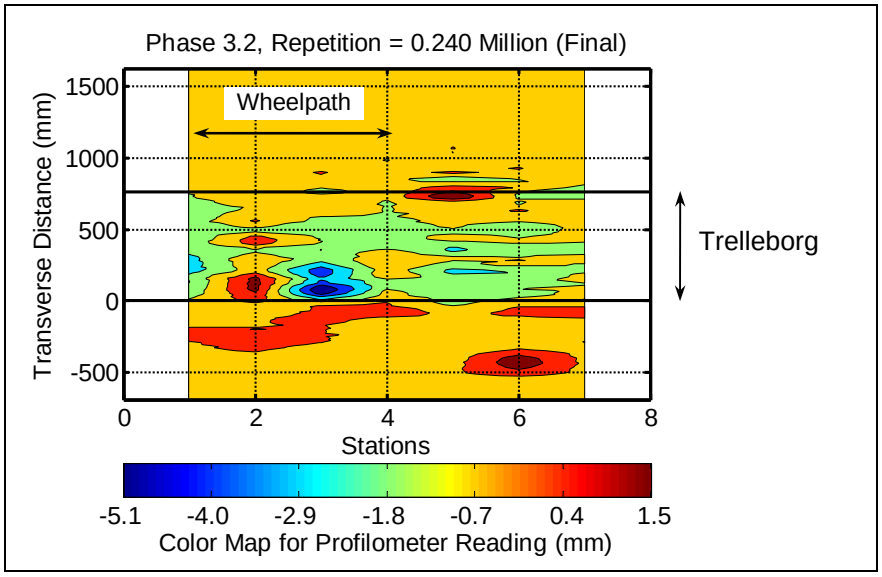

Figure 4.83: Phase 3.2: Contour plot of deformation (dual wheel, channelized on edge with impact).

(Max. downward deformation of 5.1 mm [Station 3], max. upward deformation of 1.5 mm [Station 2])

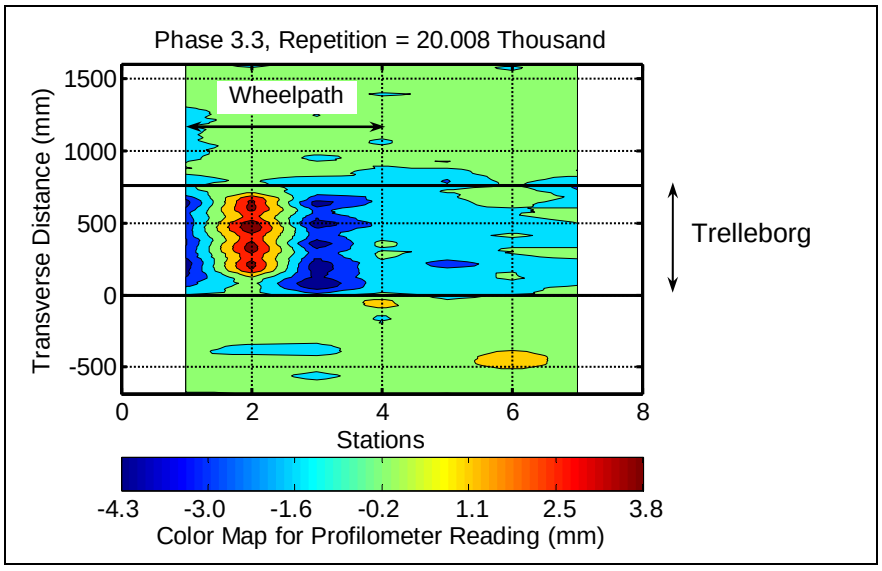

Figure 4.84: Phase 3.3 (20,000 reps): Contour plot of deformation (aircraft, channelized on edge).

(Max. downward deformation of 4.3 mm [Station 3], max. upward deformation of 3.8 mm [Station 2])

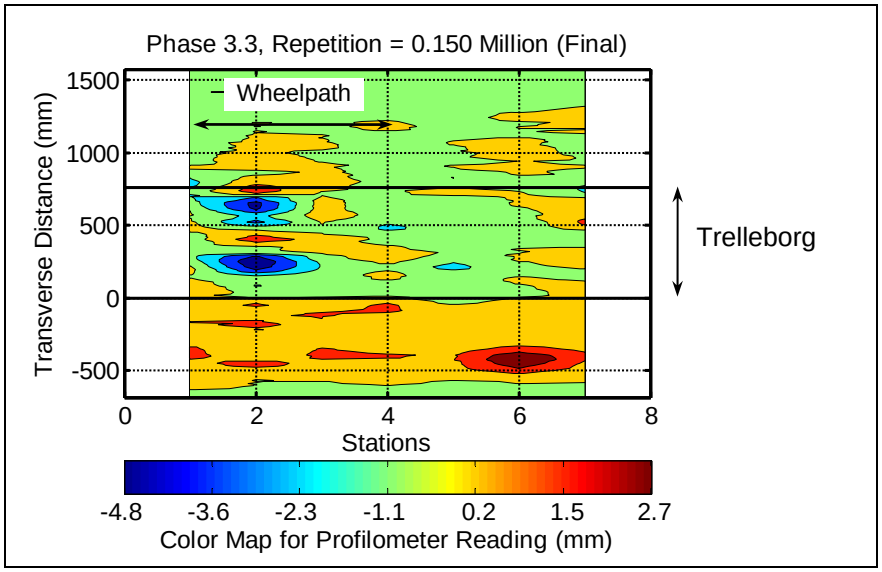

Figure 4.85: Phase 3.3 (final): Contour plot of deformation (aircraft, channelized on edge).

(Max. downward deformation of 4.8 mm [Station 2], max. upward deformation of 2.0 mm [Station 2])

5. CONCLUSIONS

A relatively unique opportunity was recently identified for accelerated traffic load testing of a new bridge expansion joint design not previously used in California. This study was part of the construction of the new East Span of the San Francisco–Oakland Bay Bridge and assessed whether the new expansion joints (which were designed to function in harmony with the bridge decks in the event of a high-magnitude earthquake) planned for linking the Self-anchored Span with the Transition and Skyway spans would withstand truck traffic loading. A test structure incorporating one of the full-scale joints was constructed close to the actual bridge and tested with the California Department of Transportation / University of California Pavement Research Center Heavy Vehicle Simulator in a series of phases.

A total of 1.36 million load repetitions, equating to about 46 million equivalent standard axle loads on a highway pavement, were applied in seven phases during the three-month test. On completion of this testing, no structural damage was recorded by any of the Linear Variable Differential Transducers (LVDTs) or strain gauges installed on the steel plates, steel frames, bolts, and washers. There was also no visible damage on any of these components. Excessive overloading with a 150 kN half-axle load (approximately four times the standard axle load) on an aircraft tire in the last phase of the test caused some damage to the Trelleborg unit in the joint. The damage included abrasion, tearing, shoving and permanent deformation of the rubber inserts, and deformation and shearing of one of the steel supports directly under the wheel load.

Although no vehicle suspension dynamics (i.e., vehicle bounce) or speed effects were considered, based on the results of this limited testing, it was concluded that the Caltrans seismic expansion joint would perform adequately under typical Bay Bridge traffic. The distresses observed on the Trelleborg unit under high loads in the last phase of testing are unlikely to occur under normal traffic. However, the Trelleborg unit was found to be the weakest point of the expansion joint, as expected. On the actual bridge structure, these units should be checked periodically to confirm the findings of this study, and to assess any effects of higher speeds and vehicle dynamics that were not identified. The joints will require periodic maintenance and replacement in line with manufacturer's specifications.

The findings from this study indicate that the Caltrans seismic expansion joint tested would be appropriate for typical Bay Bridge traffic.

No seismic or structural testing was undertaken and no recommendations toward the expansion joint's seismic or structural performance are made. Ride quality, skid resistance, and tire noise studies were carried out by Caltrans in a separate study and are reported on in separate Caltrans reports.

6. REFERENCES

1. JONES, D. 2005. **Quality Management System for Site Establishment, Daily Operations, Instrumentation, Data Collection and Data Storage for APT Experiments.** Pretoria, South Africa: CSIR Transportek. (Contract Report CR-2004/67-v2).

APPENDIX A: TEST STRUCTURE DESIGN AND INSTRUMENTATION

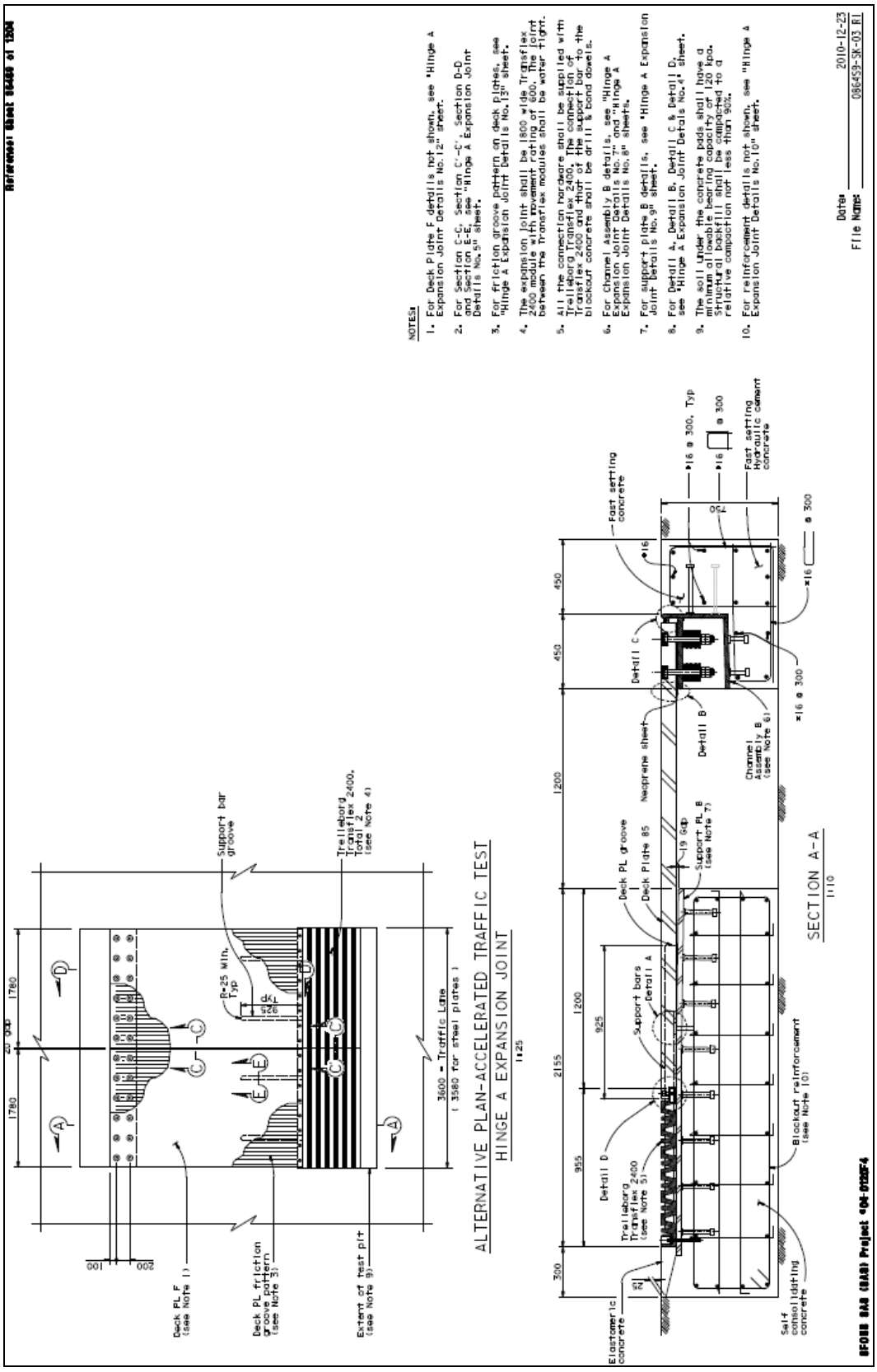

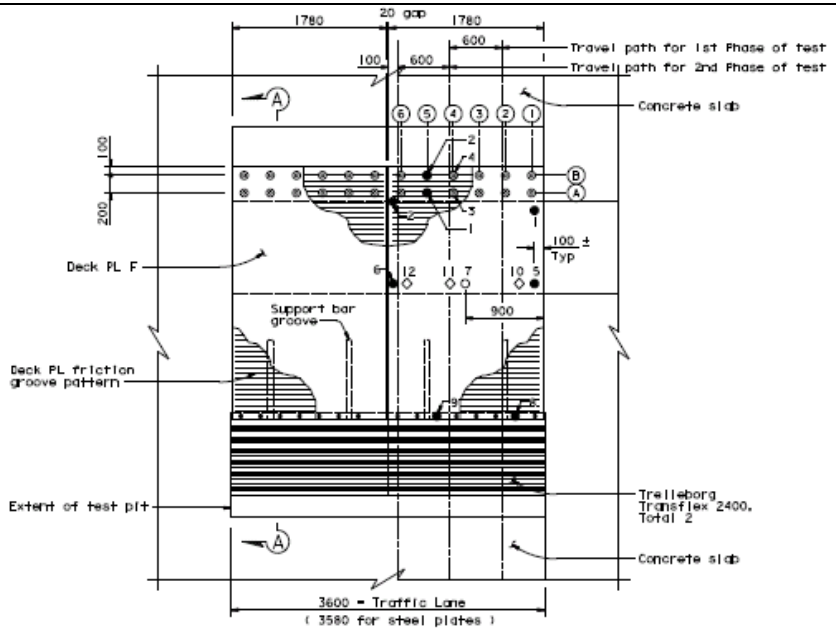

PLAN-SEISMIC JOINT INSTRUMENTATION

HINGE A EXPANSION JOINT (See Note 1)

1:25

INSTRUMENTED LOCATION			
MONITORED LOCATIONS	INSTRUMENT	MEASURED RESPONSE	LOCATION
● 1	LVDT	Vertical Deformation	Bolt head A⑤ at Phase 1 and A③ at Phase 2
● 2	LVDT	Vertical Deformation	Bolt head B⑤ at Phase 1 and B③ at Phase 2
○ 3	LVDT	Vertical Deformation	Bottom washer at Bolt A④ at Phase 1 and 2
○ 4	LVDT	Vertical Deformation	Bottom washer at Bolt B④ at Phase 1 and 2
● 5	LVDT	Vertical Deformation	Top of deck plate at outside edge
● 6	LVDT	Vertical Deformation	Top of deck plate at inside edge
○ 7	LVDT	Vertical Deformation	Bottom of deck plate at mid width
● 8	LVDT	Vertical Deformation	Bolt head at the connection between Trelleborg and the deck plate: Bolt 2 at Phase 1 and Bolt 4 at Phase 2
● 9	LVDT	Vertical Deformation	Bolt head at the connection between Trelleborg and the deck plate: Bolt 6 at Phase 1 and None at Phase 2
◇ 10	Strain Gauge	Strains parallel to traffic	Bottom of the deck plate at outside edge
◇ 11	Strain Gauge	Strains parallel to traffic	Bottom of the deck plate at mid width
◇ 12	Strain Gauge	Strains parallel to traffic	Bottom of the deck plate at inside edge

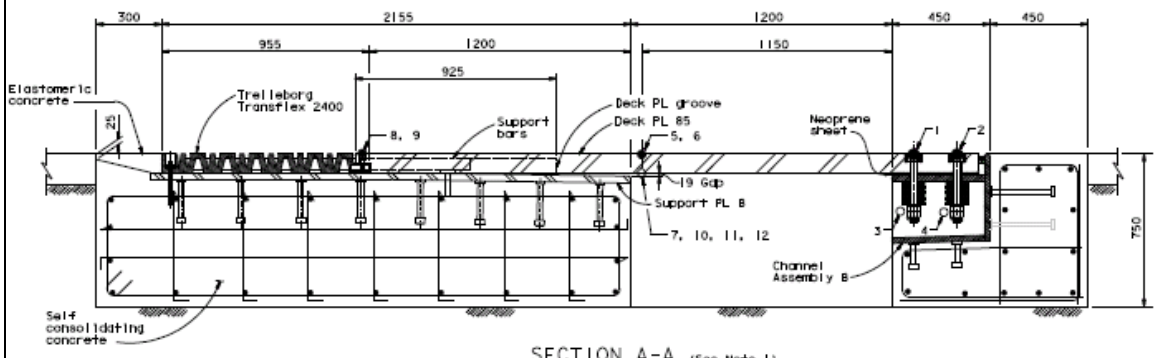

SECTION A-A (See Note 1)

1:10

NOTES:

1. For details not shown, see "086459-SK-03-R1" sheet.
2. Laser profilometer shall be used for daily monitoring of neoprene distortion at Transflex.
3. Deflection of the test wheel shall also be monitored in real time.
4. Additional strain gages shall be per direction of Caltrans.
5. Bolts shall be inspected daily. Any loosening shall be reported to the Engineer.

Date: 2011-07-20

File Name: 086459-SK-04

SFOBB BAS (BAS) Project #04-0120F4